UNIVERSITY OF CAPE TOWN
IYUNIVESITHI YASEKAPA • UNIVERSITEIT VAN KAAPSTAD

CHARACTERISATION OF BRIDGE-TRACK INTERACTION OF A MULTI-SPAN VIADUCT SUBJECTED TO HEAVY HAUL LOADING

by

Emilia Joyce Mupwedi

Supervisor

Professor Pilate Moyo

Co-Supervisor

Dr. Kabani Matongo

Dissertation submitted in partial fulfilment of the requirements for the degree of Master of Science in Structural Engineering

Department of Civil Engineering
University of Cape Town, Private Bag Rondebosch, 7700
South Africa 77

University of Cape Town

The copyright of this thesis vests in the author. No quotation from it or information derived from it is to be published without full acknowledgement of the source. The thesis is to be used for private study or non-commercial research purposes only.

Published by the University of Cape Town (UCT) in terms of the non-exclusive license granted to UCT by the author.

University of Cape Town

PLAGIARISM DECLARATION

1. I am presenting this dissertation in partial fulfilment of the requirements for my degree.
2. I know the meaning of plagiarism and declare that all of the work in the dissertation, save for that which is properly acknowledged, is my own.
3. This thesis has been submitted to the Turnitin module (or equivalent similarity and originality checking software), and I confirm that my supervisor has seen my report and any concerns revealed by such have been resolved with my supervisor.
4. I hereby grant the University of Cape Town free licence to reproduce for the purpose of research either the whole or any portion of the contents in any manner whatsoever of the above dissertation.

Signed by candidate

24/08/2022

Emilia Mupwedi
MPWEMI001

Date

ABSTRACT

In many countries, railway transportation has been the primary mode of transportation, and engineers have been pushing boundaries to increase productivity and reduce costs for decades. The rail is the most important component of the railway infrastructure because it serves as the driving surface, direction guidance, and force transmission. Continuously Welded Rail (CWR), which are defined as rails that have been welded together, are now used in modern railways. When the rail is built on a bridge, the bridge's and rolling stock's behavior adds additional forces to CWR rails. As a result of the coupling effects of tracks and deformed superstructures, additional rail stresses are superimposed on other forces. These extra stresses are caused primarily by the longitudinal elongation of the superstructure as a result of temperature, braking, traction, and deck movement. The interaction of these forces between the rail and the bridge is therefore known as Track-Bridge-Interaction (TBI). Therefore, the horizontal forces must be precisely managed to prevent rail failure.

This research presents a characterization of TBI for heavy haul railways and management of longitudinal forces to minimize the possibility of failure due to superimposed longitudinal forces. The Olifants River Viaduct (ORV), a 1 km long bridge with CWR and two continuous spans of 11 spans at each end and a drop span in the middle, was used as a case study in the research. The ORV has been equipped with monitoring systems to help manage the tracks. Thus, data from these systems were used to categorize the interaction forces. The research focused on categorizing the trains crossing the ORV into six (A-F) categories; the categorization was based on the train length and the commodities being hauled. The research also studied the speed variations of each train crossing the bridge. The speeds were analysed using python and statistical tools MS Excel. Lastly, the impact of crossing trains on rail forces, rail temperature, ambient temperature, and deck movement was analysed using python and statistical tools in excel.

The study showed that the most frequent train to cross the bridge are category D trains with six locomotives and 342 wagons, while the train speed is dependent on the train length and the commodities hauled. Thus, the short trains in categories (A, B, and E) cross the bridge at higher constant speeds while the long trains in categories (C and D) cross the bridge at reduced speeds

than the short trains but exhibit speed variations and sometimes cross the bridge at speeds exceeding the 50 km/h limit. Therefore, higher dynamic forces should be expected from short trains crossing the bridge at high constant speeds, but no additional forces should be expected on the rails from these trains as they experience no speed variations. At the same time, the long trains experience significant speed variations of both acceleration and decelerations, which imposes additional forces on the rails due to traction and braking. The imposed forces on the rails are predominantly due to crossing trains with significant speed variations of acceleration and deceleration, the acceleration change ranges from 5-30 km/h, and deceleration change ranges from 5-20 km/h. The braking and acceleration effect causes a change in the rail forces, rail temperature, and deck deflection, which in turn imposes additional forces on the rails. Therefore, high speed variation induces additional longitudinal forces on the rails. However, the imposed acceleration forces are higher than the braking forces, but the braking imposed forces are the most critical forces as they tend to cause an increase in the tensile and compression forces when the forces are at their peaks, and there is a train present on the bridge, while acceleration causes a decrease in the rail forces at those times. The deck movement forces imposed on the rails were predominantly due to ambient temperature, which showed a positive linear relationship between the two. The deck expands with increasing ambient temperature and contracts with a decrease in ambient temperature. In contrast, the compression forces were within the given limits of 1100 kN, while the tension forces exceeded the rail force limit of 1400 kN when the rail temperature was between $0 - 20℃$, and the deck deflection above 83 mm in the negative direction, and a present train on the bridge, making the rail more susceptible to failure during winter.

DEDICATION

I dedicate this work to my dear mother (**Orga Shetunyenga**) and aunt (**Saima Shetunyenga**) for their unwavering love, trust, and sacrifices, which have enabled me to progress thus far in life. Because of them, I am who I am now, and I will be forever grateful.

ACKNOWLEDGEMENT

First and foremost, I want to express my gratitude to God for his gift of wisdom and strength, which has sustained me throughout this research. I would like to thank and acknowledge the following individuals as well:

I am deeply grateful to my supervisor, Professor Pilate Moyo, for his guidance and supervision during the entire Master's period. He bestowed me with the commitment and the awareness to follow the best possible route by his unmatchable style of encouragement. I also thank him for his moral support and for sharing valuable knowledge with me and my co-supervisor, Dr. Kabani Matongo, for his continued support and advice throughout this research.

My utmost gratitude goes out to the Civil Engineering Department at the University of Cape Town (UCT) for supporting me during the darkest days of my life. I Further extend my gratitude to the Concrete Materials and Structural Integrity Research Unit (CoMSIRU) for being present at the seminar presentations. They have given me valuable comments and recommendations that led in the right direction to successfully complete this research.

I would also like to thank and acknowledge the UCT Postgraduate Funding Office and WML Coast Consulting Engineers for providing partial funding for this research.

My siblings, Samuel Mupwedi, Elalia Mupwedi, Grace Nghiishililwa, Joyce Nghiishilwa, Marlene Hasheela, and the entire family at large for their continued support.

Lastly, a special thank you goes out to my partner Junias Kalumbu and my friends Jackline Zambwe, Rudolph Endjala, Shade Muluti, Sarty Sheetekela, Jaziitha Simon, Hilja Ndakola, Shalongo Angula, and Samuel Ndeutapo for their love, patience, concern, support, and for being readily available whenever I needed assistance.

Table of Contents

LIST OF FIGURES

LIST OF TABLES

LIST OF SYMBOLS AND ABBREVIATIONS

CWR	-	Continuously Welded Rail
DAS	-	Data Acquisition System
HEP	-	Head End Power
HH	-	Heavy Haul
IHHA	-	International Heavy Haul Association
MS	-	Monitoring System
ORV	-	Olifants River Viaduct
RDP	-	Radio Distributed Power
RNT	-	Rail Neutral Temperature
SS	-	Saldanha System
SHM	-	Structural Health Monitoring
TFR	-	Transnet Freight Rail
WIM-WIM	-	Wheel Impact Monitoring & Weigh-in-Motion

1. INTRODUCTION

1.1 Background

Heavy Haul (HH) operates the world's longest and heaviest freight trains, moving large quantities of bulk goods from mining areas to special export terminals. Significant advances have been made in all aspects of rail freight technology over the last few decades to make this possible, including the quality and reliability of the relevant private infrastructure. In a rapidly changing and highly competitive world, HH line owners and operators can maximize profitability in the upward phase, depending on commodity prices, markets and economic trends in both exporting and consuming countries. In addition, engineers are constantly forced to optimize train operations or reduce losses in the event of a recession. Railroad parameters such as the number of trains, axle load, and the number of freight cars increase (or decrease), and further simulations are usually performed to optimize the ratio of "railroad capacity to operating costs." However, this method generally does not explore the impact of longer/heavier train operations on the life of existing civil engineering structures servicing HH lines. Therefore, railway bridges and rail lines can deteriorate or be damaged under highly variable operating conditions.

A large percentage of HH tracks now consists of continuously welded rails (CWR), defined as rails that have been welded together into lengths exceeding 400 ft (121.92m) because it offers advantages such as reduced maintenance costs, fewer rail defects, and failures, reduced wear on vehicles, and lower energy costs for traction (Florida Department of Transportation, 2013). When the rail is constructed on a bridge, the behavior of the bridge leads to additional forces for CWR rails. Since both the track and the bridge may move, any force or displacement applied to one will cause forces to be applied to the other. In CWR, the rails are restrained; as a result, there is an internal build-up of stresses due to temperature change and traversing trains. If there is an increase in temperature, there is a build-up of compression stresses, and if there is a decrease in temperature, there is a build-up of tension forces because the rails are restrained from movement and thus cannot expand and contract, and therefore, resulting in a build-up of stresses along the horizontal direction. In addition, both the track and bridge are prone to longitudinal forces such as temperature-induced forces, traction and braking forces, and forces

induced by bridge movement (Sung et al., 2005). Direct bearing on the rail top from the wheel-tire or bearing laterally through the flange or longitudinal friction are used to impart forces to the rail structure (UIC, 2001). Track-Bridge Interaction (TBI) describes the interaction between the track and the bridge in terms of forces, forces in the rail and deck, and displacement of various bridge and track elements (UIC, 2001), and has been studied in most recent years by Mirković et al. (2018), Ramos et al., (2019), Mubarack & Upadhyay, (2021), and Kang et al., (2021), were they both analysed the management of stresses on railway bridges. Therefore, if the interactions are under control, the bridge will support the track without being subjected to anomalies.

Within this context, the Olifants River Viaduct Bridge (ORVB) was used as a case study in this research. The bridge is a prestressed single box girder bridge of a total length of 1035 m and is made up of 23 spans of 45 m each. The line on the bridge is an 861 km long single-track line connecting the mining areas in Sishen, Northern Cape Province, to the Saldanha Bay Commercial Harbour and has been operating since 1976 through the Iron Ore Export Line. Like any other continuously welded rail line, the ORV's track and supporting infrastructure (bridge) is subjected to longitudinal forces on the continuously welded rails and longitudinal forces on the bridge. The longitudinal forces on the rails and the bridge are induced by temperature changes, traction, braking, and forces caused by the bridge movement. Thus, the ORV must be managed, and forces kept within given limits to avoid rail failure due to high compression and tensile forces. Therefore, this research aims at addressing the risk of rail failure by characterizing the TBI forces induced on the ORV during the passage of the train and the effect the crossing trains have on the rail forces and deck expansion.

1.2 Significance of the study

Given the importance of the railway line and the annual revenue it generates for South Africa, closure of the line that might result from rail failure is bound to be catastrophic for Transnet. Thus, understanding the variation of train loading will improve the understanding of the bridge-track interaction and hence the management of the bridge and track to minimize rail failure and bridge damage and optimize train operations.

1.3 Research aims and objectives

With increased rail traffic and increased capacity accumulated over the years, the loading of the Viaduct has therefore been of interest to TRF. Hence, the main aim of this research was to address the risk of rail failure by analysing the interaction forces and understanding how the rail line behaves during the passage of the train and the effect a crossing train has on the rail and the supporting structure by mainly focusing on the three objectives below:

1. Characterisation of the trains operating on the ORV
2. Investigate the variation of the train speed on the ORV
3. Investigate the effect a passing train has on:
    - Rail forces
    - Rail temperature
    - Ambient temperature
    - Deck deflection

1.4 Scope and Limitation of the study

The research was limited to the data obtained from the ORV monitoring systems as it only aimed at understanding the trains operating on the ORV. Therefore, the analysis was done on data collected from the Weigh-in-Motion system, and the UPM600 Saldanha system for the year 2016.

1.5 Outline of the dissertation

The dissertation is presented in five chapters which outline different aspects of the dissertation.

Chapter 1: Provided an introduction to the dissertation. The background, research aims, and objectives were discussed in this chapter, as well as the scope and limitations of the dissertation.

Chapter 2: Critical review of the literature were discussed in this chapter to provide technical background required to undertake the study. The track-bridge interaction phenomena, factors affecting the bridge-track interaction, the potential failure modes, and the management of the rail forces in continuously welded rails were covered in this chapter.

Chapter 3: Provides the methods used to carry out the research. The monitoring systems and the sensor layouts were discussed in this chapter, as well as the train configuration basis, speed extractions and the speed profile presentations. The rail force calculations as well as any other assumptions taken were also discussed in this chapter.

Chapter 4: Analyses of the findings were discussed in this chapter. The train configuration, variation of the speeds and the speed profiles results are presented in this chapter. The bridge response to the imposed rail forces due to temperature, acceleration and deceleration was also presented in this chapter.

Chapter 5: The closing remarks of the study and recommendations for future research were presented in this chapter.

2. LITERATURE REVIEW

2.1 Introduction

The literature review firstly covers the aspect of track-bridge interaction and the problems accompanied by it. Secondly, the tracks lateral stability and the rail's potential to failure was looked at and the inherent factors affecting it. This revealed that CWR has inbuild issues, which should be taken into account while designing and operating railway bridges. Finally, previous studies carried out on the ORV was discussed to provide a theoretical background in the current research on the effect of vehicle speeds crossing the ORV in the past. The detailed background of the Viaduct is explained in-depth in Busatta & Moyo, (2015).

2.2 Track-bridge interaction

The trains run on the rails, which are laid on the bridge deck. As a result, the train, track, and bridge function as a single dynamic system, with the train and track connected by the wheel-rail interactive relationship and the track and bridge connected by the track-bridge interaction (Zhai et al., 2019b). The track therefore connects the train and the bridge together. Thus, track-bridge interaction is due to the two subsystems connected by wheel-rail contact, and relative vertical movement between the two is not allowed. As a result, the use of expandable decks that can be moved relative to the CWR track creates discontinuities in the bed's characteristics. This discontinuity is responsible for the relative movement between the roadbed and the track as the roadway expands and contracts, resulting in additional stress due to the forces exerted on the rails and structures and by the traffic load. The CWR on the bridge includes the transfer of forces due to the thermal expansion of the rail and the displacement of the bridge deck, plus the vertical traction and braking forces from the train and locomotive from the rail to the bridge deck and part of the rail itself (UIC, 2009b). As a result, any forces or displacement acting on either the bridge or the track will induce forces in the other. As a result, the track and the bridge interact as follows:

1. The force applied to the CWR rail causes additional force on the deck and the rails and bearings that support the movement of the rail and deck.
2. As the deck moves, the rails move, indirectly creating additional force on the rails and bridge bearings.

Therefore, traction, braking and thermal forces will increase horizontal forces on the track and bridge, affecting the bearing design and substructure. Figure 2.1 show the major components of the train-track-bridge dynamic interaction, as well as their relationships.

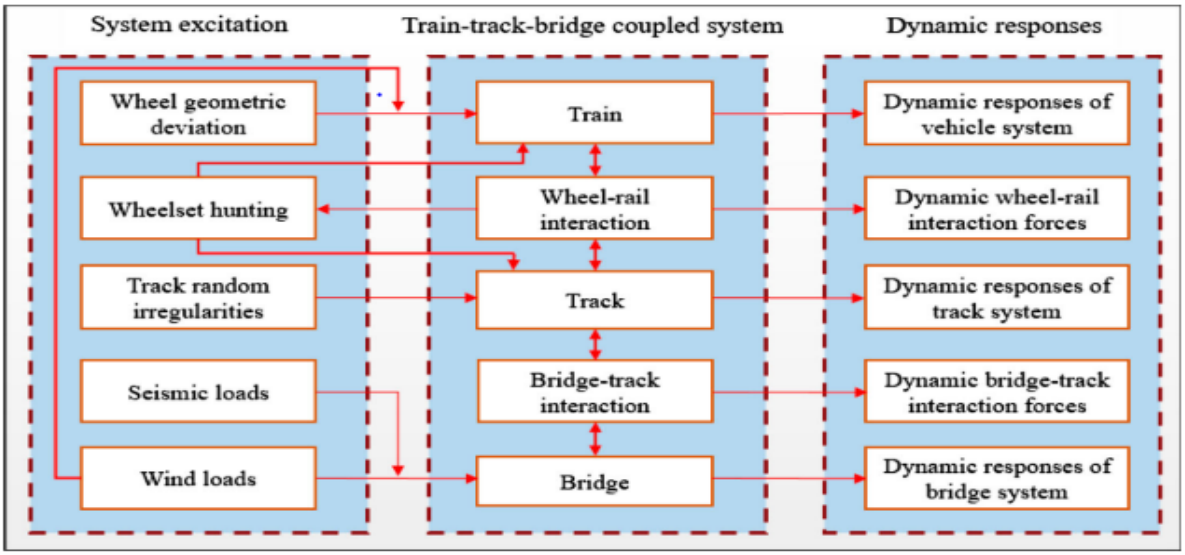

Figure 2.1: Train-tack-bridge dynamic interaction elements (Zhai et al., 2013)

As early as 1849, when Stokes analysed the vibration of a railway bridge in England in 1947, researchers have studied and attempted to lessen the effect of train-bridge interaction. Many track-bridge dynamic interaction (TBDI) models have been developed since then, and they can be classified into the following categories, as shown in Figure 2.2, which illustrates the evolution of the train-bridge interaction model: P denotes the moving load, M and m represent sprung and unsprung mass, M1 and M2 indicate the mass of the bogie and the car body.

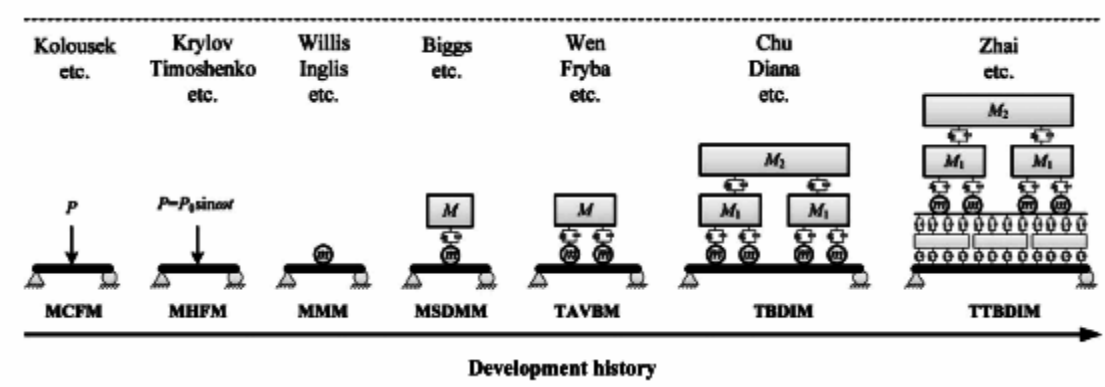

Figure 2.2: Train-bridge interaction model evolution (Zhai et al., 2019a)

2.2.1 Bridge behaviour

According to UIC, 2001, the behaviour of the bridge depends on certain aspects such as static arrangement of the bridge, bearing behaviour, supports behaviour, total stiffness, and the bending behaviour of the deck. The behaviour of the deck also depends on the following components:

1. Expansion length
2. Span length
3. Support stiffness of the deck
4. Deck's height

2.2.1.1 Static arrangement

The number of decks and the number of supports per deck define the static configuration of the bridge. The position of the permanent and moveable supports, the span length, the length of the expansion lengths, and the position of any rail expansion all contribute to its definition. The most frequent arrangements are outlined in (UIC, 2001).

2.2.1.2 Support behaviours

The bearing behaviour, support resistance to horizontal displacement, foundation stiffness, and total stiffness all play a role in the behaviour of the supports. The type of bearing and characteristic employed has a significant impact on the deck's displacement resistance. As a result, the bearing stiffness must be considered.

2.2.1.3 Deck bending behaviour

The vertical traffic load on the bridge produces a significant track-bridge interaction force as a result of the curvature of the roadway causing a vertical displacement of the upper part of the roadway. The interaction effect is primarily determined by deck compliance and the position of its neutral axis but is also affected by the stiffness of the fixed elastic support and the height of the deck. Large forces are generated in the track and the supports as a result of the displacement caused by interaction between the deck and the track.

2.2.2 Track behaviour

The behaviour of the track depends on whether the track is ballasted or unballasted. It also depends on the frequency of the maintenance of the track, present track defects, the applied

vertical load on the rail and the frequency of that load. Hence, the behaviour of the track is governed by the following parameters:

1. Track resistance
2. Cross-sectional area of the rail

2.2.2.1 Ballasted track

According to the UIC, (2001b), the track's resistance to vertical displacement is determined as follows:

1. The rail's resistance to displacement relative to the sleeper. The rail fastening provides this resistance, and its amount is determined by the clamping action's efficiency.
2. The resistance to displacement of the rail assembly in relation to the deck. This resistance is caused by the ballast's proclivity to resist sleeper movement, as well as friction between the ballast and the deck.

2.2.2.1.1 General principle governing track behaviour

The resistance of the track to longitudinal displacements is determined by the displacement of the rail relative to its supporting structure. When the displacement is small, the resistance increases quickly, but once the displacement reaches a particular magnitude, it remains nearly constant. On a loaded track, longitudinal displacement resistance is greater than on an unloaded track. Figure 2.3 shows the longitudinal resistance of the track.

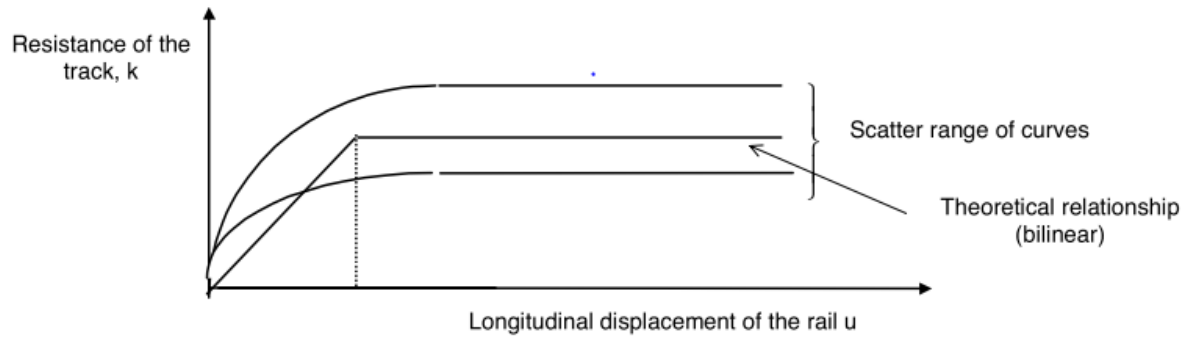

Figure 2.3: The track's longitudinal resistance as a function of longitudinal displacement (UIC, 2001)

2.2.3 Factors affecting track-bridge interaction

The interaction effects are caused by cases in which the track and the bridge move relative to one another. According to UIC, (2001b) code, the reasons for this force are as follows:

1. Temperature variation
    a. Compression and tension forces in the case of CWR.
    b. Deck and thermal rail expansion whenever an expansion joint is present.
2. Acceleration and horizontal braking forces.
3. Deck end rotation due to vertical loading
4. Supporting concrete structure deformation due to creep and shrinkage.

2.2.3.1 Effects due to temperature variation

The aspect of temperature change depends on the following:

1. In a free-moving structure, a change in the uniform component of the temperature generates a change in length.
2. In the case of a track with an expansion joint, the temperature difference between the deck and the rails.

The temperature of the deck when the rail is fixed is used as a reference for a bridge. The bridge temperature does not deviate from the reference temperature by more than 35 °C, and the rail temperature does not deviate by more than 50 °C. The temperature difference between the deck and the track should be less than 20 °C.

2.2.3.2 Braking and acceleration effects

The forces exerted at the rail top due to acceleration and braking are assumed to be uniformly distributed across the rail length. The vertical traffic loads force the deck to bend, causing the end portion to rotate and the upper edge of the deck end to shift.

2.2.3.2.1 Traction forces

The velocity of the locomotives depends on the traction effort of the locomotive and the motion resistance force. The locomotive traction motors produce the traction force, and the resistance force is the sum of all the forces influencing the train while it is moving (Rassõlkin & Hõimoja, 2012). Thus, the train accelerates if the traction effort is greater than the resistance force,

inducing a force on the rails as the train accelerates. Figure 2.4 shows the traction force. The force is in the same direction as the accelerations. The induced force is indirectly proportional to the speed of the train. Trains traveling at a low speed tend to exhibit a higher traction force compared to trains traveling at high speeds (Han, 2017).

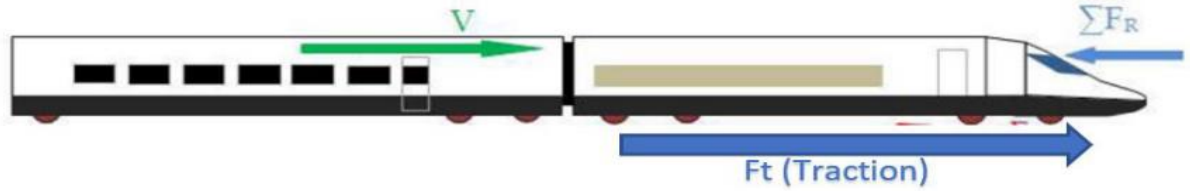

Figure 2.4: Traction (Han, 2017)

2.2.3.2.2 Braking forces

According to Ahmad et al., (2013), railway braking is a critical subject contributing to human safety and cost-effectiveness. In terms of continuously welded rails, the braking force of the train induces additional forces in the rails. The induced force depends on the acceleration of the train and the installed braking system of the train. There are, therefore, numerous research projects focused on the mitigation of additional rail/bridge forces due to train braking. Figure 2.5 illustrates the braking phenomena of the train.

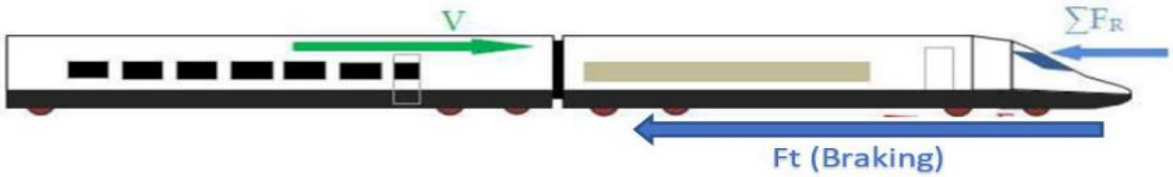

Figure 2.5: Braking (Han, 2017)

2.2.4 Thermal stresses

Fastenings are typically used to secure the rails to the sleepers as they impart a predefined clamping force. This clamping force is usually large enough to convey all of the rail's longitudinal movement to the sleepers, with the resistance to rail/sleeper sliding being greater than the ballast's longitudinal movement resistance. However, because the ballast hinders the free movement of the track under the influence of heat and traffic forces, the track is subject to longitudinal forces (Kumar & Upadhyay, 2012).

A central area that completely prevents expansion and contraction is covered by the continuous weld track, with two "breathing" areas at each end, about 150 m long. The expansion device at the end of the CWR has a 50mm aperture change and allows the end of the CWR to move freely. Therefore, significant longitudinal thermal stresses occur in the fixed middle zone of CWR. Figure 2.6 shows the thermal effect on CWR.

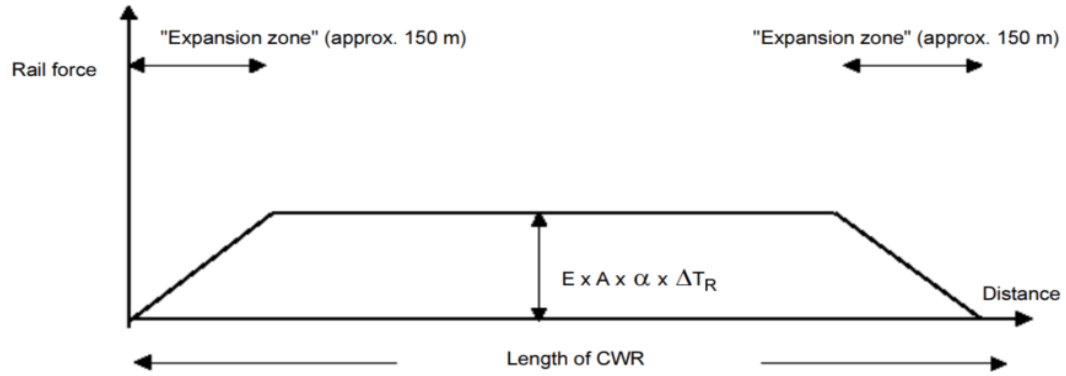

Figure 2.6: Force diagram for CWR under temperature variation (UIC, 2001)

In CWR, thermal stresses are caused by temperature changes relative to the rail neutral temperature (RNT) (Mirković et al., 2021). The temperature at which the tensions in the rail are equal to zero is known as the rail neutral temperature (RNT). A compressive force is generated when the rail temperature exceeds the RNT, and a tensile force is generated when the rail temperature falls below the RNT. The generated longitudinal normal force of the rail caused by the temperature change is calculated as follows (UIC, 2001):

$$F = EA\alpha\Delta T \qquad \textit{Equation 2.1}$$

Where;

F - longitudinal force in the rail

A - rail cross-sectional area

α - thermal expansion coefficient

ΔT - change in temperature

Figure 2.7: Depicts the longitudinal stress distribution of a long-welded rail directly fastened on a simply supported steel bridge.

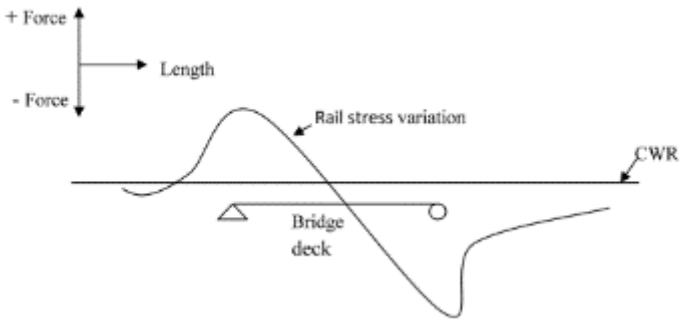

Figure 2.7: Rail stresses due to temperature variation in the bridge deck ***(Kumar & Upadhyay, 2012)***

2.3 Lateral track stability

The ability of ballast, sleepers, and fasteners to provide lateral and vertical strength to maintain track stability is known as track resistance. The lateral resistance of the track is an important factor in determining the failure resistance of the track's structure. The track passive structure holding force is proportional to the lateral deviation of the track; that is, as the lateral deviation of the track grows, so does the shear strength between the sleeper and the ballast (Esveld, 2001).

2.3.1 Rails

Resistance to lateral failure is provided by the strength of the steel and the vertical axis stiffness. As a result, larger rails will be more resistant to failure. However, given the same temperature rise, a larger track will effectively create a greater failure force than a smaller track since the stresses in both are the same, and the difference is due to the area of the cross-section of the track (Esveld, 2001).

2.3.2 Rail-to-Sleeper connection

Kink resistance and some lateral support are provided by rail fasteners. Elastic fasteners effectively prevent track slippage while also providing stronger connections and more stiffness. The elastic fasteners give greater stiffness, resulting in a stepped structure with equally distributed moment resistance and lateral restraints. This results in a changed effective buckling length and "end" conditions of the track, making the track construction more resistant to failure.

It is also necessary to have a good connection between the track and the sleepers in order to generate longitudinal ballast that will resist creep under traffic.

2.3.3 Sleeper to Ballast Interactions

The sleeper and ballast interaction provides most of the passive restriction in the longitudinal direction, provides creep resistance, thus inhibiting the change of RNT and DNT, and prevents rail failure in the transverse direction. Sleepers are essential to resist rail failure because they provide the connection between the track and the ballast. Thus, the longitudinal force generated on the track and the lateral force exerted by the track are transmitted to the ballast and the ground. As reported by the Railway Administration of Australia, the efficiency of these forces depends on these factors:

1. Type, size, shape, weight, and spacing of the sleeper.
2. The area of contact with ballast to generate friction.
3. Type of ballast and compaction.
4. Profile ballast-cradle ballast and shoulder ballast.

2.4 Potential failure modes

2.4.1 Rail buckling

The formation of large misalignments in continuously welded rail (CWR) is known as rail buckling and often results in catastrophic derailments. The major factors causing buckling are high compressive forces, weakened track conditions, and vehicle loads. These factors are directly affected by the parameters below and which in turn influence track buckling (Florida Department of Transportation, 2013):

1. Curvature of the track
2. Alignment
3. Rail Neutral Temperature
4. Track Lateral Resistance
5. Track Longitudinal Resistance
6. Dynamic Train Loading

The above parameters must be controlled and maintained to minimize the presence of buckling failure in railroads. Figure 2.8 shows an example of buckled tracks.

Figure 2.8:Rail buckling illustration (Kish & Mui, 2003)

Hagaman, (1991) defined buckling as the sudden track misalignment caused by temperature and creep induced stress. Buckling mainly occurs in the lateral direction but may also take place in the vertical direction. Track buckling occurs when the lateral buckling load is generated by the compressive force caused by thermal expansion, creep, and dynamic vehicle loading exceeding the passive restraining force of the track's structure (Hagaman, 1991).

According to Kumar, (2006), buckling is mainly caused by high compression forces in rails, weakened track conditions, and vehicle loading. As a result, the railway force must maintain stability and balance between the active buckling force, incidental lateral load, and passive restraint force generated by the structure. Hence, it is critical to address the factors that cause buckling as well as the passive resistance of the structure. Figure 2.9 shows a logical separation of the factors to consider while regulating track stability and buckling. The goal of this study was to analyse the right-hand branch in Figure 2.9 for characteristics that promote buckling.

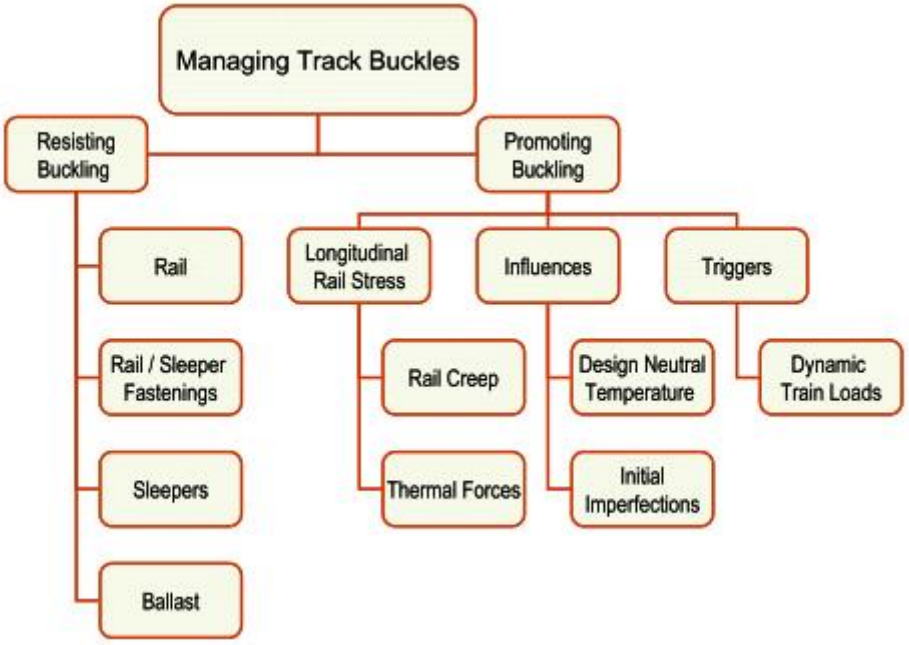

Figure 2.9: Managing track buckles components (Ole, 2008)

2.4.1.2 Conditions Conducive to Buckling

Buckling is promoted by many factors, either by the generation of compression forces in the rail or by triggering. For this research, only longitudinal and trigger factors will be discussed in detail.

2.4.1.2.1 Longitudinal Rail Stress

2.4.1.2.1.1 Thermal Forces

The main contributing factor in the occurrence of track buckling is longitudinal forces in the rail caused by temperature (Australian Transport Safety Bureau, 2005). The expansion and contraction experienced by the rails due to temperature change causes a variation in the longitudinal stresses of the rails that are restrained in the longitudinal direction or bound at the ends, and thus, causing either compression or tension forces to be generated in the rail (Marks, 2001). The buckling potential of the track is directly proportional to the temperature of the rail being raised above the neutral temperature of the rail.

A study on track buckling detection and rail stress management was carried out by Kish & Harrison, (2011). The authors found that during high temperatures, when the temperature of the rail is higher than rail neutral temperature (RNT), the rail can buckle due to high compressive forces, and during low temperatures, when the rail temperatures are below RNT,

the rail can break due to high tensile forces. Thus, it was concluded that the track buckling hazard detection and rail stress management predominantly depend on the rail neutral temperature (RNT) of the track condition. In a derailment incident report by the Australian Transport Safety Bureau, (2005), the derailment of the Koolyanobbing and Booraan lines was due to high compressive longitudinal forces and longitudinal rail movement. In another paper Kish & Samavedam, (1991) on dynamic buckling of continuous welded rail. The paper investigated CWR track buckling under thermally induced forces and vehicle loads. The buckling response is expressed in a relationship between the maximum lateral track displacement and the temperature increase above the neutral temperature, as shown in Figure 2.10. The structure becomes unstable at point B. The upper buckling temperature is denoted by TB,max, the maximum temperature limit before the track buckles. Still, the track could also buckle at TB,min from its stable equilibrium position A and S.

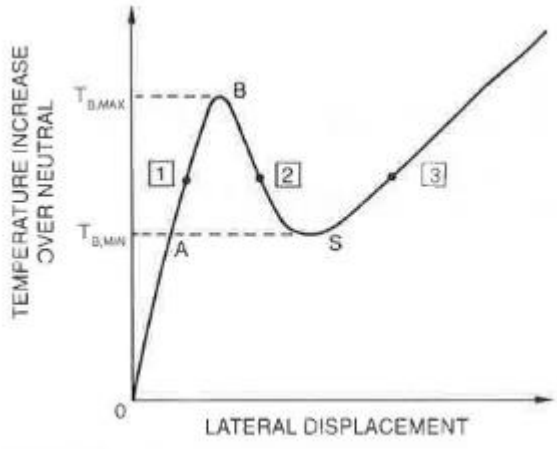

Figure 2.10: Typical buckling response (Kish & Samavedam, 1991)

2.4.2 Rail break

Considering rail breaks are the leading cause of train derailments, they have become a major source of concern for railroads due to their financial and safety implications. Rail breakdowns can occur as a result of the growth of an undetected defect or a fault developed after an inspection, as well as extremely low temperatures and dynamic stress, due to the limits of existing detection systems in evaluating rail flaws. This research focused on rail breaks due to dynamic loading and low temperatures. Figure 2.11 shows a typically broken rail due to high tensile forces.

Figure 2.11: Broken rail (Network Rail, 2021)

2.4.2.1 Dynamic Vehicle Loads

Kish et al., (1993), reviewed the parametric studies of continuously welded rail. Kish et al., (1993), found that the dynamic load of the train is the cause of rail breakage and thus concluded that vehicle loads significantly affect the rail temperature, which decreases with increasing axle loads, thus, causing tension forces in the horizontal direction. The authors also found that the wheels of a fast-moving heavy train tend to generate dynamic bulging waves on the track shown in Figure 2.12, which generally trigger the buckling process. Thus, like emergency braking, strong dynamic braking is a vehicle load that can activate rail buckling.

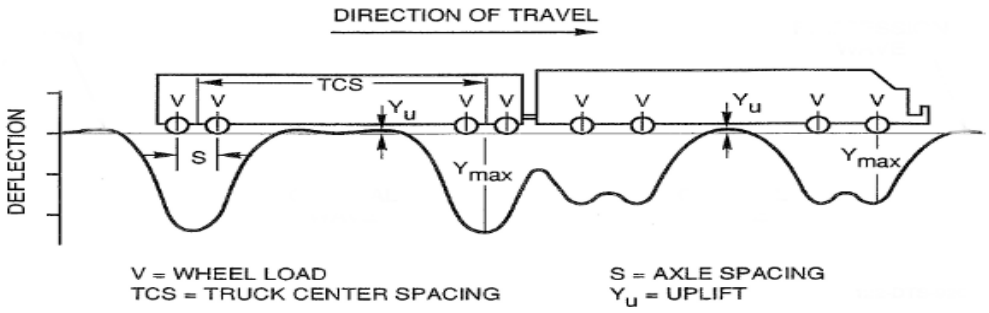

Figure 2.12: Rail under vehicle loading (Kish et al., 1993)

According to an incident report by the Australian Transport Safety Bureau, (2005), a derailment occurred on the rails of Koolyanobbing and Booraan in 2005. In addition to rail-induced temperature forces, the derailment was due to the high tensile forces of the freight train exerted on the rails.

2.5 Management of rail forces in CWR

The maintenance of CWR affects the accumulated rail stresses, the track stiffness, creep resistance, lateral resistance, and the stability of the track. Consequently, operations of this type must only be undertaken within a limited range of rail temperatures. Thus, in order to properly manage the rail forces on the track, the following parameters should be understood as they directly affect the resistance of the rail to failure.

1. Materials
2. Rail temperature
    a. Stress free temperature
    b. Change in rail temperature

2.5.1 Materials

2.5.1.1 Rails

All flat-bottom rail profiles are suitable for CWR track. It is recommended that intermediate section rails are introduced where it is required to join rails having cross-sectional areas which differ by more than 22%. New rails should not be drilled. It is recommended that serviceable rails undergo ultrasonic examination prior to CWR conversion. Existing fish bolt holes should preferably be removed prior to CWR conversion, but this is not essential, particularly in lower-speed and lower-tonnage track categories.

2.5.1.2 Fastenings

Only fastening systems that provide sufficient guaranteed longitudinal and torsional resistance to rail movement relative to the sleepers shall be used in CWR. The end of a CWR section of track over which rail movement can occur is called "the breathing length". Expansion switches can be fitted at the end of a section of CWR track where it abuts an adjoining section of jointed track or at a specific location such as a bridge.

2.5.1.3 Type and spacing of sleepers

Concrete, wooden, or steel sleepers are suitable for use in CWR. However, the type and shape of the lateral resistance is heavily influenced by the mass of the sleeper, the surface area of the sleeper end, and the sleeper spacing. Sleeper can significantly affect the lateral resistance and stability of the track. The mass of the sleeper, the surface area of the sleeper end, and the sleeper

spacing have a major effect on the lateral resistance. In addition, steel sleepers require a particular tamping technique to ensure that the ballast penetrates the hollow underside of the sleeper completely.

2.5.1.4 Ballast-bed dimensions

The mass, particle size, shape, cleanliness, and compaction of the ballast determines the longitudinal and lateral track's resistance. The particle size must be between 22,4 and 63 mm, and the individual particles must be sharp-edged and uniformly distributed. The recommended minimum depth of ballast below the sleeper soffit is 300 mm, and not less than 200 mm. The horizontal distance between the end of the sleeper and the ballast slope is 400 mm for speeds up to 160 km/h and 500 mm for higher speeds. The top of the ballast shoulder must be level with the top of the sleeper.

The width of the ballast shoulder may, with advantage, also be increased to the higher value in sharp radius curves or where tilting trains operate. The lateral resistance of the track can be increased to a limited extent by widening and raising the level of the ballast at the sleeper ends. The lateral and longitudinal resistance of the track depends largely on the degree of compaction of the ballast, being greatest when the ballast is fully compacted and least when the ballast is freshly tamped. The depth of the ballast and the width of the ballast shoulder may, during installation, fall below the above recommendations temporarily, provided high ambient temperatures can be guaranteed not to occur, or a temporary speed restriction is imposed. However, the full ballast dimensions should be obtained prior to commencement of operating at line speed.

2.5.1.5 Alignment

The quality of the alignment has a significant effect on the lateral resistance of CWR track. A greater degree of misalignment is usually found in curves compared with a straight track. The minimum curve radius in which CWR track may be safely installed depends on the rail section, the fastenings, the type of sleeper, the ballast profile, and the anticipated longitudinal thermal stresses. CWR may be installed on curves sharper than 300 m radius provided special measures, such as fitting anchoring devices to the sleepers, are taken.

2.5.1.6 Track geometry

At high rail temperatures, major alignment errors can cause track buckling. Therefore, that alignment errors should be minimized by proper maintenance practices. The following factors determine the maximum allowable error in any segment of CWR track:

1. section of the rail,
2. type of sleeper,
3. type of fastening,
4. condition of the ballast,
5. ballast bed stability
6. current temperature.

2.5.2 Rail Temperature

In order to properly manage the track, the following temperatures should be understood.

2.5.2.1 Stress-free temperature

Tn is the temperature at which there are no thermal stresses in the rails.

2.5.2.2 Change in temperature

Increment is an incremental margin from the allowable temperature, either up or down, which ΔT provides either a lesser or greater margin of safety against buckling.

In extreme situations, prior to undertaking work that may affect the stresses in the rail or reduce the lateral resistance of the track, ballast cleaning, sleeper replacement, or significant changes to track geometry, a decision must be taken whether or not temporarily to convert the track back to jointed track. The rail temperature shall be monitored and recorded during such maintenance operations, and the work must cease, and all ballasting and tightening of fastenings must be completed before the limiting temperatures are reached.

2.5.3 CWR Inspection

According to UIC, (2001a), tracks on the CWR can be inspected in a number of ways, including foot patrols, driving cabs, track inspection coaches, and local measurement. The frequency of the inspection is determined by line speed, traffic volume, and the condition of the track. When evaluating CWR track, special attention should be given to the parameters below:

1. the completeness of the ballast,
2. the vertical and lateral alignment,
3. the completeness of any anti-creep devices or other anchorages,
4. the suitable operating speed.

Depending on the type of inspection, the inspection should be performed at different levels of detail and at different frequencies, taking into account the nature of the structure and the preliminary conditions. According to UIC, (2009a), apart from normal monitoring, train and track personnel are always monitored as they cross the bridge. Three levels of control are distinguished:

2.5.3.1 Routine inspection

Annual inspection from the ground by trained inspectors. Inspectors must be trained and understand the basics of the bridge. Standard equipment includes basic tools such as hammers, cameras and luminaires. When the water is low, the foundation should be inspected.

2.5.3.2 Principal inspection

Sophisticated visual inspection with an emphasis on safety every 3 years (or 2nd year). These checks do not cover the entire structure, but they also provide the ability to simultaneously perform special detailed tests that can address specific components or problem areas.

2.5.3.3 General inspection

A very accurate inspection that tests every part of the bridge near the contact every 4-6 years (by hammering on the concrete surface). However, the frequency of inspections should reflect the type of bridge and the defects found. In practice, this means that the frequency of inspections depends on the type and condition of the bridge. General inspection results in a complete and detailed report on the condition of the structure.

2.5.4 Rail temperature monitoring

Rail stress management remains a concern and is a rapidly developing area for all rail companies worldwide. Rail tension is difficult to quantify and is a serious structural issue. This is due to the fact that high tensile forces can cause rail breakage, while high compressive forces can cause track buckling and, in the worst-case scenario, derailment. As a result, all causes that

could create longitudinal forces or displacements in the track or structure must be taken into account. Creep and shrinkage, temperature fluctuations, vertical load, tensile and braking forces are all examples of these effects. Any of these actions has the potential to transfer power from the rail to the deck via the rail fasteners and ballast (European Committee for Standardization, 2003).

2.5.4.1 Stress free temperature

Continuously welded rails (CWR) are mainly affected by rail stress and the lateral resistance of the track. Thus, effective rail stress management is a facet of railway engineering. Therefore, railway companies manage their tracks better by rail restressing, which contributes to ensuring the safe and efficient passage of rail traffic within the network.

Mitchell & Mandal, (2012), investigated the monitoring of rail stresses in continuously welded rails through stress-free temperatures SFTs as it is crucial in understanding rail load monitoring and management. Mitchell & Mandal, (2012) found that when exposed to rail traffic, the actual stress-free temperature (SFT) deviates from design neutral temperature (DNT), which is a temperature that is designed to keep the track from becoming stressed. However, many SFT measurement techniques have proven to be difficult to use in their specific applications. Thus, SFT tend to be measured only in the problem domain of interest because of the cost and revenue lines associated with the measurement process (Shah S et al., 2011). That is, railroads generally rely on precautions to control the risk of buckling. According to Salient Systems Inc, (2009), a global leader in real-time fault detection in the rail industry, the only way to ensure safe track conditions is to constantly monitor the system, and in order to be truly effective, the SFT measurement technology must do the following:

1. Reliable and accurate decisions of current SFTs with minimal truck occupancy and effort.
2. Provides a means of continuous monitoring so that window time is not missed if the SFT may swing out of safety.

2.5.4.2 Rail Creep Monitoring

The vertical movement of rails caused by the dynamic effects of rail traffic is referred to as rail creep. This occurs when the thermal and tensile forces exceed the vertical resistance of the truck (Mandal & Lees, 2019). Traditional rail creep monitoring is regarded as one of the most effective methods for understanding the rail stress of the truck behaviour at a specific point. This method is used all over the world to track changes in SFT.

The rails are installed at the desired stress-free rail temperature, also known as the initial stress-free rail section or design neutral temperature (DNT) (Ahmad et al., 2013). The rail expands or contracts as the rail temperature rises or falls from this first rail laying or DNT according to Equation 2.2.

$$\Delta L = L \propto (T_{NO} - T_N) \qquad \textit{Equation 2.2}$$

Where:

ΔL - expansion/contraction in rail (mm)

L - length of rail section (mm)

$\propto$ - coefficient of thermal expansion

T_{NO} - initial rail laying temperature (°C)

T_N - current stress-free temperature (°C)

Equation 2.2 is used to calculate the change in SFT caused by rail movement on a straight railway track (Shah et al., 2011).

2.5.4.3 Rail Stress Monitors

With Rail Stress Monitoring, a full bridge circuit's longitudinal and longitudinal strain gauges are configured to positively increase the bridge output voltage due to longitudinal and longitudinal expansion to compensate for temperature related bidirectional expansion. The resulting vertical extension from the bridge circuit results in vertical tension in the rail . RSM measures rail temperature using an in-built temperature sensor. SFT is calculated using Equations 2.3 and 2.4 based on longitudinal tension and rail temperature (Ahmad et al., 2013).

$$\varepsilon_3 = \frac{\sigma_3}{E} + \alpha(T_r - T_N) \qquad \textit{Equation 2.3}$$

$$T_{NO} + \frac{\varepsilon_3}{\alpha} = \frac{\sigma_3}{E\alpha} + T_r \qquad \text{Equation 2.4}$$

2.5.4.4 Longitudinal stress method

SFT can alter as a result of longitudinal and vertical rail movement, it is therefore critical to evaluate both longitudinal and vertical strain when determining SFT (Ahmad et al., 2013). The longitudinal stress factor takes both longitudinal and vertical strains into account. Equation 2.5 can be used to compute the longitudinal stress due to strains (Barry et al., 2009), while Equation 2.6, is merely a reorientation of the basic equation for thermal stress, and can then be used to calculate the SFT using the longitudinal stress using Equation 2.4.

$$\alpha_3 = \frac{E}{1 - v^2}(\varepsilon_3 + v\varepsilon_2) \qquad \text{Equation 2.6}$$

$$\sigma_3 = E\alpha(T_N - T_r) \qquad \text{Equation 2.5}$$

2.6 Management of CWR done on other bridges

2.6.1 Overview

Engineers are always trying to mitigate the damage induced by a structure during service life. According to Piazzaroli et al., (2019), Structural Health Monitoring reduces maintenance costs and ensures more comfort and safety to users by detecting damage at an early age; hence the overall objective of Structural Health Monitoring is to develop reliable techniques directed at diagnosing structural failures. In recent years, bridges have been fitted with a weigh-in-motion system to monitor and manage railway bridges. Therefore, this sub-chapter gives an overview of studies carried out worldwide on the management of continuously welded rail bridges fitted with weigh-in-motion systems to provide a standing ground for the current research.

2.6.2 Bridge management using SHM

James (2003), carried out an analysis on the effect of traffic loading on railway bridges. The research used data from a weigh-in-motion (WIM) system, which recorded data of the train speed, loads from each axle, and the axle spacings. The research considered only the single track to medium span bridges, and the load effects were analysed by two methods: the classical extreme value theory, where the family of distributions modelled the load. The second method

that adopted the peak over thresholds is the Generalised Pareto Distribution. The findings showed that for the studied causes, an increase in allowable axle load to 25 tonnes was accepted for bridges built to the standard of 1940 and designed to load model A of that standard.

Beskhyroun et al., (2011) and Žnidarič et al., (2016) developed a weigh-in-motion system based on piezoelectric for railway transport. The individual wheel axle loads, the weight of each rail car, the number of rail cars, total train weight, velocity, and direction of the crossing train were all estimated using the developed method. The weigh-in-motion is used to measure and manage railway parameters in real time. Both authors agreed that the development of railway WIM was a success because it demonstrated its clear potential for railway applications and management.

A bridge weigh-in-motion algorithm was created in another study by Silva & Karoumi, (2015) to track trains crossing a steel railway bridge. The WIM system estimates traffic loads, speeds, and axle spacings. The system saves useful information, such as peak and root mean square vertical bridge deck accelerations. The system employs two strain gauges from a previously deployed sensor network, which were established primarily to monitor the strains for fatigue development (Silva & Karoumi, 2015).

Karoumi et al., (2005), monitored traffic loads and dynamic effects of an instrumented railway bridge. The objective of this study was to gain a better understanding of actual traffic loads and how they affect railway bridges. The investigation detailed the instrumented integral-type railway bridge by researching actual railway traffic loads and their effect on the bridge, as well as the ongoing development and testing of the Bridge Weigh-in-Motion (B-WIM) system. The preliminary results demonstrated the high quality of the measured data as well as the significance of the B-WIM algorithm implemented. The results show that the developed algorithm can provide accurate WIM data such as static loads, axle distances, and speeds “design trains”.

2.6.3 Monitoring of railway stress

Different systems and models have been established over the years to monitor and manage stresses in continuously welded rails. Yan et al., (2015) examined the stresses in continuously

welded rails on bridges, as well as the aspect of rail steel fatigue. Yan et al., (2015) also looked into the possibility of avoiding rail expansion joints. The components of total stress in CWR, according to the authors, are greatly influenced by:

1. the railway line type
2. the bridge position on the railway route
3. climate zone

The Queensland Rail developed a technology to facilitate improvements in the management of continuously welded rail (QWR) track. This led to the introduction of new track maintenance methods to aid construction and maintenance teams to efficiently manage the tasks associated with controlling the longitudinal thermal forces in continuously welded rail. The implementation of this new technology has resulted in a decrease in the resources required to maintain the neutral temperature in continuously welded rail (CWR) track (Marks, 2001).

2.7 Management of the Olifants River Viaduct Railway Bridge

2.7.1 Overview

The Olifants River bridge is a 1035 m continuously welded rail situated on the Sishen-Saldanha line in the western province of South Africa. The line is dedicated on transporting iron ore from the mines in Sishen to the port in Saldanha. The thermal expansion of the deck and the rails interact and therefore impose additional forces on the rails. The bridge is equipped with two expansion joints and monitoring systems to measure track bridge interaction parameters. The complete overview of the ORV can be found in (Fulvio & Moyo, 2015) and Chapter 4 of this thesis.

2.7.2 Train configuration

Busatta & Moyo, (2019) researched the heavy haul train dominant frequencies to study the repetitive heavy axle moving loads imposed on the bridge by the crossing trains. The research considered the trains crossing the ORV from 1st of January 2017 to 28th February 2017. A total of 219 trains were recorded from the automated WIM-WIM system. Busatta & Moyo, (2019) established a system that categorized the trains into four categories (A-D) according to the

variability and commodities of the operated trains. Table 2.1 shows the established train categorization, which depends on the train length. Busatta & Moyo, (2019) further went on to conclude that most of the trains crossing the ORV were found to be in category D with 342 wagons and have a configuration of LC "A" +114W+LC "B" +114W+LC "C" +114W+LC "D" and four locomotive consists.

Table 2.1: Train configuration (Busatta & Moyo, 2019)

Category	No. of Locos [a]	No. of Wagons [a]	Type of Configuration [b, c]	%
A	1-2	12-59	LC"1" + *k* Ws	15
B	2-3	86-152	LC"1" + *l* Ws	1
C	2-4	184-232	LC"1"+ *m* Ws + LC"2" + *n* Ws + LC"3"	9
D	4-6	282-342	LC"1" + *r* Ws + LC"2" + *s* Ws + LC"3" + *t* Ws + LC"4"	75

2.7.3 Traffic loading and train speed

Busatta & Moyo, (2019) further investigated the Heavy Haul train speeds as it crosses the ORV and found that the heavy haul trains showed varying speeds while crossing the ORV. The longer the train, the larger the speed variation occurring when traversing the ORV. The varying speed was due to the train length and the environment where the line is situated. Non-uniform speed due to acceleration or deceleration introduces additional forces to the rail and thus influences the rail forces. These additional forces could increase the rail forces beyond the threshold that could lead to buckling or breaking of the rails, leading to derailment of the trains. Derailment of the train on the bridge could lead to the bridge's closure and thus economic consequences.

According to Busatta & Moyo, (2018), who assessed the performance of the ORV by monitoring traffic loading and dynamic effect using data from the WIM system from the 20th of March 2016 to April, 30th 2016, found that the most frequent train crossing the ORV has a configuration of LC "A" +114W+LC "B" +114W+LC "C" +114W+LC "D" with 4 Locomotive (LC) and 342 Wagons (W). Furthermore, the authors found that the train speed can be greater than 50 km/h on the ORV, and the maximum wagons axle load was often greater than 400 kN while the mean loading was found to be around 330-340 kN. Busatta & Moyo, (2018), therefore, concluded that traffic loading could be used to investigate the actual performance of the ORV under these repetitive loading.

A characterization of HH trains crossing the ORV was carried out by Kiiza, (2019). The research focused on speed behaviour and the influence of speed on rail forces. For this research, only the latter will be discussed. The author found that the 342-wagon train with 6 locomotives consist was the dominant train traversing the ORV. The short trains were found to cross the ORV at a constant speed with a constant speed profile and the long RDP train at non-uniform speed with a decelerating and accelerating speed profile.

2.7.4 Longitudinal forces

Maree, (2000) and Bester, (2015), investigated the derailment that occurred on the ORV on the 24th of September 1982 when the line was still carrying 26 tons per axle. The derailment occurred at the center of the bridge right before installing the measuring system, which was later put into service in October of the same year. The cause of the derailment was a kick out of the track due to excessive compressive forces in the rails. The compressive forces are due to the continuously welded rails of the ORV over a relatively long distance. Thermal forces were hindered in the longitudinal direction; the temperature thus induced tensile and compressive forces in the rails. The final contribution to the derailment was the bridge movement. It was approximated that the bridge was only 38% consolidated at the time of the derailment. Thus, contributing to the destabilization of the track by reducing the effect of shoulder and crib ballast and, in return, decreasing the lateral resistance of the track. The total force at the expansion joints was calculated as follow:

$$F_{tot} = F_i + 0.7F_{lt} + F_T \qquad \textit{Equation 2.7}$$

Where:

F_{tot} - total forces

F_i - interaction forces

F_{lt} - long term interaction forces

F_T - temperature forces

The interaction forces are due to bridge movement, traction, and braking forces, and the temperature forces are induced forces due to high or low temperatures. The temperature varied from 30°C to 58°C on the day of the derailment. Therefore, it imposed a temperature force of -1004 kN on the rails. When the compressive force in the rails is high enough, it can cause

lateral movement in the form of a double wave kick out of the rails (Maree, 2000). Thus, the critical compression force was calculated as follow:

$$F_{cr} = -2.95\left(\frac{EIq}{f}\right)^{0.5} \qquad \textit{Equation 2.8}$$

Where:

E - modulus of elasticity

I - moment of inertia

q - rail resistance to lateral buckling

f - alignment error

Thus, the authors found that the critical compression force due to a 12 mm alignment error was close enough to the derailment force. Concluded that the interaction forces for similar decks could be calculated with the knowledge of the daily fluctuation in temperature and bridge movements. They also recommend redistribution of forces prior to winter and summer seasons.

2.8 Chapter Summary

The track-bridge interaction phenomena was defined as the interaction of forces between the track and the bridge. As a result, any forces or displacement acting on either the bridge or the track will induce forces in the other. The major components of the track-bridge interaction were defined. The behaviour of the track depends on certain aspects such as static arrangement, bearing behaviour and support behaviour. While the track behaviour depends on whether the track is ballasted or unballasted and it also depends on the frequency of the maintenance of the track. Track resistance to longitudinal displacement is the general principle governing track behaviour. Temperature, acceleration, deceleration, and the deck end rotation due to vertical loading were found to be the factors affecting track-bridge interaction.

Potential failure modes of the rails due to this interaction were found to be mainly rail buckling due to high compressive forces and rail breaks due to high tensile forces. Rail buckling is the formation of large misalignment in continuously welded rails caused by temperature and creep

induced stress. While rail break is the sudden separation in the rails. The literature showed that these failure modes are predominantly governed by temperature.

Investigation on managing continuously welded rails were reviewed and structural health monitoring (SHM) is mostly used to manage the tracks. SHM is based on weigh-in-motion systems that are installed on the rails to monitor traffic loads, dynamic effects and rail stress. The review demonstrated high quality data and the significance of WIM systems, but there is a short fall of research on the specific contributions on induced rail forces in heavy haul rails.

Based on this further work based on track-bridge interaction of heavy haul rails carrying a long sequence of moving loads is needed. This dissertation will focus on, firstly, categorizing the trains crossing the Olifants River Viaduct. Secondly, analysing the speed variations and speed profiles of the trains crossing the ORV. Finally, determining the effect the crossing trains have on the rail forces, rail temperature, deck deflection, and the ambient temperature.

3. METHODOLOGY

3.1 Introduction

Over the years, the TBI has predominantly been analysed by implementing models that mimic the interaction forces. Therefore, this chapter will discuss the methodology that was adopted for this research. Overall, the study focused on categorizing the TBI forces induced on the Olifants River Viaduct Bridge by monitoring traffic loading and interaction forces during the passage of the trains.

3.2 Olifants River Viaduct

The ORV is an equally spaced 23 span bridge that was constructed in 1976 and consists of a single prestressed concrete girder that is 1035 m long and supported by 22 reinforced concrete piers that are 43 m apart with the tallest pier having a height of 50 m. The bridge is situated in the Western Cape province of South Africa and connects the mines in Sishen to the ports in Saldanha. In addition, the bridge has two expansion joints that are located at piers 11 to 12. Figure 3.1 below shows the ORV, and further description of the ORV can be found in (Busatta & Moyo, 2018). The bridge is owned and managed by Transnet SOC Ltd, and it operates the rail line through the operational division Transnet Freight Rail (TFR). The bridge contains continuously welded rails along it inter length of 861 km and the rail line traffic is mainly made up of iron ore freight trains.

Over the years, the demand for transported goods (iron ore and coal) increased gradually, which led to Transnet increasing the rolling stock to meet the demand for transported goods by changing from head-end power (HEP) to radio distributed power (RDP) technology. This technology allows locomotives to be placed at intermediate points within a train to reduce in-train forces. Subsequently, trains can be much longer than traditional head-end power trains. The conceptual design for the line to withstand the new capacity can be found in Kuys, (2000). As a result, the International Heavy Haul Association (IHHA) classified the rail line as a Heavy Haul railroad as it meets the heavy haul (HH) classification of supporting trains weighing 5000 metric tons and hauling revenue worth 20 million metric tons annually. Due to the increase in demand for transported goods, TFR operates the longest and largest RDP train globally, with 342 wagons and six locomotives. Research has been carried out on the ORV over the years in

an attempt to understand the effect of traffic loading and speed has on the bridge and the supporting infrastructure; Kuys, (2009) and in most recent years Busatta & Moyo, (2019) assessed the performance of the Viaduct The focus was given to monitoring traffic loads and dynamic effects. The ORV is equipped with a WIM-WIM system on span 21, Monitoring System on span 20, and a Saldanha UPM60 system along the expansion joints. The data obtained from these monitoring systems was used in this research.

Figure 3.1: Olifants River Viaduct (Busatta & Moyo, 2018)

3.2.1 Freight Network in South Africa

Heavy Haul trains have been in operation since the 1970s to export iron ore and coal in South Africa. Due to the increased demand for the transported commodities, two major export lines were built to connect the mining areas to their destinations. The export lines are the 861 km long Sishen-Saldanha Bay export line that exports iron ore and the 748 km long Black Hill-Richards Bay that exports coal (Busatta & Moyo, 2018). This research only focused on the Sishen-Saldanha Bay iron ore export line shown by the oval shape in Figure 3.2**.**

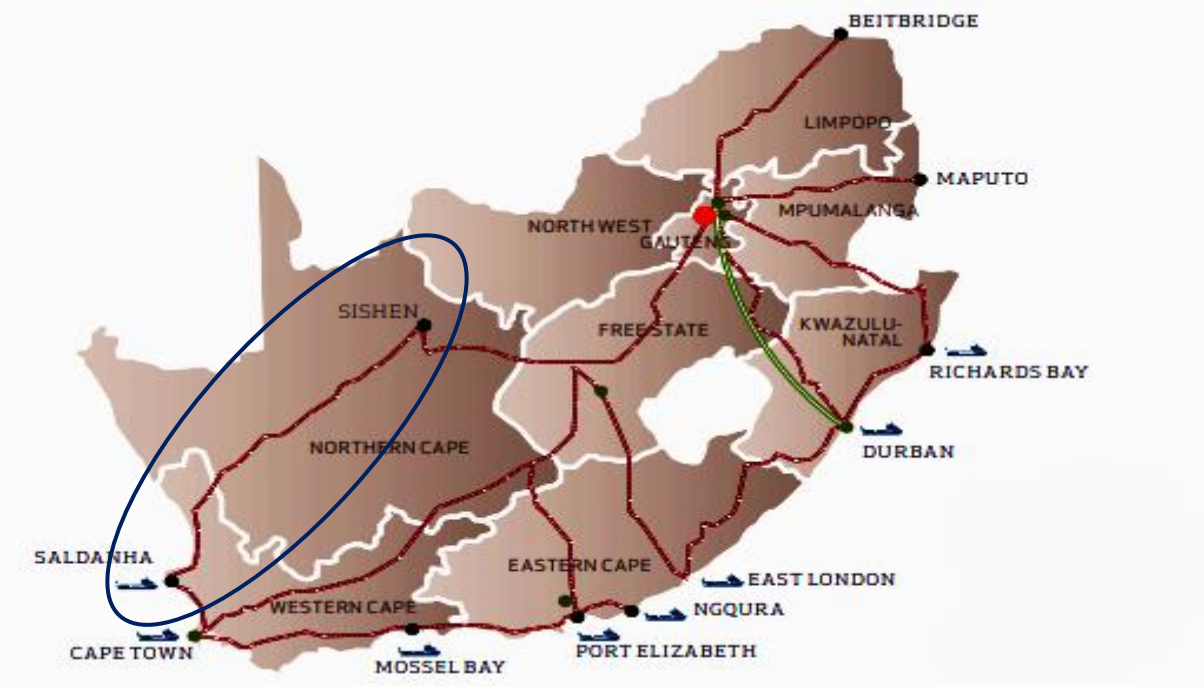

Figure 3.2: Freight Railway Network (Transnet Sustainability Report, 2014)

3.2.2 Heavy Haul Trains

According to Xia & Zhang, (2011), heavy haul trains are widely used to transport minerals in South Africa. They reduce scheduling and human activity because they are several kilometres long in design. In 2007, the ORV was crossed by a 216-wagon head-end train, but the head-end train could not withstand the increasing demand of commodities being transported. Thus a Radio Distributed Power (RDP) train was introduced (Bush, 2009). The RDP train allows locomotives to power the train from intermediate points and thus reducing the in-train forces and improving brake propagation (Ngwenyama et al., 2013). The RDP train is 4.1 km long, classified as the longest Heavy Haul train in the world. The train is composed of 3 rakes of 114 wagons and six locomotives. The 114 wagon rakes sum up to 342 wagons which are approximately 3.85 km long; the six locomotives make up the remainder of the distance and thus equating to 4.1 km.

3.2.3 Wagons

The mainline wagons working on the ORV have four axles. The most common wagon that operates on the ORV is the CR-13 wagon fitted with Scheffel self-steering bogey (Kuys, 2009).

The 4-axle wagon has a nominal axle load of 20 tonnes when empty, 120 tonnes when loaded, thus equating to 300 kN static load per axle and 50 kN when unloaded.

3.2.4 Locomotives

The mainline locomotives working on the ORV have six axles with engines that are either Head End Power (HED) or Radio Distributed Power (RDP), or both. There are 4 types of locomotives that operate on the ORV, mainly 43D (216kN/axle), 9E 280 (kN/axle), 15E (300kN/axle) (Hettasch, 2016). The 15E electric locomotive is the frequently used locomotive along the ORV line and is shown in figure 3.3.

Figure 3.3: 15E Locomotive

3.2.3 ORV Monitoring system

The ORV is equipped with two monitoring systems; Weigh-in-Motion (WIM) system, which TRF manages, and the Saldanha System to measure rail forces, deck deflection, and temperature. The WIM_WIM system identifies wheel irregularities with high dynamic forces into the track structure and weighs the trains to determine skewing bogies. This research used data from the WIM system to categorize the trains, and the Saldanha system was used to evaluate the TBI phenomena; thus, both systems are elaborated in detail below.

3.2.3.1 Wheel Impact Monitoring & Weigh-in-Motion (WIM-WIM) System

In February 1998, the first WIM-WIM system was installed on the Sishen-Saldanha Iron Export Line (Tomas, 2000). The WIM system comprises of strain gauges applied in situ to the rail, a signal conditioner to calibrate and condition the strain gauge channel, a high-speed

computer with data acquisition analysis, communication facilities, and lighting protection to minimize chances of lightning damage. The WIM-WIM system is located on the rail at span 21 and consists of 32 strain gauges welded on the rail containing 32 channels that are sampled at 2.5k Hz per channel and a computer-based data acquisition system inside the viaduct girder and can measure speeds up to 150 km/h, but the ORV has a speed limit of 50 km/h. Figure 3.4 and Figure 3.5 show the typical sensors and sensor arrangements of the WIM-WIM system.

Figure 3.4: Typical WIM-WIM sensors

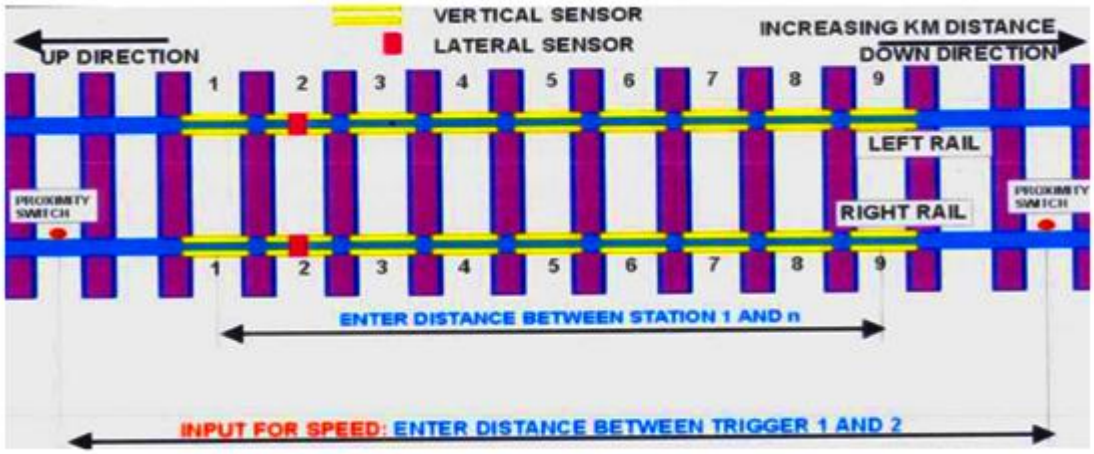

Figure 3.5: Typical WIM-WIM sensor arrangement (Matongo, 2018)

The main aim of the WIM system is to weigh the trains and detect excessive wheel irregularities and incorrectly loaded wagons. According to Hettasch (2016), the Olifants River Bridge WIM data is denoted by SLK.SLK.L04.WIM.01 and is managed by the freight rail operators Transnet. The system uses a trigger to detect a traversing train and determine the wagon and locomotive type, the speed of each locomotive and wagon, and the mass. In addition, the system uses the contact forces caused by the strain of the wheel in the rails. Figure 3.6 shows the general output layout of the system. Data from the WIM-WIM system was used to categorize the trains and determine the speed profiles of the trains.

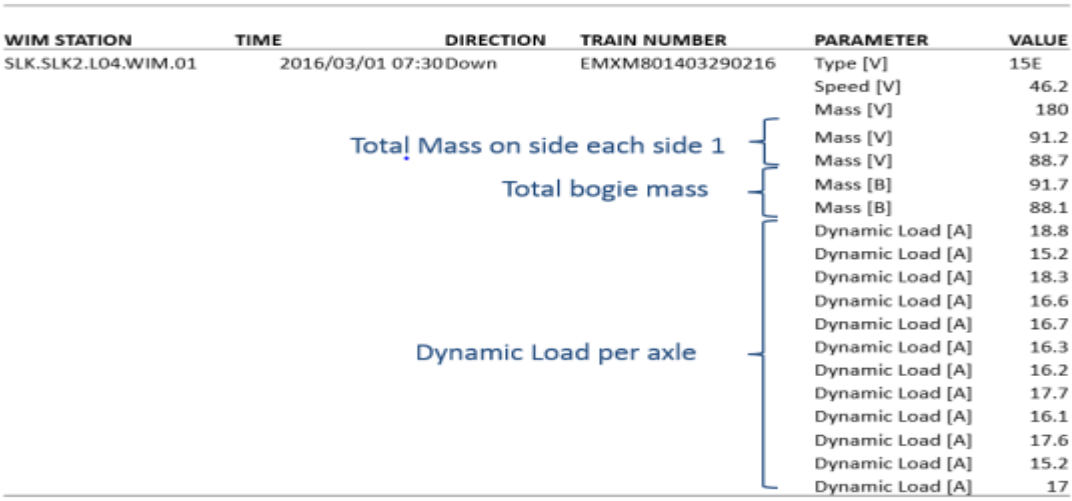

Figure 3.6: Typical screenshot of the WIM-WIM output (Matongo, 2018)

3.2.3.1.1 Train Categorization and Statistical summaries

A Python script was developed and used to group the trains in loaded and loaded trains by using the direction given on the WIM-WIM output file, which is either “UP” or “DOWN.” UP refers to trains traveling from the ports in Saldanha to the mines in Sishen, while DOWN refers to the trains traveling in the opposite direction. To determine whether the train is loaded or unloaded, an assumption was made that trains traveling from the mines will be loaded and the trains traveling from the ports will be unloaded. The assumption was verified by checking the total mass of the wagons in each direction which should be 200 kN (20 tons) when empty and 1200 kN (120 tons) when loaded. The data extraction script can be found in Appendix A.

Given that the ORV is a single track, no trains cross the railway simultaneously. The unique timestamp identified each train, and all vehicles with that same timestamp were grouped into an individual train. A Python script was used to group the trains with identical timestamp and the script is outlined in Appendix A. The trains were further categorized using the initial (A-D) categories established by Busatta & Moyo, (2019) in Table 3.1. The categorization uses the length of the trains and the commodity they carry. Finally, the maximum and the minimum train speed computation were developed and tabulated for the loaded and unloaded trains. This showed each category's minimum, maximum, and median speed values.

Table 3.1: Train Categorization (Busatta & Moyo, 2019)

Category	No. of Locos	No of Wagons	Type of Configuration
A	1-2	12-59	LC"1" + kWs
B	2-3	86-152	LC"1" + lWs
C	2-4	184-232	LC"1" + mWs + LC"2" + nWs + LC"3"
D	4-6	282-342	LC"1" + rWs + LC"2" + sWs + LC"3" + tWs + LC"4"

3.2.3.1.2 Speed profiles

The speeds of the train were extracted for both the loaded and unloaded trains from the WIM-WIM system and graphed to determine the speed profiles of the trains. This was established by developing a python script that graphed the loaded and unloaded speeds of the trains separately. The speed profile plotter script is outlined in Appendix A. Speed profiles present the variation of the vehicle's speed in a train. Thus, the effect on the loading spectra was observed by considering the speed of the train as it crossed the ORV for both the loaded and the unloaded trains.

3.2.3.2 Saldanha UPM60 Systems

There are currently two measurement systems installed on the ORV that measures the rail forces, namely the Saldanha System (SS) and the Track Testing Centre System (TTCS). Both systems employ UPM60 scanners to measure rail force, deck deflection, and temperatures. Measured parameters are transmitted to the bridge computer situated at the traffic control office in the Saldanha Bay by the Saldanha system. Should the Saldanha System fail or malfunction,

the TTC System acts as a backup system. Figure 3.7 shows the Track Testing System and the UPM60 systems.

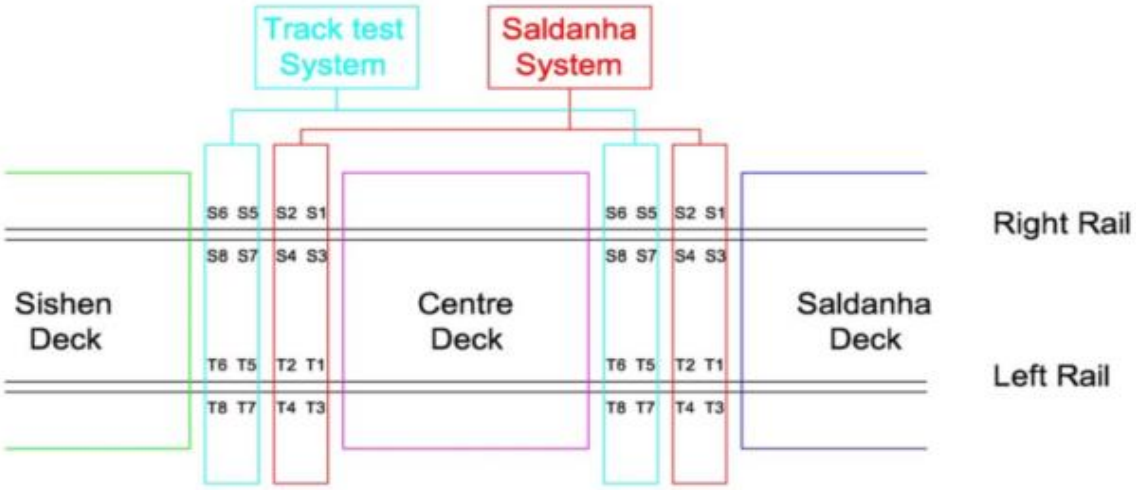

Figure 3.7: Screenshot of the Saldanha UPM60 System layout (Freyer RV, 2004)

3.2.3.2.1 Rail force

Strain gauges are mounted on the neutral axis of the rail directly above the expansion joint to measure the tensile and compressive forces generated on the rail. The rails must be released to compensate for the strain gauges. To destress, one need to cut the rails to keep the track stress-free. The output value of the amplifier can then be set to zero. The system consists of 16 channels that monitor rail forces, and all the 16 channels were analysed simultaneously using MS Excel data analysis tools. Warning and alarm levels are set by computer programs and are triggered as soon as the danger level is reached. Currently, the Olifants River bridge has the following alarm and warning levels:

Tension warning value: 1400 kN
Tension alarm value: 1500 kN
Compression warning value: -1100 kN
Compression alarm value 1: -1200 kN
Compression alarm value 2: -1400 kN

3.2.3.2.2 Deck Deflection

A W100 deflection gauge (± 100 mm LVDT) is mounted inside the concrete ceiling above the expansion joint. If the bridge is in the neutral position, the deflector will be fixed in the zero position. The W100 deflection meter has a measuring capability of 100 mm from zero in both negative and positive directions. The deflection consists of 4 channels, with two channels placed in the Saldanha direction and the other two placed in the Sishen direction. The data from the 4 channels was analysed using MS Excel data analysis tools.

3.2.3.2.1 Temperature

Different temperature sensors are used for the two systems. The Saldanha system uses PT100 thermal resistors for rail, ambient and concrete temperatures. Due to the bridge configuration, these devices require a separate switching unit for the UPM60 scanner. The TTC system uses strain gauge technology for all temperature measurements that require the same switching unit as the force and displacement transducers. Note that the two systems for temperature measurement are incompatible due to the different switching units.

For rail temperature measurements, the device is mounted on the right leg on either side of the rail flange of the rail and is measured in the left and right rail. Ambient temperature is measured using equipment mounted on a Stevenson screen mounted on the railing of the bridge measured from the North and South direction.

MS Excel data analysis tools for scientific analysis such as descriptive statistic, regression and sampling were used to analyse the temperatures. As per literature, the longitudinal forces of the rail due to temperature change was calculated using Equation 2.1 from the (UIC, 2001):

$$F = EA\alpha\Delta T$$

Where:

F - longitudinal force in the rail

A - rail cross-sectional area

α - thermal expansion coefficient

ΔT - change in temperature

The longitudinal force in the rails was obtained by multiplying the modulus of elasticity with the cross-sectional area of the rails, the thermal expansion coefficient, and the change in temperature. The change in temperature is the difference in rail temperature during the passage of the train. With the values of $E = 205 \times 10^3 N/mm^2$, $A = 7600\, mm^2$, and $\alpha = 11{,}5 \times 10^{-6}$ where based on information from (Maree, 2000) and the provided construction drawing of the ORV and not based on any material testing.

3.3 TBI forces

To prevent bridge failure due to excessive forces exerted on the track, the deformation of the rail during the passage of the train must be kept at a minimum. Thus, longitudinal forces due to temperature change, deck defection, braking, and traction were calculated and compared to the extracted rail forces. It is detrimental to ensure that the bridge's horizontal forces are kept within the established limits.

3.4 Summary of the research methodology

In summary, the study used data collected from the WIM_WIM system for stage 1, and Saldanha UPM60 System for stage 2. Stage 1 aimed at categorizing the trains and obtaining speed profiles. The stage is divided into four steps, primarily steps 1). the extraction and cleaning of data; 2). identifying loaded and unloaded trains; 3). Further categorizing the loaded and unloaded trains into categories using the categorization system established by Busatta and Moyo, (2015) and identifying the speed of the trains; 4). Producing the speed profiles. Stage 2 involves the extraction of the rail forces, rail temperature, and deck expansion from the Saldanha UPM60 System**.** Figure 3.8 below shows a summary of the methodology and its respective procedures.

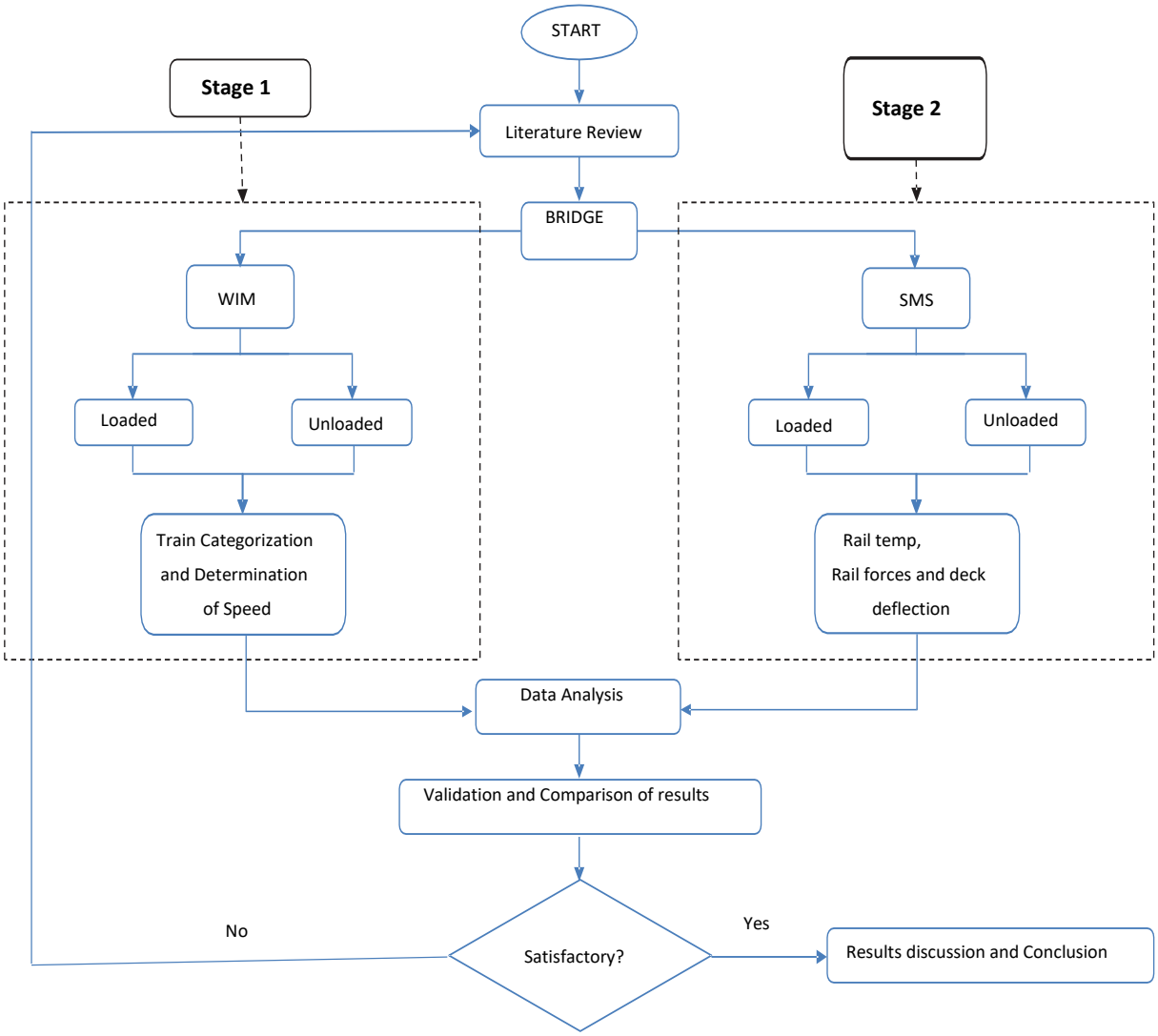

Figure 3.8: Methodology summary

4. RESULTS AND DISCUSSION

4.1 Introduction

The results were discussed in this chapter. Firstly, the observed trains with their categorization and train configuration were discussed. Secondly, the train speeds and speed profiles were discussed. Lastly, the effect a crossing train has on the bridge were discussed by looking more specifically at the rail forces, deck extension, and rail temperature.

This thesis aimed at understanding TBI forces present on the ORV and the behaviour of the bridge during the passage of a train by analyzing the most frequent train crossing the bridge, its configuration, and the speed at which it crosses the ORV, and the effect that train has on the interaction forces to deduce a conclusion based on the track-bridge interaction phenomena.

4.2 Train categorization and train configuration

Using the WIM data, a total of 4099 trains were recorded between January 2016 and December 2016, 2062 of them were found to be loaded trains, and 2037 were unloaded trains. With November and December having recorded the highest number of trains for the unloaded trains and November having recorded the highest number of loaded trains, while January recorded the lowest number of trains for both the loaded and the unloaded trains. For January, data was only available for 5 days, from the 27th to the 31st of January and thus explaining the low number of trains recorded for the month. Figure 4.1 shows the total number of trains observed for the year 2016.

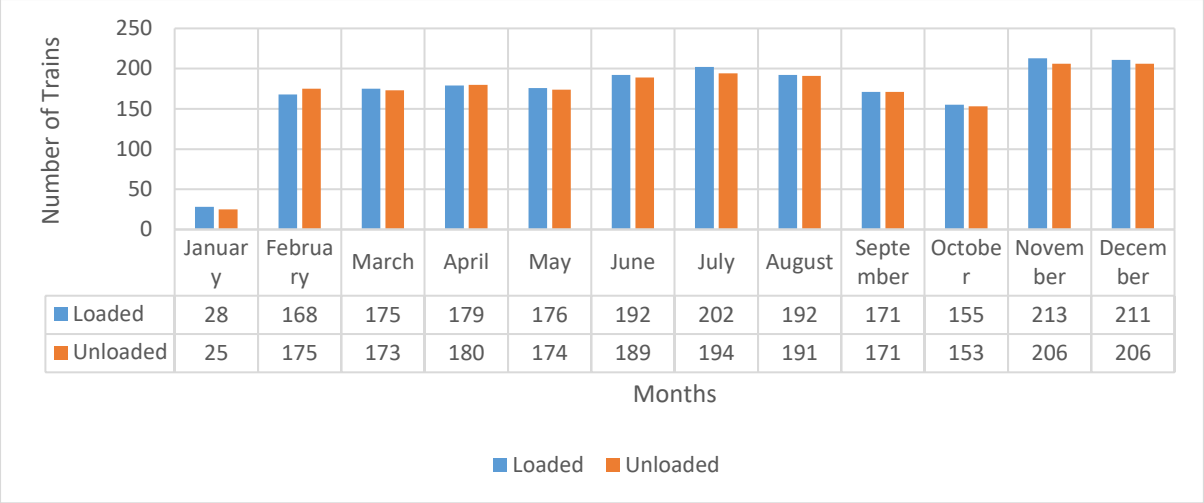

Figure 4.1: Observed trains

The trains were categorized by their length and the commodities they carried. The train length is a function of the number of wagons and number of locomotives it contains, as well as the axle loads which are defined by the commodities they carry. Table 4.1 presents a categorization allocated to each train type that crossed the bridge with its corresponding number of wagons and number of locomotives. The loaded trains were found traveling from the mines in Sishen (North) to the port in Saldanha (South), and the unloaded trains travelled from the port in Saldanha (South) to the mines in Sishen (North).

Table 4.1: Train Categorization

Category	No. of Locos	No. of Wagons	Type of Configuration
A	1-2	1-59	LC"1" + kWs
B	2-3	60-152	LC"1" + lWs
C	2-4	153-232	LC"1" + mWs + LC"2" + nWs + LC"3"
D	4-6	282-342	LC"1" + rWs + LC"2" + sWs + LC"3" + tWs +LC"4"
E	1-2	none	LC"1" + LC"1"
F	1-8	unlimited	LC"1" + rWs + LC"2" + sWs + LC"3" + tWs +LC"4"

4.2.1 Category A

Category A consist of short Head End Power trains with one locomotive consists. The number of locomotives ranged from 1-2 for one locomotive consist with the locomotive being mainly of diesel. A total of 622 trains were found in category A, with 309 of them being loaded trains and 315 of them being unloaded trains. These trains consist of 12 to 56 wagons with a median number of 48 wagons and mainly carry aggregates and dolomite blocks. The configuration of category A train is shown in Figure 4.2. The configuration composes of one locomotive consist and 48 wagons - (43D) (43D) - 48Ws.

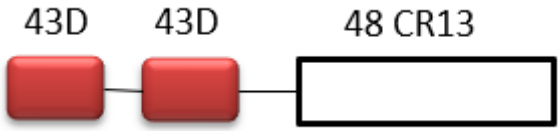

Figure 4.2: Category A configuration

4.2.2 Category B

Category B consists of 73 short HEP trains with one locomotive consists. The number of locomotives ranged from 1-2 for one locomotive consist with the type being electrical (15E) and diesel (43D). The 73 trains consist of 22 loaded trains and 51 unloaded trains with the number of wagons ranging from 92 to 124 wagons, and mainly carry a mixture of manganese and clinker ore. The configuration of category B train is shown in the Figure 4.3, having one locomotive consist and 118 wagons (15E) (43D) - 118Ws.

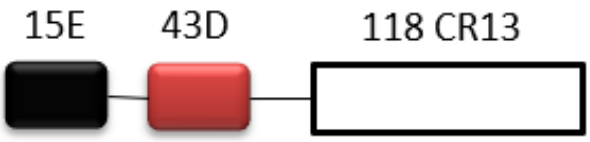

Figure 4.3: Category B configuration

4.2.3 Category C

Category C consists of 407 RDP trains with two or three locomotive consists. The number of locomotives ranged from 1-2 for one locomotive consist with the type mainly that of diesel

(43D) or electrical (15E) or both. The 407 trains consist of 197 loaded trains and 210 unloaded trains with the number of wagons ranging from 190 to 230 wagons and mainly carrying manganese ores. The configuration of category C trains is shown in Figure 4.4, having two locomotive consist and 228 wagons (15E) (43D) - 114Ws – (15E) – 114Ws.

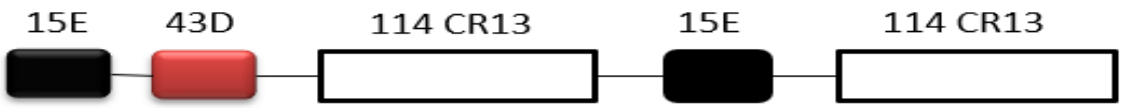

Figure 4.4: Category C configuration

4.2.4 Category D

A total of 2972 RDP trains with four locomotive consists were found to be in category D. The number of locomotives ranged from 1-2 for one locomotive consist with the type mainly that of diesel (43D) and electrical (15E). The 2982 trains consist of 1510 loaded trains and 1468 unloaded trains, with the number of wagons ranging from 338 to 342 wagons and mainly carrying manganese and iron ores. Category D trains generally have a configuration layout of (15E) (43D) - 114W – (15E) (43D) – 114W – (15E) – 114W – (15E). Figure 4.5 illustrates the train configuration of category D trains. This configuration is similar to the configuration in of Busatta & Moyo, (2018) and Matongo, (2018).

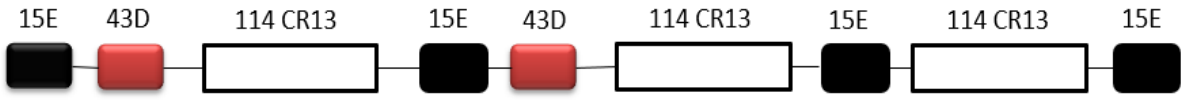

Figure 4.5: Category D configuration

4.2.5 Category E

Category E consists of a total of 40 trains that only compromises of locomotives and are not accounted for in the A-D categorization established by Busatta & Moyo, (2019). The number

of locomotives generally ranged from 1-6. The configuration of category E trains is shown in Figure 4.6 with three locomotives (15E) (15E) (15E).

Figure 4.6: Category E configuration

4.2.6 Category F

It consists of 14 mixed trains not accounted for in the A-D Bussata & Moyo, (2019) categorization. The number of locomotives generally ranged from 5-7, with 7 being the predominant locomotive. These trains consist of 22-360 wagons. The configuration of category F long train is shown in Figure 4.7 having 4 locomotive consist and 342 wagons (15E) (43D) - 114W – (15E) (43D) – 114W – (15E) – 114W – (15E).

Figure 4.7: Category F configuration

4.3 Wagon loads

The wagons used on the ORV have a load of 196 kN when unloaded and 1177 kN when loaded. The four axles on the wagons have a normal load of 49 kN when unloaded and 294 kN when loaded. Figure 4.8 shows the wagon loads for August 2016. Category A trains have loads ranging from 14126 kN to 69455 kN, category B have loads ranging from 101239 kN to 178934 kN, category C have loads ranging from 216605 kN to 273110 kN, and finally, category D have wagon loads ranging from 331970 kN to 402602 kN. All the category loads were found to be within the established limits. According to Figure 4.8, the maximum load reached in August was 396062 N and had an axle load of 290 kN which is well within the limit of 294 kN per axle. The minimum load was found to be 3173 kN and has an axle load of 66 kN. August has a mean load of 314474 kN and a median load of 387695 kN. It can be seen that category D trains are the heaviest and most frequent trains to traverse the ORV. It was also deduced that

a single span can simultaneously be loaded by 4.5 wagons which in turn amount to 18 axles and have a mass of 5400 t per span, which was discovered to be close to the self-weight of the beam 600 t. The obtained loads are slightly lower than the loads obtained by Busatta & Moyo, (2018) because the author used $g = 9.81\, m/s^2$ and Busatta & Moyo, (2018) used $g = 10\, m/s^2$.

The wagon loading tend to follow a certain patten that is depended on the train category. When plotted, the trains in the same category were found to form a group along the graph with category A trains at bottom as they are the lightest and category D trains at the top as they are the heaviest. Figure 4.8 shows the wagons loading for August. Category A trains are shown at the bottom of the figure in Red followed by category B trains in Green then followed by category C trains in Yellow and finally category D trains in Blue. The patten is depended on the weight of the wagons which in turn determines the categories of the trains. Category E trains are not shown within this pattern as they only contain locomotives and this is a presentation of the wagon loads, while category F trains can be found within these categories as category F trains are trains that don't fit in Bussata & Moyo, (2019) categorization but where still found to transverse the bridge. Hence, all four categories contain trains that belong to category F trains even though there is no clear distinction according to the pattern formed. The loading of each month is outlined in Appendix B.

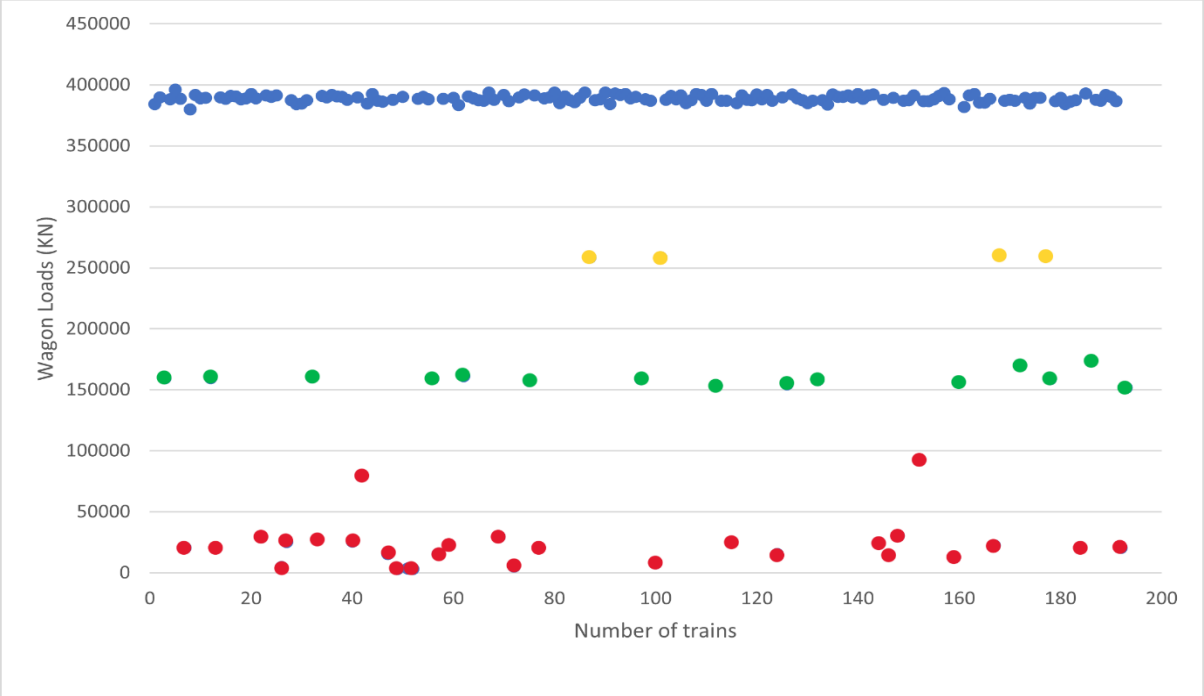

Figure 4.8: Wagon loads (August)

4.4 Train speed

The speed of the train provides an understanding of how the train behaves along the ORV and the generation of rail forces, be it due to acceleration, deceleration, or braking, which are in turn transferred to the deck and finally to the supporting infrastructure. It was observed that the wagons and locomotives within a specific train don't travel at the same speed when crossing the bridge. According to the literature and the provided documents of the ORV, the speed of the train is limited to 50 km/h when crossing the bridge in order to protect the structural integrity of the bridge.

4.4.1 Category A

The majority of category A trains were observed to cross the ORV at a constant speed. The other trains within category A had a slight difference in speed from wagon to wagon, but the change in speed was found to be within 3 km/h, and it was therefore deemed constant. The majority of the loaded trains cross the bridge at a speed of 40-50 km/h, but a small portion of the loaded trains also cross the bridge at a speed of 20-40 km/h, and the unloaded trains cross the bridge at 45-55 km/h. The maximum speed within a specific loaded train was 51.5 km/h

and the minimum speed 28.9 km/h. In contrast, the maximum speed of an unloaded train was 54 km/h and the minimum speed 39.8 km/h. In comparison, the unloaded trains of category A crossed the bridge at a higher speed compared to the loaded trains. It was also observed that not all trains travel within the ORV speed limit; 10% of category A trains crossed the bridge at a speed of 50-65 km/h, which is way above the 50 km/h speed limit. As shown in section 4.2.1, Category A trains are predominantly short trains with 12 to 56 wagons and 1 to 2 locomotive consists and can therefore travel at high speeds. The variation in speed between the loaded and unloaded trains is due to the commodities being hauled and the length of the trains. The unloaded trains travel at higher speeds compared to the loaded trains because the normal load per wagon is reduced for the unloaded trains, but the overall high speeds of category A trains are due to the short length of category A trains.

4.4.2 Category B

Category B recorded the least number of trains. Though category B trains are much longer than category A trains, they were observed to cross the bridge at a constant speed. With vehicles within a particular train having a speed variation of 2-3 km/h. The maximum speed for the loaded trains was 40-45 km/h, and the minimum speed was 35-40 km/h. The majority of the loaded trains lean towards the maximum speed of 40-45 km/h. The unloaded trains have a maximum speed of 45-50 km/h and a minimum speed of 40-45 km/h. The first vehicles within a specific train tend to have a higher entry speed and a slightly lower exit speed for the last vehicles. For a specific loaded train, the train has a maximum speed of 44.5 km/h and a minimum speed of 40.3 km/h. The high speeds recorded for category B trains is due to the length of the train. Category B trains are predominantly short trains with 92 to 124 wagons and 2 to 3 locomotive consists; thus, the trains cross the bridge at high speeds. The unloaded trains were observed to travel at a higher speed compared to the loaded trains because the load per wagon is reduced for the unloaded trains. Both the loaded and the unloaded trains travel at speeds within the given ORV speed limit.

4.4.3 Category C

Most of the loaded trains have a maximum speed ranging from 40-53 km/h, and the remaining trains have a minimum speed ranging from 20-40 km/h. The unloaded trains have a maximum

speed ranging from 45-54 km/h and a minimum speed ranging from 30-45 km/h. Eighty percent of the loaded and unloaded trains fall within the maximum speed range. In a specific train, the maximum speed for a loaded train was observed to be 48.9 km/h, and the minimum speed was observed to be 45.3 km/h. For an unloaded train, the maximum speed was observed to be 49.8 km/h, and the minimum speed was observed to be 45.0 km/h. The loaded and unloaded trains both exceed the ORV's speed limit of 50 km/h with about 4 km/h. The variation in speed across category C trains is predominantly due to the commodities being hauled and the length of the train. Category C trains are generally long trains compared to categories A and B trains, and thus travel at a reduced speed compared to categories A and B. The unloaded trains for category C travel at higher speeds compared to the loaded trains because the load per wagon is reduced for the unloaded trains.

4.4.4 Category D

For the loaded trains, the speed decelerates from the first vehicle to the 190th vehicle, and then it starts to accelerate from the 191 vehicles to the last vehicle. Overall, the trains have an entry speed of 40-50 km/h and an exit speed of 35-45 km/h. The deceleration has a speed change of roughly 15-20 km/h. The loaded trains have a maximum speed ranging from 45-50 km/h and a minimum speed ranging from 25-35 km/h. The unloaded train's speed decelerates from vehicle to vehicle till the last vehicle. Thus, unloaded trains have a maximum speed ranging from 45-50 km/h and a minimum speed ranging from 30-45 km/h. A specific loaded train has a maximum speed of 53 km/h and a minimum speed of 44 km/h. For an unloaded train, one train has a maximum speed of 50.0 km/h and a minimum speed of 28.6 km/h. It is important to note that not all unloaded trains follow this pattern. Some unloaded trains have a more decreased change in the speed variation. Category D trains were observed to enter the bridge at an extremely high speed, sometimes even higher than the speed limit of 50 km/h and exit the bridge at even higher speed greater than the 50 km/h speed limit. The variation in speed between the loaded and unloaded trains was assumed to be due to the topography of the bridge. The loaded trains are required to climb a cliff upon exit of the ORV; thus, explaining the acceleration from the 191 vehicle to the last vehicle. While the unloaded train is subjected to a much flatter terrain that slopes downwards, thus explaining why the unloaded trains decelerate from vehicle to vehicle till the last vehicle.

4.4.5 Category E

Category E trains cross the ORV at constant speeds. Therefore, there is no speed variation for category E trains. They cross the bridge at a speed of 50 km/h when traveling from the mines to the port and have an increased speed of 55-60 km/h when traveling from the port to the mines. The increased speed in the latter direction was found to be primarily due to the topography on which the ORV is situated. Hence, category E trains primarily cross the bridge at speeds higher than the established speed limit of 50 km/h.

4.4.6 Category F

Category F contains both short and long trains. The short trains were observed to behave like the trains in category A and B, and the long trains behave similar to category C, and D. The loaded short trains travel at a maximum speed ranging from 40-50 km/h and a minimum speed ranging from 30-40 km/h. The unloaded short trains travel at a maximum speed ranging from 45-50 km/h and a minimum speed ranging from 35-45 km/h. Both the loaded and the unloaded trains travel within the speed limit of 50 km/h.

4.4.7 Statistical Summaries

Table 4.2 outlines the statistical speed summaries for each category. The minimum speed is the minimum speed recorded within a particular category, and the maximum speed is the maximum speed of a train recorded within a particular category. The mean speed is the average speed of all the trains within a particular category. The median is the middle speed within a particular speed set in a category, and the mode is the most frequent speed within a particular category. The speeds in Table 4.2 are an average of the statistical summaries of speeds in each month, and the monthly statistical summaries are in Appendix C.

Category A and C loaded trains recorded the highest maximum speeds amongst all categories, with 52.47 km/h and 52.58 km/h, respectively. While category A and D unloaded trains recorded the highest speeds amongst all categories, 62.87 km/h and 59.28 km/h, respectively. Category D trains have the lowest minimum speeds, with the loaded trains having 13.73 km/h and the unloaded trains having 18.62 km/h. The mean, median, and mode speeds are all within the ORV speed limit of 50 km/h. With category E having the highest mean speed of 47.09 km/h, and category D unloaded trains having the maximum median speed of 47.71 km/h, and category B, C, and D unloaded trains having the highest mode speeds of 48.4 km/h, 48.06 km/h

and 48.25 km/h, respectively. The mean speeds have a standard deviation of 2.5 km/h, meaning the speed values are more scattered around the mean.

The maximum speeds of the loaded and the unloaded trains of category A, C trains, and category D unloaded trains exceed the ORV's speed limit of 50 km/h. However, the loaded trains tend to cross the bridge at higher speeds than the unloaded trains. Therefore, the high unloaded speed is primarily due to the unloaded wagons. When the wagons are empty, the normal load per wagon is reduced; thus, the vehicle can travel faster. The speed is also dependent on the length of the trains; the short trains travel at a higher speed than the long trains because the short trains haul fewer commodities than the long trains. Thus, the short HEP trains in category A travel faster than the long RDP trains in category D. Overall, the results of the speeds for categories A-D are similar to the results obtained in Busatta & Moyo, (2016), who also found that the train sometimes cross the bridge at speeds exceeding the 50 km/h speed limit.

Table 4.2: Statistical summaries

CATEGORY		MAX (km/h)	MIN (km/h)	MEAN (km/h)	MEDIAN (km/h)	MODE (km/h)
A	Loaded	52.5	20.6	41.7	43.4	43.3
	Unloaded	62.9	20.6	45.7	47.0	46.8
B	Loaded	47.3	35.8	42.8	45.0	45.1
	Unloaded	49.9	38.9	46.2	47.7	48.4
C	Loaded	52.6	28.2	43.9	44.7	44.6
	Unloaded	53.4	31.6	46.1	47.1	48.1
D	Loaded	47.8	13.7	44.9	45.9	47.8
	Unloaded	59.4	18.6	45.1	47.7	48.3
E	-	49.0	44.0	47.1	47.4	46.7
F	Loaded	47.2	35.5	42.4	43.2	45.2
	Unloaded	51.4	50.6	51.1	51.1	51.3

4.5 Speed Profiles

The variation of the speed of the train is presented by the speed profiles, which captured the first locomotive of the train as it enters the bridge and the last locomotive/wagon as it leaves the bridge. In addition, the speed and the number of wagons were indicated to observe if the speed of the train and wagons affect the shape of the speed profile. More speed profiles of all the categories are attached in the Appendix D, and only the most common ones are presented below.

4.5.1 Category A

Category A trains comprise 20-56 vehicles, of which 2 are 6-axle locomotives. The loaded trains crossed the bridge at constant speeds ranging from 30-50 km/h, with most of them having speeds of 40-50 km/h and the remainder having speeds of 30-40 km/h, and the unloaded trains crossed the bridge at slightly higher constant speeds ranging from 45-50 km/h. Therefore, the loaded and the unloaded category A trains exhibit a constant speed profile with speeds ranging from 30-50 km/h. However, as discussed in Section 4.4.1, some category A trains cross the bridge at speeds above the given 50 km/h limit; therefore, some trains have constant speed profiles ranging from 50-65 km/h. Hence, no difference between the loaded and unloaded category A speed profile. Figures 4.9 and 4.10 show the speed profiles of the loaded and the unloaded trains for category A, and both present a constant speed profile with the loaded train having a constant speed of 33 km/h and the unloaded train having a constant speed of 43 km/h. Since there is no change in the crossing speeds, category A trains only contribute to the dynamic loading of the bridge, and no contribution goes to the rail forces.

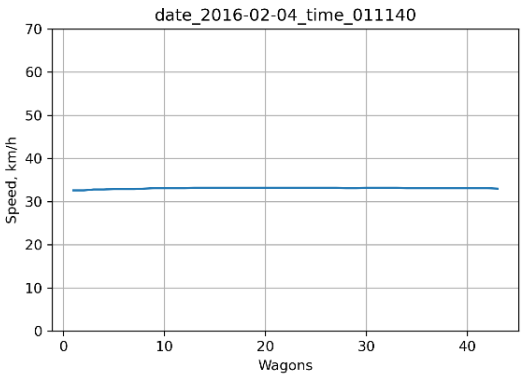

Figure 4.10: Category A speed profile (loaded train)

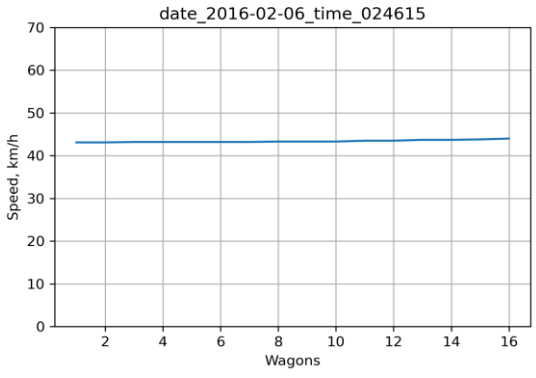

Figure 4.9: Category A speed profile (unloaded train)

4.5.2 Category B

Category B trains ranged from 92 to 124 wagons and 2-3 six-axle locomotives. The loaded trains cross the bridge with speeds ranging from 40-50 km/h, and the unloaded trains cross the bridge with speeds ranging from 45-55 km/h. Figure 4.11 shows a speed profile of a category B loaded train. The train has an entry speed of 44.8 km/h and an exit speed of 41 km/h and has a speed change of 3.8 km/h, which can be considered a constant speed. Therefore, category B loaded trains have a constant speed profile.

On the other hand, the unloaded train in Figure 4.12 has an entry speed of 50.8 km/h and an exit speed of 50.8 km/h, but the train slightly accelerated and decelerated along the way with a change in speed of less than 1 km/h. This behavior was observed within many unloaded trains of category B. This behavior is due to the wagons of the unloaded trains being empty, meaning the normal load per wagon is reduced; thus, category B unloaded trains can now travel at a faster speed and therefore exhibiting a constant speed profile. Furthermore, both the loaded and the unloaded trains of category B cross the bridge with speeds less than 50 km/h; thus, no speed profiles of speeds ranging above 50 were observed. However, since the crossing speed of category B trains was deemed constant for both the loaded and the unloaded trains, the trains only contribute to the dynamic load of the bridge, but no contribution goes to the longitudinal rail forces.

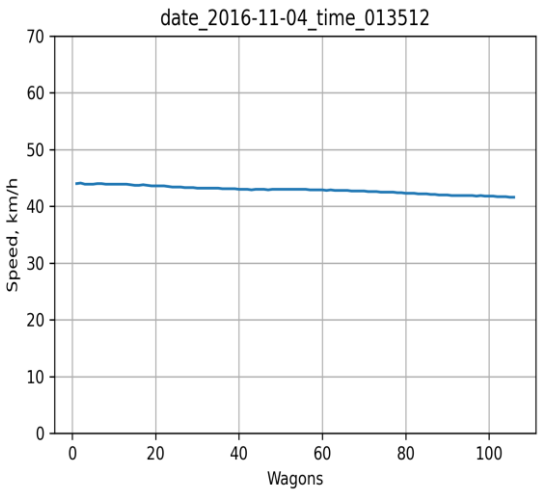

Figure 4.11: Category B speed profile (loaded)

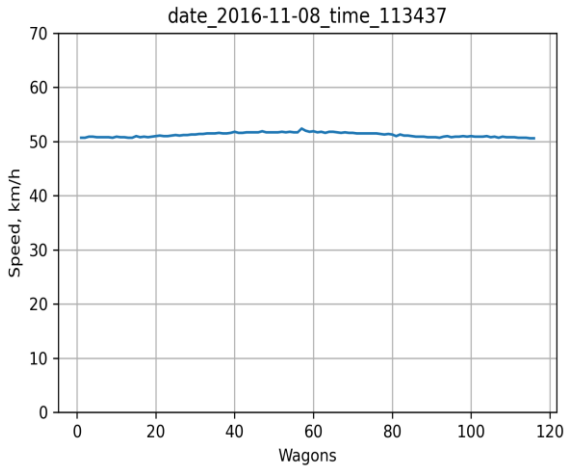

Figure 4.12: Category B speed profile (unloaded)

4.5.3 Category C

Long RDP trains with roughly 180-230 wagons plus 2-4 locomotives make up category C trains. The loaded trains cross the bridge with speeds ranging from 30-50 km/h with all the trains having speeds within the 50 km/h speed limit, and the unloaded trains cross the bridge with speeds ranging from 35-55 km/h were 10% of them crossed the bridge at speeds higher than the given speed limit of 50 km/h.

The loaded trains enter the bridge with speeds ranging from 40–50 km/h and were observed to decelerate upon entry onto the bridge, then slightly, followed by a decreased acceleration until the last vehicle. The change in speed in most loaded trains was less than 3 km/h; thus, the speed was deemed constant and therefore exhibited a constant speed profile, but not all loaded trains followed that pattern; some trains decelerated upon exit, but the change in speed was still minimal, and thus it was still considered constant. Therefore, the loaded trains mainly contribute to the dynamic loading of the bridge compared to the rail forces. The rail force contribution can be considered negligible since the change in the train speeds is less than 3 km/h. Figure 4.13 shows the speed profile of a loaded train. The train has an entry and exit speed of 49 km/h and a change in speed of roughly 3 km/h, thus presenting a constant speed profile.

On the other hand, unloaded trains enter the bridge with high entry speeds ranging from 45-55 km/h and exit the bridge with lower speeds ranging from 35-45 km/h. Therefore, the train's speed decelerates from vehicle to vehicle upon entry on the bridge with a change in speed of roughly 5-10 km/h. The unloaded trains, therefore, have a deceleration speed profile. Furthermore, the decelerating speed change induces braking forces on rails; thus, the unloaded trains contribute to the horizontal rail and dynamic bridge forces. Trains with high entry speeds tend to have a tremendous change in speed of roughly 10 km/h, which increases the braking force transferred on the rails. For example, Figure 4.14 shows an unloaded category C train with an entry speed of roughly 50 km/h and an exit speed of 46 km/h. The train has a 4 km/h change in speed and represents a decelerating speed profile.

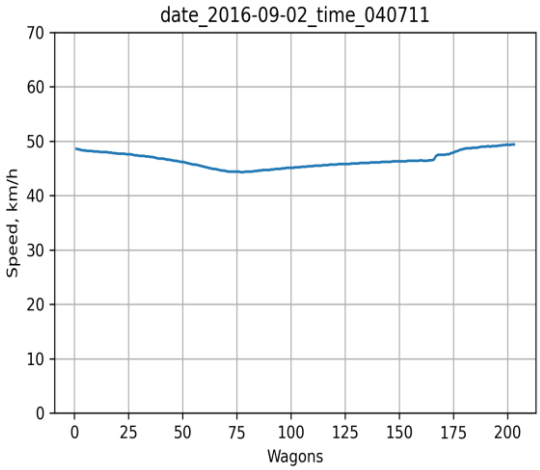

Figure 4.14: Category C speed profile (loaded)

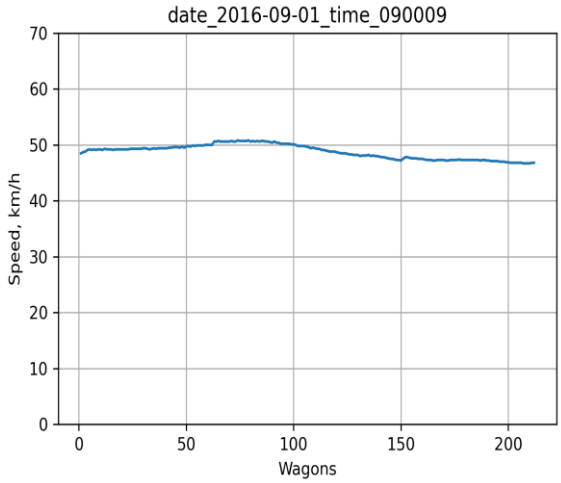

Figure 4.13: Category C speed profile (unloaded)

4.5.4 Category D

Category D trains contain long RDP trains with predominantly 342 wagons and six locomotives. The loaded trains cross the bridge with speeds ranging from 35-55 km/h, and the unloaded trains cross the bridge with speeds ranging from 35-60 km/h, with the majority of the loaded and unloaded trains having speeds ranging from 40-50 km/h. Twenty percent of the loaded and the unloaded trains exceed the 50 km/h speed limit.

The loaded trains have an entry speed ranging from 40-50 km/h and tend to decelerate upon entry on the bridge. The speed decelerates from vehicle to vehicle until the 140-150th vehicle, and then it accelerates from the 161 vehicle until the last vehicle, which has an exit speed ranging from 45-55 km/h, typically higher than the entry speed. The decelerating speed has a speed change ranging from 5-20 km/h, and the accelerating speed has a speed change ranging from 5-25 km/h. Therefore, category D trains exhibit a deceleration followed by an acceleration speed profile which typically represents a V shape. Moreover, the deceleration of 5-20 km/h experienced by the first 140 vehicles induces a braking force on the rails and, in return, contributes to the build-up of horizontal forces on the rails. At the same time, the acceleration of 5-25 km/h experienced by the remainder 202 vehicles induces a traction force on the rails and, in return increasing the horizontal rail forces. While the train itself contributes to the bridge's dynamic loading; hence, the heavier the train, the larger the dynamic loading.

Therefore, the combined effect of the braking, acceleration, and dynamic loading of the train predominantly affects the track-bridge interaction, as explained earlier in Section 2.2.3 of the literature.

Figure 4.15 shows a typical speed profile for a category D train exhibiting a deceleration speed profile followed by an acceleration speed profile. The train has an entry speed of 46 km/h, which decelerated till the 140th vehicle to a speed of 39 km/h with a speed change of 7 km/h, followed by an acceleration from the 140th vehicle till the last vehicle, which has a speed of 52 km/h and an acceleration speed change of 13 km/h. The train braked from 46 km/h to 39 km/h and thus induced a braking force on the rails, while the acceleration from 39 km/h to 52 km/h induced a traction force on the rails. The speed change due to acceleration was typically greater than the speed change due to braking; therefore, one can deduce that a higher traction force is induced on the rails than the braking forces.

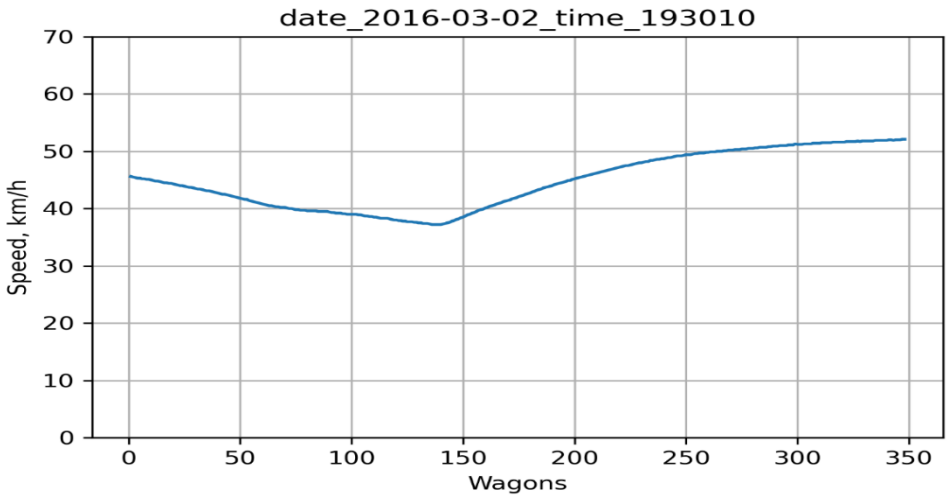

Figure 4.15: Loaded Category D Speed Profile

While unloaded trains have entry speeds ranging from 40-65 km/h and exit speeds ranging from 20-30 km/h. Upon entry on the bridge, the speed remains constant from the first vehicle to the 150-200 vehicle, followed by a change in speed from the 200 vehicles to the last vehicle. The change in speed of the last vehicles ranges from 5-20 km/h. The constant speed followed by a decrease in speed shows a parabolic shape. Therefore, the unloaded category D trains exhibit a constant speed profile followed by deceleration speed profiles, which show a parabolic shape. The appearance of the train on the bridge induces forces on the rails and

bridge, but no force is induced on the rails during the constant speed period since there is no change in speed in the first 150-200 vehicles, while the deceleration of the last vehicles induces a braking force on the rails, and the train induces a dynamic force on the bridge. Unloaded trains do not experience an increased change in speed during the crossing of the train; therefore, no contribution of the traction forces is experienced on the rails. Hence, the total track-bridge interaction forces along the bridge and the rails are primarily due to braking and dynamic forces.

Figure 4.16 shows a typical unloaded category D speed profile. The first vehicle has an entry speed of 50.1 km/h, and the last vehicle has a speed of 42 km/h. The train's speed is constant from the first vehicle to the 140th vehicle, and it gradually decreases from the 141 vehicle to the last vehicle and, therefore, exhibits a deceleration speed profile with a concave shape. The change in speed of 8.1 km/h experienced by this train induced a braking force on the rails which caused an increase in the horizontal forces of the rails.

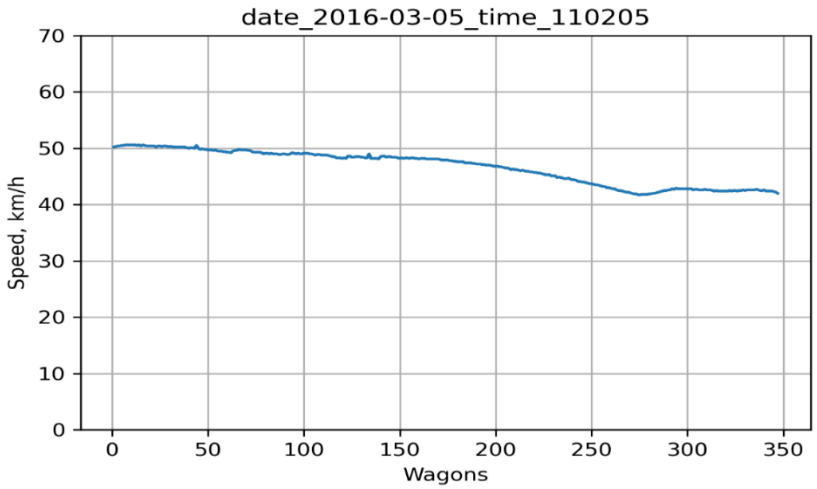

Figure 4.16: Unloaded Category D Speed Profile

In contrast, the loaded and the unloaded trains both enter the bridge at high speeds, with the unloaded speeds being slightly higher than the loaded trains, but the loaded entry speeds tend to exceed the 50 km/h speed limit while the exit speeds are the opposite of each other, with loaded trains having higher exit speed compared to the unloaded trains. The ORV is 1km long, and the RDP train is 4.2 km long; therefore, only half of the train loads it when the bridge is fully loaded. In addition, the difference in speed profiles between the loaded and the unloaded

trains was assumed to be due to the topography of the bridge. The loaded trains are required to climb a cliff upon exit of the ORV; thus, explaining why the loaded trains tend to accelerate as they exit the ORV. While the unloaded trains are subjected to a much more flatter terrain that slopes downwards, thus explaining why the unloaded trains exhibit a decrease in speed upon exit on the ORV. Therefore, the loaded train is more critical as it experiences both braking and acceleration, which tend to be significant factors in the build-up of horizontal forces on the rails in addition to dynamic forces induced by the train on the bridge.

4.5.5 Category E

Category E contains only locomotives. The locomotives were observed to cross the bridge at constant speeds ranging from 40-65 km/h. The speed depends on the direction in which the locomotive is traveling; locomotives traveling from the ports in Saldanha to the mines in Sishen tend to cross the bridge at higher speeds than those traveling in the opposite direction. The locomotives experience no speed change as they transverse the bridge; therefore, locomotives travel at constant speeds and exhibit a constant speed profile. No horizontal forces are induced on the rails as there is no change in speed and only the locomotive contributes to the dynamic forces of the bridge. Figure 4.17 shows a speed profile of a category E train with a constant speed profile at 64 km/h.

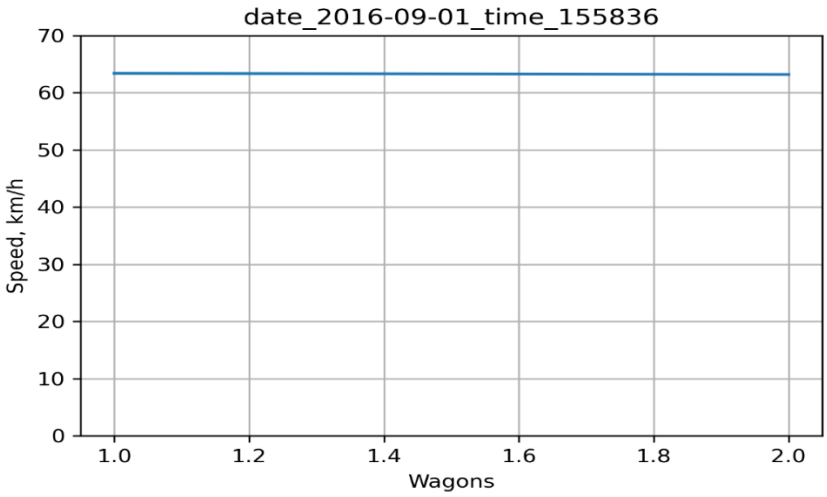

Figure 4.17: Category E speed profile

4.5.6 Category F

Category F contains short HEP trains and long RDP trains that were not included in the established categorization of Busatta and Moyo. Though the short trains do not necessarily

have the same number of 6 axle locomotives and four-axle wagons as category A and B trains, still exhibit the same constant speed profile as those categories. The long trains in category F also tend to exhibit the same profiles as category C and D. Thus, the loaded and unloaded short trains have a constant speed profile as in categories A and B. In contrast, the long-loaded trains have a deceleration, followed by an acceleration speed profile, and the unloaded trains have a constant speed profile from the first vehicle till the 200 vehicle, followed by a deceleration from the 300th vehicle till the last vehicle as in category C and D.

The short trains only contribute to the dynamic forces of the bridge, and no horizontal forces are induced on the rails as they experience no speed change. While the long-loaded trains experience speed variation and therefore induce braking and traction forces on the rails in addition to dynamic forces induced on the bridge by the train. While the unloaded trains only experience a decrease in speed and thus, induce braking forces on the rails and dynamic forces on the bridge due to the train. Figure 4.18 shows category Fs V shape speed profile, which is precisely the same as the category D speed profile.

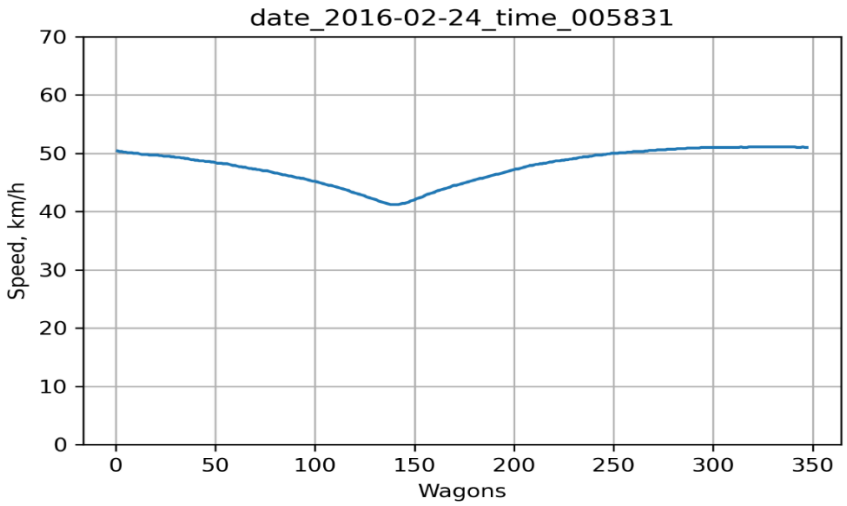

Figure 4.18: Speed profile

4.5.7 Speed profile summary

Overall, category A & B have constant speed profiles as they tend to cross the bridge at constant speeds, while the long trains with the non-uniform speeds have decelerating and accelerating speed profile and this is similar to the profiles found in Kiiza, (2019).

4.6 Presence of the train on the bridge

The ORV is subjected to high forces due to continuously welded rails used to construct the bridge. The forces are due to high temperature, deck movement, and rail traffic. Therefore, the forces need to be kept within limits to prevent buckling and derailment of the rails. Thus, this section characterizes the interaction forces by closely looking at the rail forces, deck deflection, air, and rail temperature.

The research used 2016 data from the Saldanha UPM60 systems, which was recorded every three minutes. The data contains 16 strain channels, four-deck deflection channels, two rail temperature channels, and two air temperature channels, and they were all analyzed simultaneously. The system has a tension limit of 1400 kN and a compression limit of 1100 kN. For the rail forces, the forces above zero represent forces due to tension, and those below zero represent compression forces. At the same time, for the deck deflection, negative values indicate deck contraction, which induces tensile forces, and a positive value indicates deck expansion which induces compression forces. Finally, negative temperature values induce compression forces, while positive temperature induces tensile forces.

Based on the speed profiles of category D trains, they experience a significant change in speeds, both acceleration, and deceleration, which induces additional forces in the rails due to the change in speed. Therefore, during the presence of a category D train on the bridge, a change in the rail forces, deck deflection, and rail temperature is experienced and is represented by a jump in all three parameters. The short trains in categories (A, B, and E) experience no speed change; thus, they exhibit no effect on the rail forces, deck deflection, and rail temperature. Therefore, no jumps are captured on the rail forces, deck deflection, and rail temperature due to those trains. Figure 4.19 shows the shape of the jumps experienced by the rail forces, deck deflection, and rail temperature. The rail forces and the deck deflection both experienced a similar jump shown in Figure 4.19 (a). In addition, the jump in the rail temperature exhibit a linear line, as shown in Figure 4.19 (b).

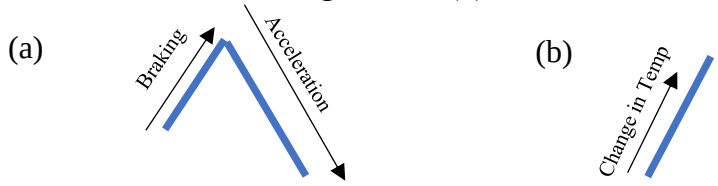

Figure 4.19: Jump shapes experienced in the rail forces, deck deflection, and rail temperature (a) rail force and deck deflection jump; (b): rail temperature jump

The shape of the jump in the rail forces is dependent on the time the train is present on the bridge. The rail forces are high in tension during morning hours; thus, a train crossing the bridge during the morning hours causes an increase in the rail forces when the train brakes, followed by a decrease in the rail forces when the train accelerates. However, a train crossing the bridge in the afternoon when rail forces are high in compression causes a decrease in rail forces due to braking, followed by an increase in the rail forces due to acceleration. Therefore, during the day, the jump in the rail forces takes the shape of a V, the category D speed profile shape, while a train crossing the bridge during the morning hours has a reverse V shape.

4.6.1 Track-Bridge Interaction

According to the rail force jump presented in Figure 4.19 (a), an increase in the rail forces and deck deflection is experienced when the train brakes, followed by a decrease in the rail forces as the train accelerates. Figure 4.20 shows the relationship between the speed profiles, rail forces, rail temperature, air temperature, and deck deflection, with 4.20 (a) showing the rail forces vs. temperature (air and rail) for a train that crossed the ORV on 2016-05-01 at 22:49, while 4.20 (b) shows the deck deflection vs. rail forces for the same train, and 4.20 (c) shows the speed profile.

As the train decelerates, an increase in rail force is experienced, while a decrease in rail force is experienced when the train starts to accelerate again. In contrast, the acceleration also causes an increase in the rail temperature. In can be seen from Figure 4.20 (a), a deceleration from 42 km/h to 31 km/h caused the rail force to jump from 1120 kN to 1140 kN; thus, adding a braking force of 20 kN, while the acceleration from 31 km/h to 44 km/h decreased the rail forces from 1140 kN to 1010 kN, therefore, adding a 130 kN force. The acceleration also caused an increase in the rail temperature, which changed from 12 ℃ to 18 ℃ and had a temperature increase of 6 ℃ with the air temperature at 15.9 ℃. Therefore, the 130 kN change in the rail forces due to acceleration is a sum of the traction force plus the temperature-induced force.

This relationship was observed throughout all category D loaded trains with acceleration and deceleration speed variations greater than 3 km/h. While for trains with a minimal deceleration speed (3 km/h difference) and an acceleration of more than 5 km/h, only the effect of the acceleration is recorded on the rail forces showing a downward sloping curve. Not all unloaded

trains are shown on the rail forces. Unloaded trains tend to decelerate upon entry on the bridge, so only the jumps of trains presenting significant deceleration variations are captured on the rail forces.

During the passage of the train, a similar jump is observed in the deck deflection. However, the shape of the jump is the reverse of the jump observed in the rail force, as shown in figure 4.20 (b). In Figure 4.20 (b), the deck is in tension with an air temperature of 15.8 ℃. The deflection jumped from -56 mm to -56.5 mm, followed by -56.5 mm to -56.1 mm. The deck deflection increases when the train brakes, followed by a decrease in deck deflection when the train accelerates. The magnitude of the jump is depended on the change of speed; thus, the higher the deceleration/acceleration speed change, the greater the deflection jump. In contrast, the air temperature dramatically affects the magnitude of the deck deflection. An increase in the air temperature causes the deck to expand, while a decrease in the air temperature causes the deck to contract, which imposes additional forces on the rails.

Based on this, the deceleration of the train speed increases the tensile forces of the bridge and causes a decrease in the deck deflection. At the same time, the speed acceleration decreases the rail forces pushing them into the compression region simultaneously, causing an increase in deck deflection and increasing the rail temperature, which increases the compression forces. Therefore, there is indeed an interaction between the rail and the bridge, as the track-bridge phenomena stipulate. In addition to dynamic forces on the bridge, additional rail forces should be expected when significant speed variations are experienced.

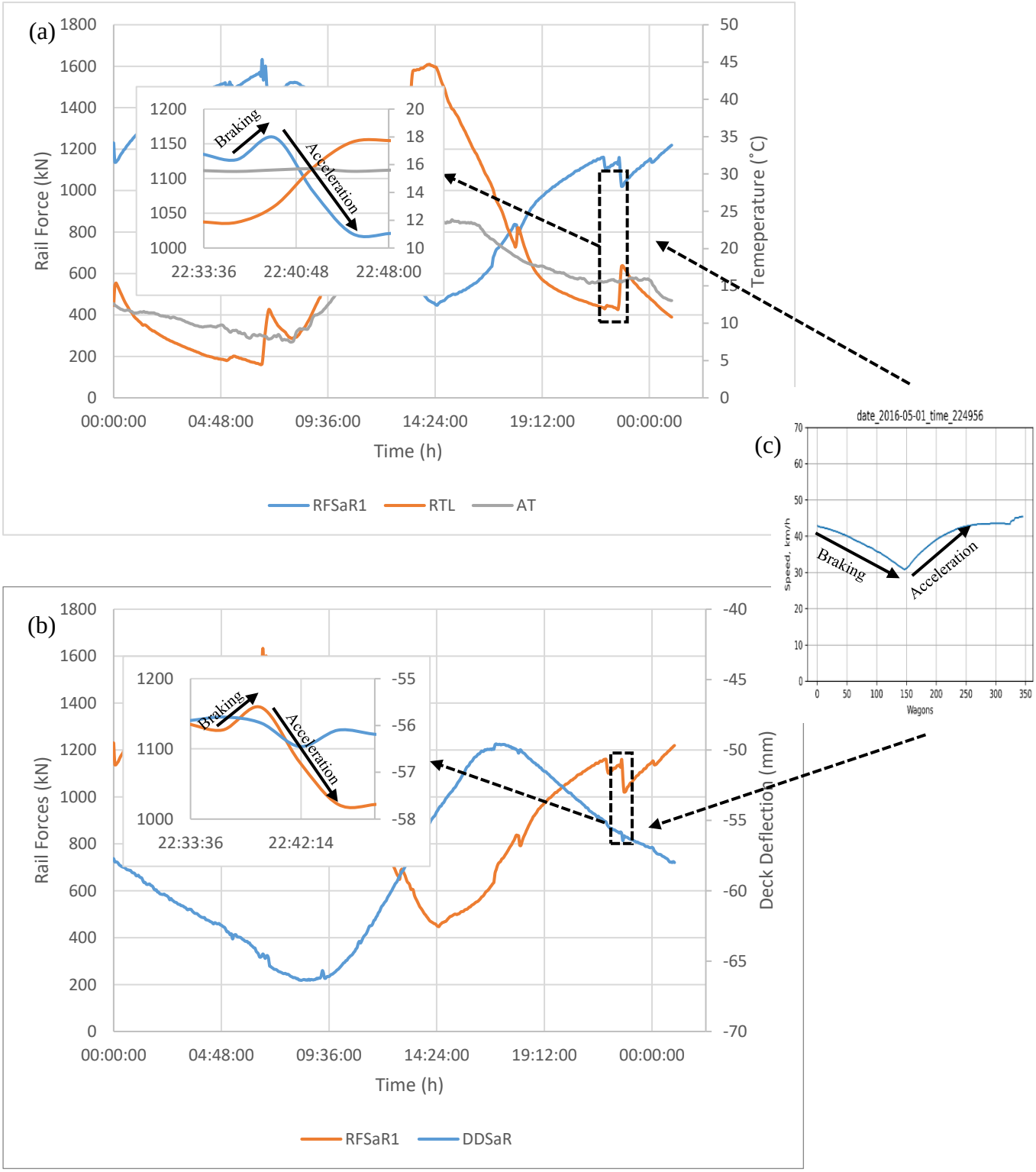

Figure 4.20: Track-bridge interaction. (a) rail forces vs temperature; (b) rail force vs deck expansion; (c) speed profile (2016-05-01 at 22:49)

4.7 Air Temperature

It is reasonable to assume that air temperature affects both rail temperature and the deck expansion, and as a result, both affect the rail forces. A drastic change in the rail temperature and deck deflection results in additional forces in the rails. Though train speed cannot be directly linked to air temperature, a train present on the bridge during a turning point on a hot or cold day will spike a jump in the rail forces as it brakes/accelerates, thus increasing the rail forces above the threshold and therefore posing as a threat during those periods. Therefore, air temperature is the interlinkage between the four (speed, rail force, rail temperature, and deck deflection) parameters.

An increase in air temperature causes an increase in rail temperatures which also causes an expansion of the deck, while a decrease in air temperature causes contraction of the deck and thus resulting in compression and tensile forces, respectively. Additional rails forces will constantly impose a risk on the rails because air temperature cannot be managed as it is naturally occurring and is the main contribution to the additional forces. The relationship between air temperature and the four parameters was investigated using regression models.

A scatter plot of the rail and air temperature showed an R square value of 0.77, implying that the data points are close to the regression line and that the regression model can explain 77% variability in the rail temperature. While the rail force and air temperature have an R square value of 0.79, meaning the data points are close to the region line, and 79% of the variability in rail forces is due to air temperature. In contrast, the scatter plot of deck deflection, and the air temperature showed an R square value of 0.49 which means that the data values are scattered around the regression line, and the regression model can account for only 49% of the deck deflection variability. Table 4 shows the R square values for rail temperature, rail force, deck deflection, and air temperature. The R squared values showed that there is indeed a relationship between the air temperature and the four parameters. The regression models can be found in Appendix I.

Table 4.3: R Squared Values

Parameters	**R square value**
Rail temperature	0.77
Rail force	0.79
Deck deflection	0.49

For 2016, the air temperature ranged from 0 - 45 degrees, with the lowest temperature recording the highest tensile forces and the highest temperature recording the highest compression forces. The annual air temperature for 2016 can be found in Appendix. A closer look at the air temperature was done from the 1st to the 5th of January 2016, as shown in Figure 4.21. The air temperature ranged from 20 to 35 degrees for the five days with a sinusoidal pattern. The deck deflection and the rail temperature follow this pattern, but there is a significant deviation in the rail temperature during the day compared to the air temperature. The deviation in the rail temperature from the air temperature is shown with black arrows in Figure 4.21. This deviation implies additional parameters that might influence the rail temperature during the day. The rail forces are high in compression during the day when the air temperature is high and high in tension at night when the air temperature is low. The jumps on the rail forces and the rail temperature are due to the presence of a train on the bridge.

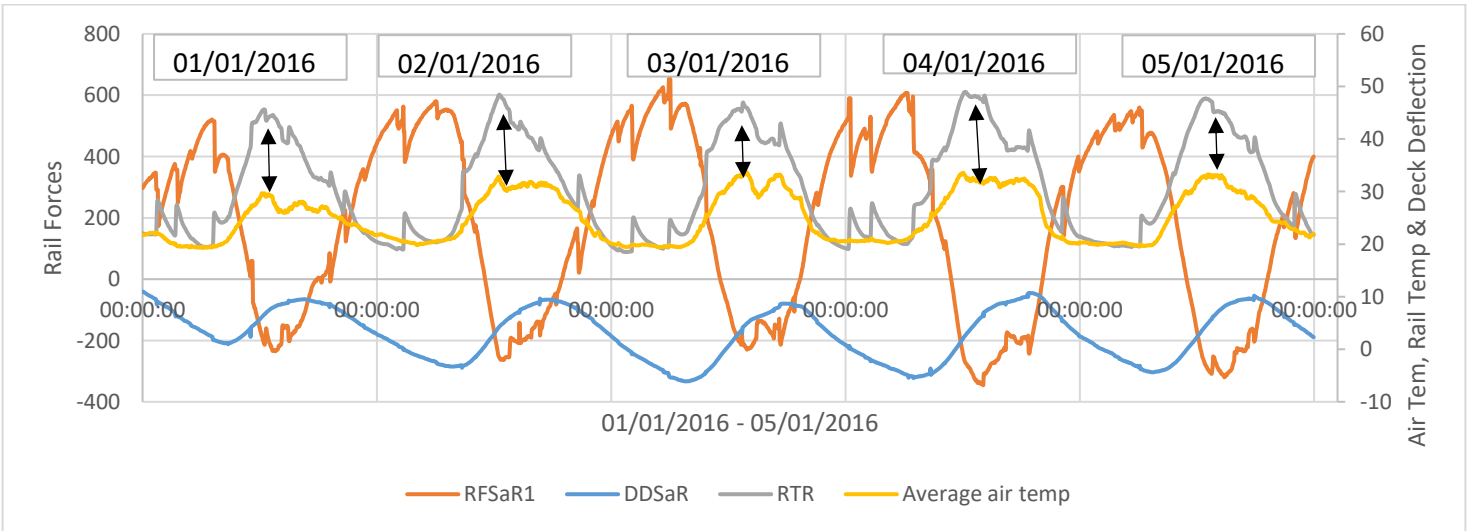

Figure 4.21: Air Temperature Relationship

4.8 Rail forces

The additional rail forces are due to the variation of the train speed, which causes a jump in the rail forces. In addition, a force is induced on the rails as a train accelerates or decelerates. Therefore, the total rail forces depend on the velocity at which a train is traversing the bridge and the time the train crosses the bridge.

The influence on the rail forces is critical when a train is present on the bridge during the tensile or compression turning points because the rail forces are their maximum during these points; thus, a jump in the rail forces at such a time will drastically increase the rail forces and add to the additional longitudinal forces on the rails. Figure 4.22 shows the rail forces for the 1st of December 2016, which illustrates the rail force peaks and their turning points. A train crossing the bridge during the peaks is likely to cause rail failure compared to a train crossing the bridge at any other time. The jumps occurring on the tension turning point are the opposite in shape of those occurring during a compression turning point, but both cause an increase in the rail forces and add to the longitudinal forces. Hence, the focus has been given to trains crossing the bridge during the turning point of the rail forces.

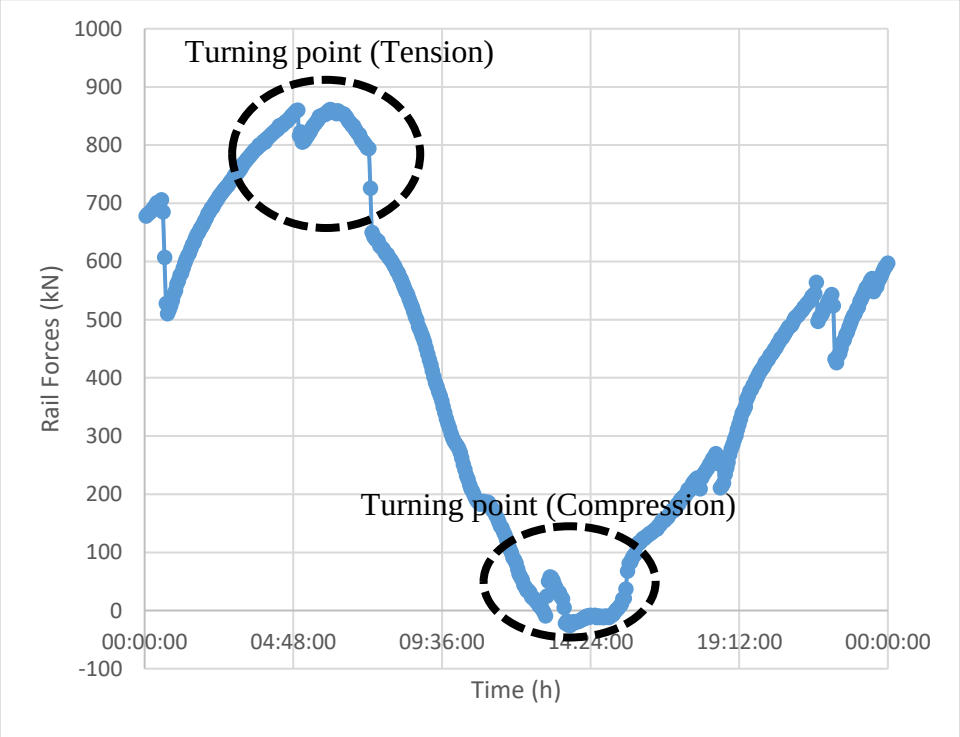

Figure 4.22:: Rail Force (1/12/2016)

4.8.1 Rail forces vs. Speed

The short trains in categories A, B & E cross the bridge at constant speeds and do not experience speed variations. Hence, no jumps are observed in the rail forces for such kinds of trains. Hence, no additional horizontal forces are induced on the rails due to those trains. However, a jump is recorded in the rail forces as a category D train crosses the bridge as they experience significant speed variation that induce additional forces on the rails. The loaded category D trains present a big jump in the rails compared to the unloaded category D trains, but only the unloaded trains with significant speed variations are captured on the rails.

The magnitude of the rail force jump is dependent on the acceleration and deceleration speed variation. Category D trains have an entrance speed of 40-55 km/h and experience a deceleration upon entry on the bridge of approximately 5-25 km/h, which adds an additional force on the rails. If the train is present on the bridge during a tension turning point, this additional force is presented as an upward jump in the rail force, increasing the tensile forces. However, the trains have an exit speed of roughly 40-65 km/h, which causes an acceleration of roughly 5-25 km/h, which causes a downward jump in the rails. The downward jump decreases the rail forces and pushes them into the compression region. Thus, the shape of the jump due to acceleration and deceleration has the same shape as a loaded category D speed profile but in the opposite direction.

Figure 4.23 (a) shows the rail force diagram for the 27th of January 2016, and Figure 4.22 (b) shows a speed profile of a train that crossed the ORV on the 27th of January 2016 at 12:23 pm during a compression turning point. A jump is observed on the rail forces at the time that the train crossed the bridge. The Category D train in question has a decelerating and accelerating speed profile. The train speed decelerated from 30 km/h to 18 km/h and then accelerated from 18 km/h to 33 km/h with a speed change of 12 km/h and 15 km/h, respectively. As a result, the rail forces jumped from 130 kN to 60 kN for this particular train and again jumped from 60 kN to 140 kN. Thus, having a rail force change of 70 kN and 80 kN, respectively. The jump in the rail force has the same shape as the category D speed profile; thus, when the train decelerates, a decrease in the rail forces is experienced, while an accelerating train increases the rail forces. In return, the speed change added additional forces on the rails, with the deceleration decreasing the rail forces and pushing them in the compression region while an accelerating

train increases rail forces and pushes them in a tension region. It is important to note that the shape of the jump in the rail force is depended on the time the train crosses the bridge. Trains crossing the bridge during the morning hours experience a reverse effect in the shape of the jump compared to the train explained above.

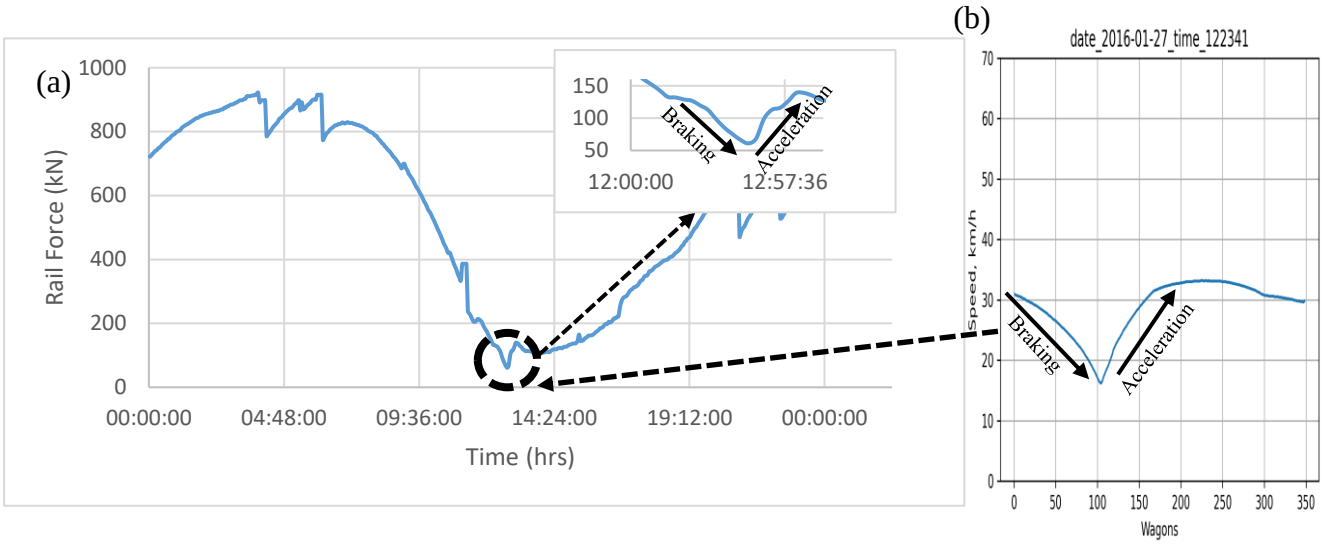

Figure 4.23: (a) Rail Force; (b) Speed Profile

The trains decelerate upon approach of the bridge; thus, the change in speed deceleration while on the bridge is somewhat controlled. However, the acceleration of the train while on the bridge is much more significant as now the train has to accelerate to exit the bridge. In contrast, the change in speed due to acceleration is greater than the change due to deceleration which implies a greater acceleration force is induced on the rails compared to the braking force. However, a braking train during a tension turning point increases the rail forces, while an accelerating train decreases the rail forces; thus, the braking effect is more critical as it causes an increase in the rail forces, making the rail more prone to failure. Thus, the change in the rail forces is directly proportional to the change in speed. The higher the change in speed, the higher the change in the rail forces and the higher the induced horizontal force on the rails. The train speed is independent of the season and the time of day, but the effect of the rail depends on the time of day. Therefore, additional tensile forces should be expected during morning hours and additional compression forces should be expected during afternoon hours when the train is present on the bridge during those times.

4.9 Rail Temperature

As discussed in Section 2.2.4 of the literature, temperature is a major contribution to the additional horizontal forces imposed on the rails. It is common knowledge that low temperatures are expected during sunrise and sunset, while high temperatures are expected during the day. Thus, the low temperature at sunrise influences the rail temperature, which adds additional tension forces on the rails, while high temperatures induce additional compression forces. During the passage of the train, a jump heading in the positive direction is observed on the rail temperature profile. Figure 4.24 shows the annual maximum and minimum rail temperature observed on the left and right rail. The grey and yellow show the maximum rail temperatures, while the blue and orange show the minimum temperature. The rail temperature across the rails differs, with the left rail having the highest and the lowest rail temperatures. This implies that high compression forces are induced on the rails due to high temperatures, while high tensile forces are induced due to low temperatures.

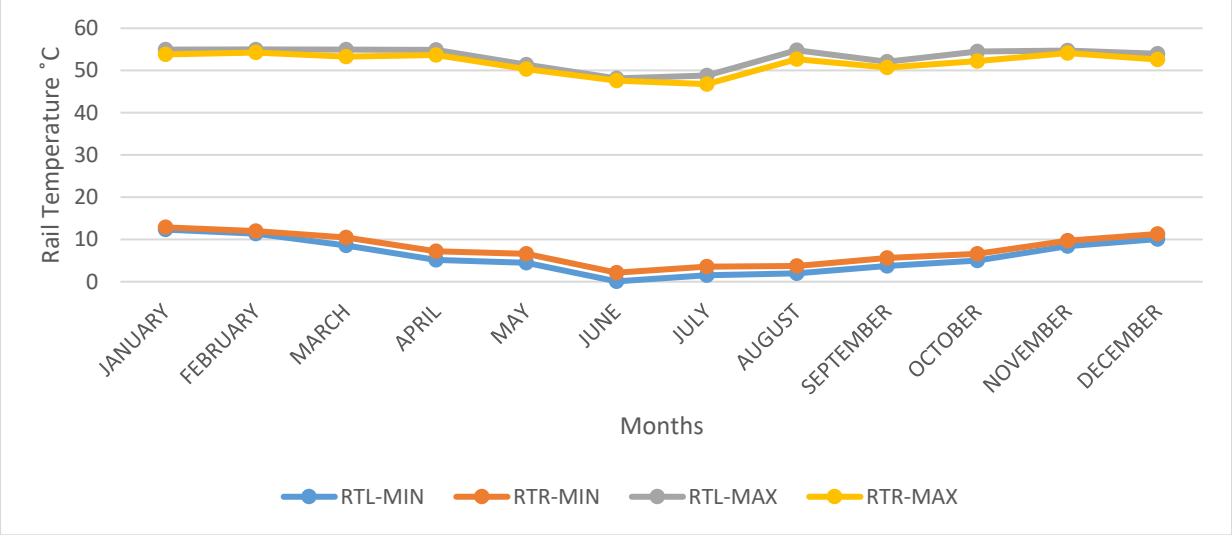

Figure 4.24: Rail temperature

4.9.1 Rail temperature vs. rail forces

The rail forces are widely dependent on the rail temperature, which is influenced by the surrounding temperature and the variation of train speeds. For example, during summer, when the temperature usually is high, the rails are heated and try to expand but are restricted, which causes a build-up of compression stresses on the rails, thus resulting in an additional

longitudinal force on the rails. At the same time, low temperatures cause a tension build-up of forces, which adds to the longitudinal forces on the rails. Figure 4.25 shows the annual Rail Forces vs. Rail Temperature for 2016. During colder months, high tension forces were experienced with the rail forces exceeding the 1400 kN limit. These tension forces are primarily due to trains crossing the bridge during tension peak points while the rail temperature is low. The trains caused a jump in the rail temperature, increasing the rail temperature, which added additional longitudinal forces on the rails, thus increasing the rail forces. The magnitude of the rail temperature jump depends on the train's acceleration variation.

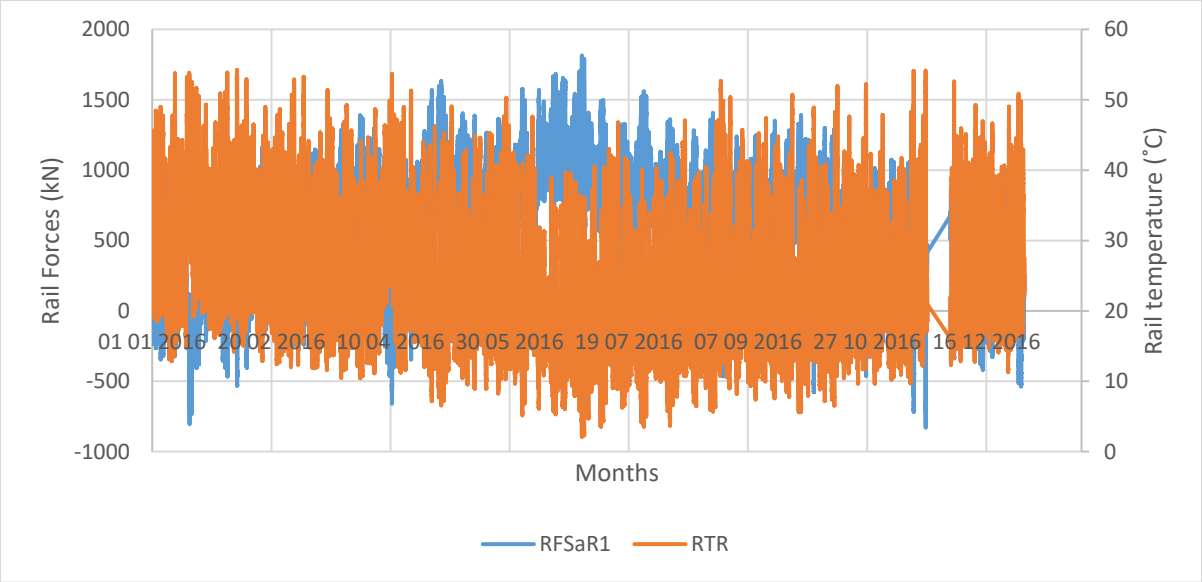

Figure 4.25: Annual rail forces vs. rail temperature

As discussed earlier, the presence of a train on the bridge causes a jump in the rail temperature, which induces an additional force in the rails. The direction of the jumps in the rail forces is dependent on the time a train is present on the bridge. When the train crosses the bridge while the rail forces are at a tension peak, a braking train causes an upward jump in the rail forces showing an increase in rail force, while a downward jump is caused by an accelerating train causing a decrease in the rail forces. However, an accelerating train also causes an increase in rail temperature, which causes an increase in rail temperature. Hence there is an interaction between the train, rail force, and the rail temperature.

Figure 4.26 (a) below shows the rail forces vs. rail temperature, and (a) shows the speed profile of a train that crossed the bridge at 02:54 am on the 30th of July during a turning point in the tension forces. The speed of the train decelerated from 48 km/h to 41 km/h and accelerated from 41 km/h to 48 km/h. The train has a speed change of 7 km/h for both acceleration and deceleration. A tiny jump due to train braking is visible in the upward direction on the rail forces, while a big jump due to acceleration sloping downwards is visible on the rail forces. At the same time, a jump sloping in the upward direction is visible on the rail temperature due to the train acceleration. As a result, the forces jumped from 930 kN to 940 kN upwards, followed by a decrease in the rail forces from 940 kN to 790 kN, and the rail temperature changed from 12°C to 18°C. Resulting in an upward rail force change of 10 kN, a downward rail force change of 150 kN, and a temperature change of 6°C. The train acceleration caused an increase in the rail temperature and a decrease in the rail forces, while the increased rail temperature also caused a decrease in the rail forces; one can assume that the total decrease in rail forces is due to both acceleration and rail temperature. Therefore, the rail force and rail temperature change confirm the interlinkage between the train, track, and rail temperature. Overall, the acceleration of a train and the imposed temperature change decreases the rail forces when the train is present on the bridge during a tension turning point, while they increase the rail forces when the train is at a compression turning point.

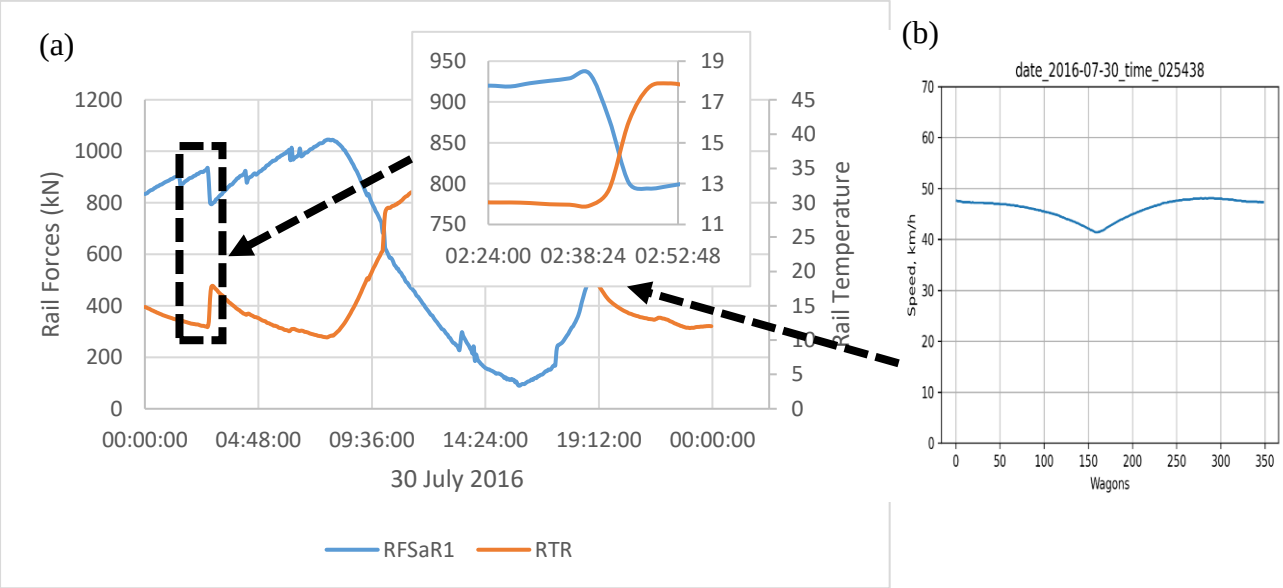

Figure 4.26: (a) Rail force vs. Rail Temperature; (b) Speed profile

4.9.2 Rail Temperature Induced Forces

The thermal induced rail force is determined as a function of change in rail temperature. Figure 4.27 below summarises the rail forces due to temperature and the forces due to traction. The temperature-induced forces were calculated using Equation 2.1 from Section 2.2.4 in the literature, and the force values can be found in Appendix H. It can be seen that the rail forces due to temperature are higher than the forces due to traction; therefore, it can be concluded that the change in rail force is ultimately due to temperature when compared to traction forces. Furthermore, it can be concluded that the higher the temperature change, the higher the induced temperature forces.

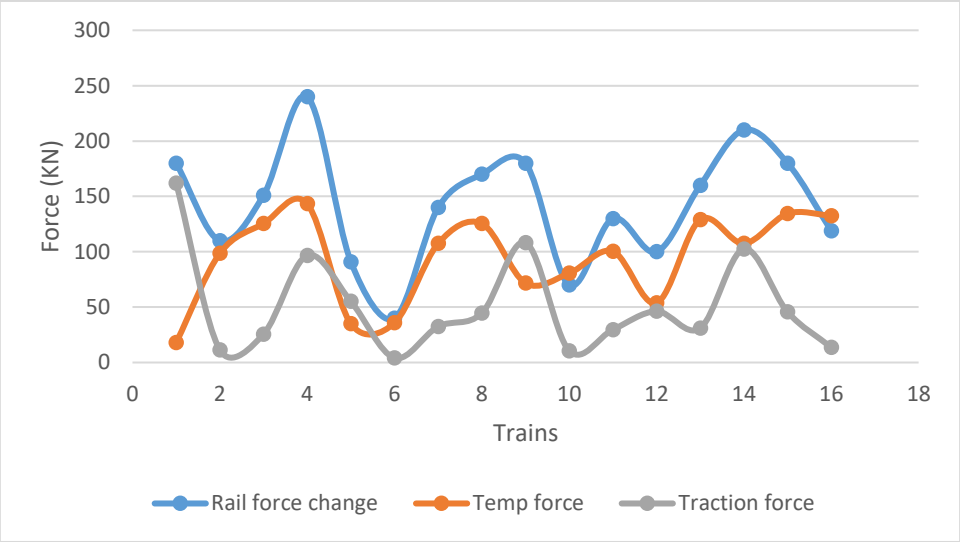

Figure 4.27: Rail Forces Comparison

4.9.3 Descriptive Statistics

Descriptive statistics and regression analysis will be discussed in this subchapter to show the linear relationship between rail forces and rail temperature. The descriptive statistics and regression statistics are shown in Table 4.3, while Figure 4.28 shows the rail forces vs. rail temperature graph. The analysis produced an $R^2 = 0.7385$, which is approximately equal to 73.9%, which means 74% of the variability in rail force is explained by the regression line and the data points are closer to the regression line Thus, demonstrating a stronger correlation between the rail forces and the rail temperatures and further validates the observation.

The kurtosis of the rail force and rail temperature gives negative values of -0.29 and -0.45, respectively, which implies that both rail force and rail temperature have a flat standard deviation. The rail forces were observed to cross the 1400 kN limit when temperatures are between $0℃ - 20℃$. Therefore, high tensile forces are expected during that temperature range, and special care should be taken during such periods in order to avoid rail breakage due to the decreased temperature and high tensile forces. The compression forces are observed to increase as the temperature approaches $60℃$; thus, caution should be taken when temperatures are that high to prevent rail buckling.

Table 4.4: Descriptive Statistics

Descriptive Statistics		
	RF	RT
Mean	609,43	23,26
Standard Error	0,99	0,02
Median	637,00	20,72
Mode	840,00	18,29
Standard Deviation	406,51	9,88
Sample Variance	165253,72	97,57
Kurtosis	-0,29	-0,45
Skewness	-0,24	0,63
Range	2645,00	52,10
Minimum	-830,00	2,14
Maximum	1815,00	54,24
Sum	103498310,00	3950461,17
Count	169828,00	169828,00
Confidence Level(95,0%)	1,93	0,05
Regression Statistics		
Multiple R	0,86	
R Square	0,74	
Adjusted R Square	0,74	
Standard Error	207,86	
Observations	169828,00	

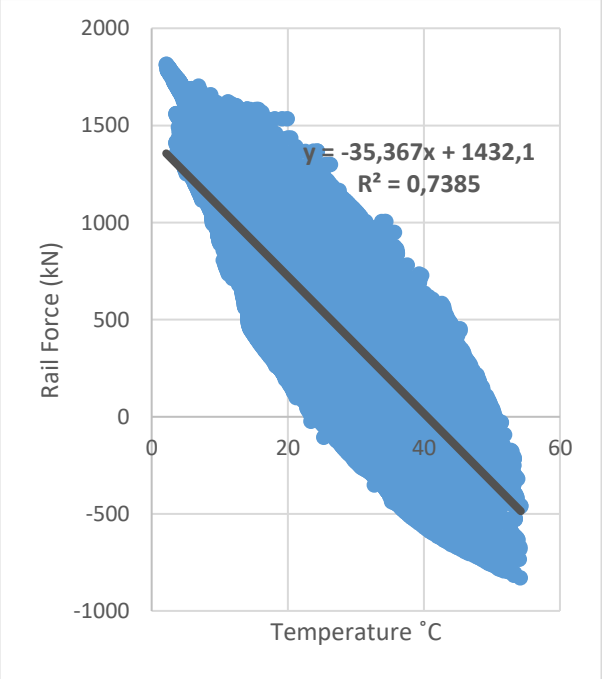

Figure 4.28: Rail Force vs. Rail Temperature

4.10 Deck Deflection

The deck deflection measures the change in length relative to the original deck length. The deck expands during high temperatures and contracts during low temperatures; thus, a positive deck deflection value implies expansion with an increase in compression forces, while a

negative value implies contraction resulting in an increase in tension forces. When the deck expands/contracts, the forces increase towards the center where the expansion joints are located. These forces are then transferred to the rail via friction between the ballast and the concrete deck, thus resulting in additional rail forces in the longitudinal direction. Figure 4.29 shows the annual deck deflection for 2016. It can be seen that during January - February, when the temperature is high, the deck values are above zero, signifying expansion, while during the colder months, June-August, with reduced temperature, the deck values are below zero, signifying contraction. At the same time, it can be observed that the deflection across the four channels is not uniform. A difference in deflection was observed between the Saldanha right rail, and the Saldanha left rail, with Saldanha left rail recording the highest deflection amongst the four deflection channels. The Sishen right rail and left rail were found to have the exact amount of deflection. The horizontal deflection due to the vertical operating loads was within the limits of 3 mm as stipulated in UCI 776.

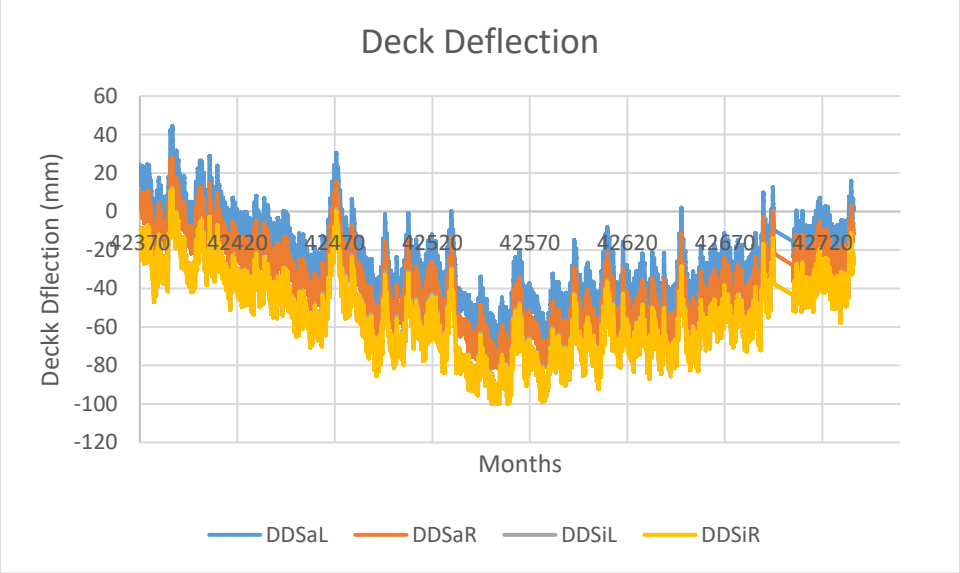

Figure 4.29: Annual Deck Deflection

4.10.1 Deck Deflection vs. Train Speed

The bridge deflection increases with an increased train dynamic loading. Hence, the larger the dynamic loading, the larger the deck deflection. The maximum deflection due to braking was recorded to be 2 mm, and the minimum deflection ranged from 0.1-0.9 mm. The maximum

deflection due to acceleration was observed to range from 1-2 mm, and the minimum deflection due to traction was observed to range from 0.2-0.7 mm. It is important to note that the deflection due to braking of the observed trains was in accordance with UCI Leaflet 776, which stipulates that the deflection due to braking must be less than 5 mm. Hence, it can be deduced that the change in deflection is directly proportional to the change in train speed.

An increased deflection change due to an increased train speed was found to increase the compression forces of the rails, and a reduced deflection change due to train braking was found to increase the tensile rail forces. The short trains in category A and B traveling at a constant speed were found to have deflection change ranging from 0.01-1 mm, and the long trains from category C and D were found to have deflection change ranging from 0.01-2.4 mm. The category D trains have a tremendous change in deflection amongst all categories. The acceleration aspect of category D trains tends to be a major contribution to the rail forces. Figure 4.29 (a) presents the deck expansion for the 5th of July 2016, and Figure 4.30 (b) presents the speed profile of a category D train that crossed the ORV on the 5th of July 2016 at 02:29 am. The train has a deceleration followed by an accelerating speed profile with a v shape. The deck deflection changed from -84.4 mm to 83.4 mm, then from 83.4 mm to 85.8 mm. The change in deflection due to braking was 1 mm, and the change in deflection due to traction was 2.4 mm.

4.10.2 Deck Deflection vs. Rail Force

A closer look at the deck deflection vs. rail forces is presented in Figure 4.30. Again, just like the rail forces, a jump is observed in the deck deflection during the presence of a train on the bridge. The jump is linked to the speed of the train's variations and the surrounding temperature. When the train is braking, a decrease in the deck deflection is experienced by the deck, followed by an increase in the deck deflection. The decrease in the deck deflection causes an expansion in the rail forces, while the increased deck deflection causes a contraction in the deck, thus inducing tensile forces on the rails. The tensile forces contribute to the longitudinal forces on the rails and might cause the bridge to fail. Figure 4.30 (a) shows the deck deflection vs. rail force relation for the 5th of July 2016, while Figure 4.30 (b) shows a speed profile of a train that crossed the bridge on the 5th of July 2016 at 02:29. The decreased deck deflection and increased deck deflection confirm the theory elaborated above.

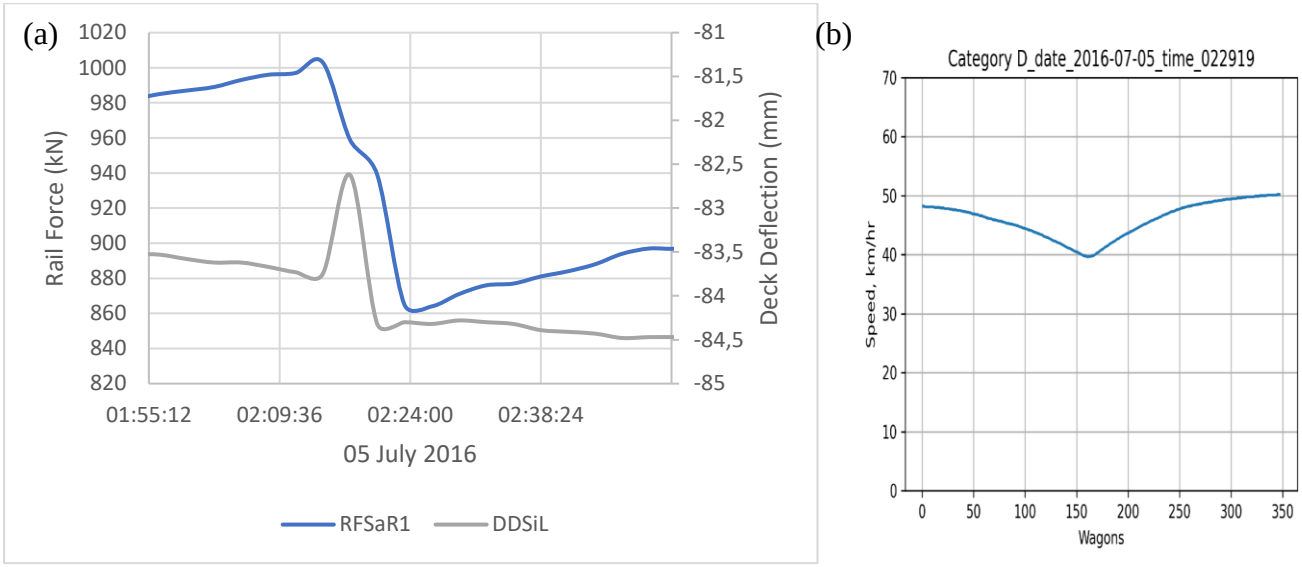

Figure 4.30: (a)- Deck Deflection; (b)- Speed Profile

Figure 4.31 presents the annual relationship between the deck and the rail forces, while Table 4.5 shows the descriptive statistics of the relationship. The relationship gives an R square value of 0.49, which indicates that the points are scattered around the linear regression line. The correlation also gives a negative Kurtosis for the deck deflection and rail forces of -0.58 and -0.29, respectively. This indicates that the deck deflection and the rail forces have a flat distribution. The tensile rail forces increase with an increase in the negative deck values. The rail forces exceed the 1400 kN limit when the deck deflection is around -55 mm. the compression forces should be expected to increase when the deck deflection values increase in the positive direction.

Table 4.5: DD vs. RF Descriptive statistics

Descriptive Statistics		
	DD	RF
Mean	-37,67	609,43
Standard Error	0,05	0,99
Median	-39,29	637,00
Mode	-52,62	840,00
Standard Deviation	21,47	406,51
Sample Variance	461,06	165253,72
Kurtosis	-0,58	-0,29
Skewness	0,28	-0,24
Range	109,44	2645,00
Minimum	-81,20	-830,00
Maximum	28,24	1815,00
Sum	-6397295,27	103498310,00
Count	169828,00	169828,00
Confidence Level(95,0%)	0,10	1,93

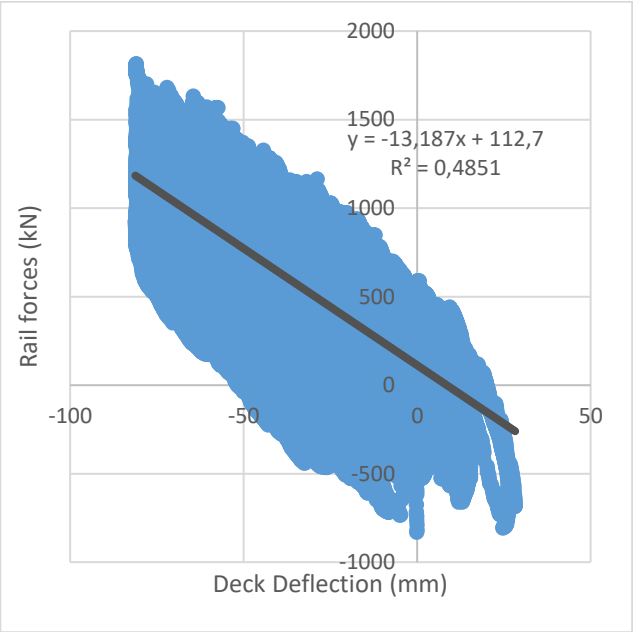

Figure 4.31: Deck Deflection vs. Rail Force

4.10.3 Deck Deflection vs. Rail Temperature

Table 4.6 shows the descriptive statistics of the deck and the rail temperature, while Figure 4.32 shows the relationship between the rail forces and the deck deflection. The relationship shows an R square value of 0.23, which indicates that the regression line explains only 23% of the variation in the deck deflection and the data is scattered around the linear regression line. Thus, only 23% of the rail forces is due to the deck deflection and 77% of it can be assumed to be due to other factors such as speed variation, rail, and ambient temperature.

Table 4.6: DD vs. RF Descriptive statistics

Descriptive statistics		
	DD	RT
Mean	-37,67	23,26
Standard Error	0,05	0,02
Median	-39,29	20,72
Mode	-52,62	18,29
Standard Deviation	21,47	9,88
Sample Variance	461,06	97,57
Kurtosis	-0,58	-0,45
Skewness	0,28	0,63
Range	109,44	52,10
Minimum	-81,20	2,14
Maximum	28,24	54,24
Sum	-6397295,27	3950461,17
Count	169828	169828
Confidence Level(95,0%)	0,10	0,05
Observations	169828	

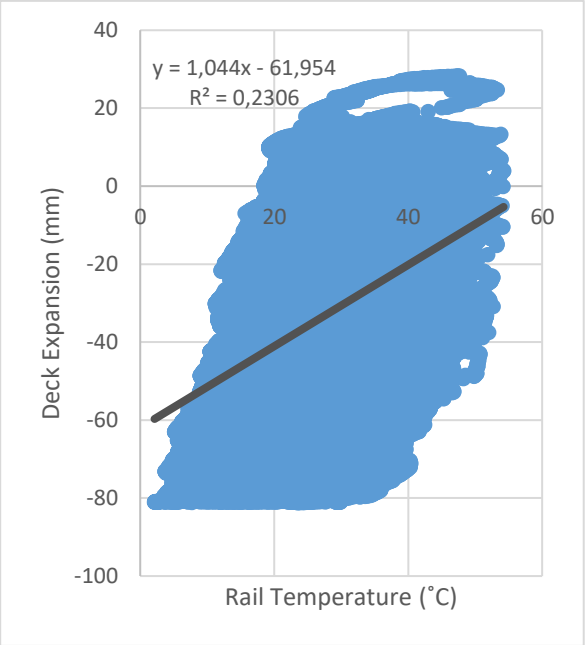

Figure 4.32: Deck Deflection vs. Rail temperature

4.11 Chapter summary

The trains crossing the ORV were categorized into groups, and the category groups depend on the train length and the commodities they carry. Category A consists of short HEP trains with one locomotive consist, and usually carry aggregates and dolomite blocks. Category B trains are also short HEP trains with one locomotive consists which carry manganese ores and ore clinker. Category C trains are long RDP trains with three locomotive consists that predominantly carry manganese ores. Category D trains are also long RDP trains with four locomotive consists and mainly carrying iron and manganese ore. Categories A, B, and E cross the bridge at a constant speed, while C and D cross the bridge at varying speeds. Categories A, B, and E have a constant speed profile. Whereas the loaded trains of category D have a deceleration followed by an accelerating speed profile, the unloaded trains have a decelerating speed profile. The short HEP trains with no speed variation contribute to the dynamic loading of the bridge, and no additional forces are imposed on the rails. At the same time, the RDP trains with speed variations contribute to the rail forces and the dynamic loading of the bridge.

The high rail forces were primarily due to increased temperature changes and speed variations of trains. The deck deflection was deduced to be directly proportional to the speed and the surrounding temperature.

5. CONCLUSION AND RECOMMENDATIONS

5.1 Summary

A total of 4067 trains were analysed for this research. The research characterized the TBI of the ORV by focusing on the speed variations of the crossing trains and the induced rail forces due to speed variation, deck deflection, air temperature, and rail temperature.

5.2 Conclusions

The following conclusions were drawn based on the analysed results:

1. The most frequent train crossing the ORV belongs to category D. The train has six locomotives and 342 wagons, while category B trains were found to be the least trains crossing the ORV. The mass of a single loaded span was relatively close to the beam self-weight. In addition, the loads per axle are well within the maximum axle load limits. Therefore, no wagon was overloaded.
2. The short trains from Categories A, B, and E cross the bridge at constant speeds, while the long trains from categories C, D, and F exhibit speed variation when crossing the bridge. The loaded trains in all categories crossed the bridge at low speed compared to the unloaded trains. The short trains in category F behave similarly to the short trains in category A and B, whereas the long trains in category F behave similarly to the long trains in categories C and D.
3. Slightly higher dynamic forces are expected by the short trains that cross the bridge at high speeds. There is no acceleration and deceleration in the short trains, so we do not expect additional rail forces due to the short trains. Based on this, the longest trains have a significant change in acceleration and deceleration speeds, which implies additional forces in the rails due to acceleration and deceleration.
4. The speed at which the trains cross the bridge is dependent on the commodities hauled by the trains and the train length. Thus, category A and B trains crossed the bridge at higher speeds because they hauled less than category C and D trains.

5. The loaded and the unloaded trains of categories A and B exhibit a constant speed profile. While the loaded trains of category D exhibit a deceleration followed by an acceleration speed profile with a v shape. In contrast, the unloaded trains exhibit a deceleration speed profile with a parabolic shape. The difference in speed profiles was deduced to be due to the ORV's topography. Upon exit of the ORV, the loaded trains are required to climb up a cliff due to the increased elevation, while the unloaded trains travel on a flatter terrain that's sloping down. Hence, explaining the speed profile shapes of the loaded and the unloaded trains.
6. Air temperature is the linkage between the rail forces, rail temperature and deck deflection. Thus, a sudden change in the air temperature will cause a sudden change in the rail forces due to all three parameters being interlinked. The deck deflection and the rail temperature increase with increasing air temperature, with air temperature accounting for 77% and 49% of variability in rail temperature and deck deflection, respectively. While air temperature accounts for 79% of the variability in the rail forces. Speed is not directly affected by air temperature, but when the train transverse the bridge while the rails are experiencing high temperatures the braking effect causes a tremendous increase in the rail forces during such times. High forces should therefore be expected during air temperature peaks.
7. Crossing trains with considerable speed differences of acceleration and deceleration, with acceleration changes ranging from 5-30 km/h and deceleration changes ranging from 5-20 km/h, are primarily responsible for the imposed forces on the rails. The braking and accelerating effect causes alterations in rail forces, rail temperature, and deck deflection, all of which add to additional rail forces. As a result, increased longitudinal forces on the rails are induced by significant speed variations. The imposed acceleration forces are higher than the braking forces, but the braking-imposed forces are the most critical because they cause an increase in tensile and compression forces when the forces are at their peaks, and there is a train on the bridge, whereas acceleration causes a decrease in rail forces at those times. The deck movement forces on the rails were mostly caused by ambient temperature, which had a positive linear relationship. The deck expands when the ambient temperature rises and compresses as the ambient temperature falls. When the rail temperature was between 0-20°C, the deck deflection was above 83 mm in the negative direction, and there was a train on the

bridge, the compression forces were within the given limits of 1100 kN, while the tension forces exceeded the rail force limit of 1400 kN, making the rail more susceptible to failure during winter.

5.3 Recommendations

The track-bridge interaction phenomena is not fully understood; hence, there is a lack of research worldwide.

I. A model should be developed based on the above results to verify the results. The model should include both the lateral and vertical directions.
II. This study showed that the Olifants River Viaduct is prone to high longitudinal forces which are predominantly due to speed variations of the traversing trains and extreme weather conditions. A study based on emergency measure or countermeasures for extreme longitudinal forces should be carried out to ensure the safety of the ORV.

6. REFERENCES

Ahmad, H. A., Hajj, M. R., Inman, D. J., Sandu, C., & Taheri, S. (2013). *Dynamic Braking Control for Accurate Train Braking Distance Estimation under Different Operating Conditions*. Virginia Polytechnic Institute and State University.

Ahmad, S. S., Mandal, N. K., Chattopadhyay, G., & Powell, J. (2013). Development of a unified railway track stability management tool to enhance track safety. *Journal of Rail and Rapid Transit*, *227*(5), 493–516. https://doi.org/10.1177/0954409713501490

Australian Transport Safety Bureau. (2005). *Derailment of Pacific NationalTrain 6MP4 Koolyanobbing, Western Australia and Pacific National Train*. www.atsb.gov.au

Beskhyroun, S., Wegner, L. D., & Sparling, B. F. (2011). Piezo-based weigh-in-motion system for the railway transport. *Structural Control and Health Monitoring*, *19*(2), 199–215. https://doi.org/10.1002/stc.416

Bester, J. F. (2015). The Olifants River Bridge - The Inherent Problem.pdf. *SAICE*, 1–7.

Busatta, F., & Moyo, P. (2015). Vibration Monitoring of a Large Scale Heavy Haul Railway Viaduct. *MATEC Web of Conferences*, *24*, 1–10. https://doi.org/10.1051/matecconf/20152404007

Busatta, F., & Moyo, P. (2016). Lessons learned from the dynamic assessment of railway bridges for heavy haul transport in South Africa. *Insights and Innovations in Structural Engineering, Mechanics and Computation - Proceedings of the 6th International Conference on Structural Engineering, Mechanics and Computation, SEMC 2016, Transnet 2015*, 2028–2033. https://doi.org/10.1201/9781315641645-336

Busatta, F., & Moyo, P. (2018). Assessing the performance of a heavy haul railway viaduct through monitoring traffic loads and dynamic effects. *Experimental Vibration Analysis for Civil Structures.*, *5*, 770–780. https://doi.org/10.1007/978-3-319-67443-8_68

Busatta, F., & Moyo, P. (2019). Heavy haul train dominant frequencies - Insights and practical use. *MATEC Web of Conferences*, 1–8.

Busatta, F., & Pilate, M. (2019). Performance Monitoring of a Prestressed Concrete Railway Viaduct : Implementation of a System and First Results. *MATEC Web of Conferences*, 1–10.

Bush, D. J. (2009). Upgrade of the Sishen to Saldanha iron ore line. *9th International Heavy Haul Conference: "Heavy Haul and Innovation Development,"* 1017–1021.

Esveld, C. (2001). *Modern Railway Track* (Second Edi). https://www.esveld.com

European Committee for Standardization. (2003). *Eurocode 1: Actions on structures, Part 2: General actions, Traffic Loads on Bridges*. *1*(2005), 167.

Florida Department of Transportation. (2013). *Continuous Welded Rail Plan*. https://www.fra.dot.gov/Page/P0123

Freyer RV. (2004). *FORCE MONITORING ON THE OLIFANTS RIVER*. *March 2004*, 1–19.

Hagaman, B. R. (1991). Railways of Australia Track Buckling Project. *Transportation Research Record*, *1289*, 1–10.

Han, D. (2017). *Braking / Traction Assessment for Railway Bridge to AS5100 : 2017*.

Hettasch, G. (2016). *Wheel/rail interaction data report description*. 4–7.

James, G. (2003). *Analysis of Traffic Load Effects on Railway Bridges* [Royal Institute of Technology]. https://doi.org/KTH/BKN/B--70--SE

James, G., & Barry, G. (2009). *Mechanics of materials* (H. Gowans (ed.); 7th ed.). Quebecor World. https://doi.org/10: 0-534-55397-4

Kang, C., Wenner, M., & Marx, S. (2021). Background investigation on the permissible additional rail stresses due to track/bridge interaction. *Engineering Structures*, *228*, 1–12. https://doi.org/10.1016/j.engstruct.2020.111505

Karoumi, R., Wiberg, J., & Liljencrantz, A. (2005). Monitoring traffic loads and dynamic effects using an instrumented railway bridge. *Engineering Structures*, *27*(12 SPEC. ISS.), 1813–1819. https://doi.org/10.1016/j.engstruct.2005.04.022

Kiiza, C. (2019). *Characterisation of Heavy Haul trains*. University of Cape Town.

Kish, A., & Harrison, H. (2011). Track Buckling Hazard Detection and Rail Stress Management. *9th World Congress Railway Research*, 1–10. http://www.railway-research.org/IMG/pdf/c4_kish_andrew.pdf

Kish, A., & Mui, W. (2003). Track buckling research. *Volpe Center*, 1–19. https://rosap.ntl.bts.gov/view/dot/11985

Kish, A., & Samavedam, G. (1991). Dynamic Buckling of Continuous Welded Rail Track: Theory, Tests, and Safety Concepts. *Transportation Research Record*, *1289*, 23–38.

Kish A, Samavedam, G., & Jeon, D. (1993). *Parametric Analysis and Safety Concepts of CWR TRack Buckling* (pp. 1–112). US Department of transport. https://doi.org/dot-vntsc-fra-93-25

Kumar, R., & Upadhyay, A. (2012). Effect of temperature gradient on track-bridge

interaction. *Interaction and Multiscale Mechanics*, *5*(1), 1–12. https://doi.org/10.12989/imm.2012.5.1.001

Kumar, S. (2006). *Study of Rail Breaks : Associated Risks and Maintenance Strategies Study of Rail Breaks : Associated Risks and Maintenance Strategies*. 1–33.

Kuys, W. (2000). Ore Line Capacity Expansion: Conceptual Design of the Railway Line to Increase Capacity. *October*, *85*(12), 1722–1731.

Kuys, W. C. (2009). Ore line capacity expansion: Conceptual design of the railway line to increase capacity. *Proceedings - 9th International Heavy Haul Conference: "Heavy Haul and Innovation Development,"* 941–949.

Mandal, N. K., & Lees, M. (2019). Effectiveness of measuring stress-free temperature in continuously welded rails by Rail Creep Method and Rail Stress Modules. *Engineering Failure Analysis*, *104*(August 2018), 189–202. https://doi.org/10.1016/j.engfailanal.2019.05.032

Maree, H. (2000). *Forces in the railway track structure on the Olifants River Bridge* (pp. 17).

Marks, I. (2001). Management of Continuously Welded Rail Track in Queensland Rail. *7th Intemational Heavy Haul Conference*, 397–402.

Matongo, K. (2018). RELIABILITY BASED LIVE LOADS FOR STRUCTURAL ASSESSMENT OF BRIDGES ON HEAVY-HAUL RAILWAY LINES. *University of Cape Town -Doctoral Thesis*.

Mirković, N. B., Popović, Z. J., Pustovgar, A. P., Lazarević, L. M., & Zhuravlev, A. V. (2018). Management of stresses in the rails on railway bridges. *FME Transactions*, *46*(4), 636–643. https://doi.org/10.5937/fmet1804636M

Mirković, N., Brajović, L., Popović, Z., Todorović, G., Lazarević, L., & Petrović, M. (2021). Determination of temperature stresses in CWR based on measured rail surface temperatures. *Construction and Building Materials*, *284*, 122713. https://doi.org/10.1016/j.conbuildmat.2021.122713

Mitchell, L., & Mandal, N. (2012). *An Investigation into Monitoring Stresses in Continuously Welded Rails Through Stress Free Temperature*. 1–8. https://www.researchgate.net/publication/303805601

Mubarack, C. K. A., & Upadhyay, A. (2021). Stability of continuous welded rail on steel bridge subjected to thermal loading. *Structures*, *34*(August), 4524–4531. https://doi.org/10.1016/j.istruc.2021.10.050

Network Rail. (2021). *Broken Rail*. https://www.networkrail.co.uk/wp-content/uploads/2020/02/Broken-rail.png

Ngwenyama, J. D., Naidoo, P. N., & Mulder, J. M. (2013). *5 Years of Operational Experience and Lessons Learnt with the on South Africa ' s Iron Ore Line*. 796–803.

Ole, Z. K. (2008). *Track Stability and Buckling - Rail Stress Management A dissertation submitted by* (Issue Civil Engineering). University of Southern Queensland.

Piazzaroli, R., Alexandre, C., & Flávio, B. (2019). An SHM approach using machine learning and statistical indicators extracted from raw dynamic measurements. *Latin American Journal of Solid of Structure*, *16*(1998), 1–17. https://doi.org/10.1590/1679-78254942

Ramos, R., Schanack, F., Carreras, G., & de Vena Retuerto, J. (2019). Bridge length limits due to track-structure interaction in continuous girder prestressed concrete bridges. *Engineering Structures*, *196*(109310), 1–8. https://doi.org/10.1016/j.engstruct.2019.109310

Rassõlkin, A., & Hõimoja, H. (2012). Calculation of the Traction Effort of Switching Locomotive. *11th International Symposium "Topical Problems in the Field of Electrical and Power Engineering"*, *1*, 61–65. https://www.researchgate.net/publication/264008124

Salient Systems Inc. (2009). *System and Method for Determining Rail Safety Limits.* (Patent No. US 7,502,670 B2).

Sanjar, Shah;, Ahmad, N., Mandal, N. K., & Chattopadhyay, G. (2011). *Improvement of rail creep data to measure the stress state of a tangent continuously welded rail (CWR) track. January*.

Sanjar, Shah, Ahmad, N., Supervisor, P., Mandal, N. K., & Chattopadhyay, G. (2011). *Ensuring track safety and reducing unnecessary train speed restrictions in hot weather by the application of a unified track stability management tool* [Central Queensland University]. https://hdl.handle.net/10018/917585

Silva, I. J. G., & Karoumi, R. (2015). Traffic monitoring using a structural health monitoring system. *Proceedings of the Institution of Civil Engineers: Bridge Engineering*, *168*(1), 13–23. https://doi.org/10.1680/bren.11.00046

Sung, W. P., Shih, M. H., Lin, C. I., & Go, C. G. (2005). Critical loading for lateral buckling of continuous welded rail. *Journal of Zhejiang University: Science*, *6 A*(8), 878–885. https://doi.org/10.1631/jzus.2005.A0878

Tomas, M. D. (2000). *Wheel Impact Monitoring & Weigh in Motion (WIM_WIM) Systems.pdf* (pp. 1–10).

Transnet Sustainability Report. (2014). Enel Sustainability Report 2014. *Sustainability Report*, 1–216. https://www.enel.com/en-gb/Documents/report2014/Enel_Sustainability_Report_2014.pdf

UIC. (2001). Track/bridge interaction recommendation for calculations. In *internation unioin of railways (UIC)* (Vol. 2).

UIC. (2005). Laying and Maintenance of CWR Track-720. In *Internation Unioin of railways (UIC)* (Issue 2).

UIC. (2009a). Defects in railway bridges and procedures for maintenance: 778-4. In *International Union of Railways (UIC): Vol. 2nd editio*.

UIC. (2009b). Design requirements for rail-bridges based on interaction phenomena between train, track and bridge: 776-2. In *International Union of Railways (UIC)* (Issue June).

Xia, X., & Zhang, J. (2011). Modeling and Control of Heavy-Haul Trains. *IEEE Control Systems*, *31*(4), 18–31. https://doi.org/10.1109/MCS.2011.941403

Yan, B., Dai, G. lian, Guo, W. hua, & Xu, Q. yuan. (2015). Longitudinal force in continuously welded rail on long-span tied arch continuous bridge carrying multiple tracks. *Journal of Central South University*, *22*(5), 2001–2006. https://doi.org/10.1007/s11771-015-2721-5

Zhai, W., Han, Z., Chen, Z., Ling, L., & Zhu, S. (2019a). Train–track–bridge dynamic interaction: a state-of-the-art review. *Vehicle System Dynamics*, *57*(7), 984–1027. https://doi.org/10.1080/00423114.2019.1605085

Zhai, W., Han, Z., Chen, Z., Ling, L., & Zhu, S. (2019b). Train – track – bridge dynamic interaction : a state-of- the-art review. *International Journal of Vehicle Mechanics and Mobility*, *3114*. https://doi.org/10.1080/00423114.2019.1605085

Zhai, W., Xia, H., Cai, C., Gao, M., Li, X., Guo, X., Zhang, N., & Wang, K. (2013). High-speed train–track–bridge dynamic interactions–Part I: Theoretical model and numerical simulation. *International Journal of Rail Transportation*, *1*(1), 3–24. https://doi.org/10.1080/23248378.2013.791498

Žnidarič, A., Kalin, J., Kreslin, M., Favai, P., & Kolakowski, P. (2016). Railway Bridge Weigh-in-Motion System. *Transportation Research Procedia*, *14*, 4010–4019. https://doi.org/10.1016/j.trpro.2016.05.498

7. APPENDICES

Appendix A: Python Scripts

```
4
5   @author: Emilia Joyce Mupwedi
6   """
7
8   import numpy as np
9   import glob
10  import logging
11
12  selectionCriteria = ["SLK.SLK1.L04.WIM.01"] # enter criteria
13  criteria = len(selectionCriteria)
14
15  def readingFolderFile(file):
16      for everySelectionCriteria in range(criteria):
17          with open(file) as f:
18              empty = []
19              for everyLine in f:
20                  lineExtract = everyLine.strip()
21                  empty.append(lineExtract)
22              selection = [everyLine for everyLine in empty if selectionCriteria[everySelectionCriteria] in everyLine]
23
24      return selection
25
26  empty2 = []
27  theFiles = glob.glob("*.csv")
28  for eachFile in range(len(theFiles)):
29      outputAllFiles = readingFolderFile(theFiles[eachFile])
30      for output in outputAllFiles:
31          lineExtract2 = output.strip()
32          empty2.append(lineExtract2)
33  p = open("cout.log", "w").close()
34  for outputLines in empty2:
35      print(outputLines, file=open("cout.log", "a"))
36
```

Figure 7.1: Screenshot of the data extraction

```
@author: Emilia Joyce Mupwedi
"""

import numpy as np
import glob
import logging
import re
import matplotlib.pyplot as plt

emptyTarget = []
theTargetFile = glob.glob("*.txt")
print("reading single file: {}".format(theTargetFile[0]))

def readingTargetFile(file):
    with open(file) as l:
        empty0 = []
        for everyLine in l:
            lineTargetExtract = everyLine.strip()
            empty0.append(lineTargetExtract)
        selectionTarget = [everyLine for everyLine in empty0]
    return selectionTarget

for eachTargetFile in range(len(theTargetFile)):
    outputAllTargetFiles = readingTargetFile(theTargetFile[eachTargetFile])

    for output in outputAllTargetFiles:
        lineExtract0 = output.strip()
        emptyTarget.append(lineExtract0)

emptyTimeList2 = []
for eachOne in emptyTarget:
    bro = str(eachOne[33:41])
    emptyTimeList2.append(bro)
    emptyTimeList = list(set(emptyTimeList2))

emptyTimeList = [timeEntry for timeEntry in emptyTimeList if ":" in timeEntry]
```

Figure 7.2: Screenshot of the individual train extraction and plotting of the speed profile script

```
41
42  for eachEntry in range(len(emptyTimeList)):
43      selectionCriteria = [str(emptyTimeList[eachEntry])]
44      criteria = len(selectionCriteria)
45      def readingFolderFile(file):
46          for everySelectionCriteria in range(criteria):
47              with open(file) as f:
48                  empty = []
49                  for everyLine in f:
50                      lineExtract = everyLine.strip()
51                      empty.append(lineExtract)
52                  selection = [everyLine for everyLine in empty if selectionCriteria[everySelectionCriteria] in everyLine]
53
54          return selection
55      empty2 = []
56      theFiles = glob.glob("*.txt")
57      for eachFile in range(len(theFiles)):
58          #print(eachFile)
59          outputAllFiles = readingFolderFile(theFiles[eachFile])
60          #print(outputAllFiles)
61          for output in outputAllFiles:
62              lineExtract2 = output.strip()
63              empty2.append(lineExtract2)
64      #print(empty2)
65      fileName = str(emptyTimeList[eachEntry][0:2])+str(emptyTimeList[eachEntry][3:5])+str(emptyTimeList[eachEntry][6:8])
```

Figure 7.3: Screenshot of the individual train extraction and plotting of the speed profile script cont.

```
66
67      print("plotting to speed vs wagons graph {i}".format(i = eachEntry))
68      #speed plot
69      speedPlot = [float(re.findall(r"[-+]?\d*\.\d+|\d+", outputLines)[-1]) for outputLines in empty2 if "Speed" in outputLines]
70      dateData = [str(re.findall(r"(\d+-\d+-\d+)", outputLines)[0]) for outputLines in empty2 if "Speed" in outputLines][0]
71      #print(speedPlot)
72      linePlot = np.linspace(1, len(speedPlot), len(speedPlot)).tolist()
73      fig = plt.figure()
74      ax = fig.add_subplot(111)
75      strainPlot = ax.plot(linePlot, speedPlot)
76      plt.title("date_{date}_time_{time}".format(date = dateData, time = fileName))
77      plt.ylabel('Speed, km/hr')
78      plt.xlabel('Wagons')
79      speedPlotMax = max(speedPlot)
80      speedPlotMin = min(speedPlot)
81      lineMax = linePlot[speedPlot.index(speedPlotMax)]
82      lineMin = linePlot[speedPlot.index(speedPlotMin)]
83      ax.set_ylim(0,70)
84      ax.grid()
85      plt.savefig("traintime_speed_{}".format(fileName), dpi=300)
86      plt.show()
87
88      fileName = str(emptyTimeList[eachEntry][0:2])+str(emptyTimeList[eachEntry][3:5])+str(emptyTimeList[eachEntry][6:8])
89      for outputLines in empty2:
90          print(outputLines, file=open("train_time_{}.txt".format(fileName), "a"))
91          folderOutput = "".join(sorted(outputAllFiles))
92          print(folderOutput, file=open("outputFile.txt", "w"))
93
94  print("")
95  print("DONE!")
```

Figure 7.4: Screenshot of the individual train extraction and plotting of the speed profile script cont.

```
@author: emiliamupwedi
"""

import numpy as np
import glob
import logging
import os
import pandas as pd
import datetime as dt
from datetime import datetime
import matplotlib.pyplot as plt
import matplotlib.dates as dates

emptyTarget = []
theTargetFile = glob.glob("*.xlsx")
dfs = pd.read_excel(theTargetFile[0], sheet_name=None)
n = 6 # number of columns to plot (count from left-most colun in excel)
default = os.getcwd()

for key in dfs:
    sheet = dfs[key]
    sheet['Date'] = sheet['Date'].astype(str)
    # date = dateIntermediate
    date = list(set([x[0:10] for x in sheet['Date'].to_list()]))
    time = [y[11:len(y)] for y in sheet['Date'].to_list()]
    dateTime = [z for z in sheet['Date'].to_list()]
    print(len(date))

```

Figure 7.5: Screenshot of the deck deflection, rail forces, rail temperature, & ambient temperature plotter script

```
33
34  for everyDay in date:
35      if not os.path.exists("{league}".format(league = everyDay)):
36          os.makedirs("{league}".format(league = everyDay))
37      os.chdir("{league}".format(league = everyDay))
38      dateData = [x for x in dateTime if everyDay in x]
39      for key in dfs:
40          sheet = dfs[key]
41      plotData = sheet[sheet['Date'].str.contains(everyDay)]
42      dateDataPlot = []
43      for everyEntry in dateData:
44          year,month,day = everyEntry[0:10].split("-")
45          hour,minute,second = everyEntry[11:19].split(":")
46          dateDataPlot.append(dt.datetime(int(year), int(month), int(day), int(hour), int(minute), int(second)))
47      plotData2 = plotData.iloc[:, 2:n]
48      for column in plotData2.columns:
49          datePlot = np.array(plotData['Time'].to_list())
50          dummy = np.array(plotData['Time'].dt.strftime('%H-%M-%S').to_list())
51          # for them in plotData['Time'].to_list():
52          againPlot = dates.date2num(plotData['Time'].to_list())
53          dataPlot = np.array(plotData2[column].to_list())
54          plt.rcParams['axes.labelsize'] = 13
55          plt.rcParams['xtick.labelsize'] = 13
56          plt.rcParams['ytick.labelsize'] = 13
57          fig, ax = plt.subplots(figsize=(13,10))
58          if len(column.split(".")) > 1:
59              colName = str(column.split(".")[0] + column.split(".")[1])
60          else:
61              colName = str(column.split(".")[0])
62          nameFig = str("{day}_{col}".format(day = everyDay, col = colName))
63          strainPlot = plt.plot(datePlot, dataPlot)
64          myFmt = dates.DateFormatter('%H-%M-%S')
65          ax.xaxis.set_major_formatter(myFmt)
66          plt.gcf().autofmt_xdate()
67          plt.title(nameFig.split("_")[0]+" "+nameFig.split("_")[1])
68          plt.ylabel('Deck Expansion (mm)')
69          plt.xlabel('Time')
70          ax.grid()
71          plt.savefig("{}_Plot".format(nameFig), dpi=600)
72          plt.show()
73      os.chdir(default)
```

Figure 7.6: Screenshot of the deck deflection, rail forces, rail temperature, & ambient temperature plotter script cont.

Appendix B: Wagon loads

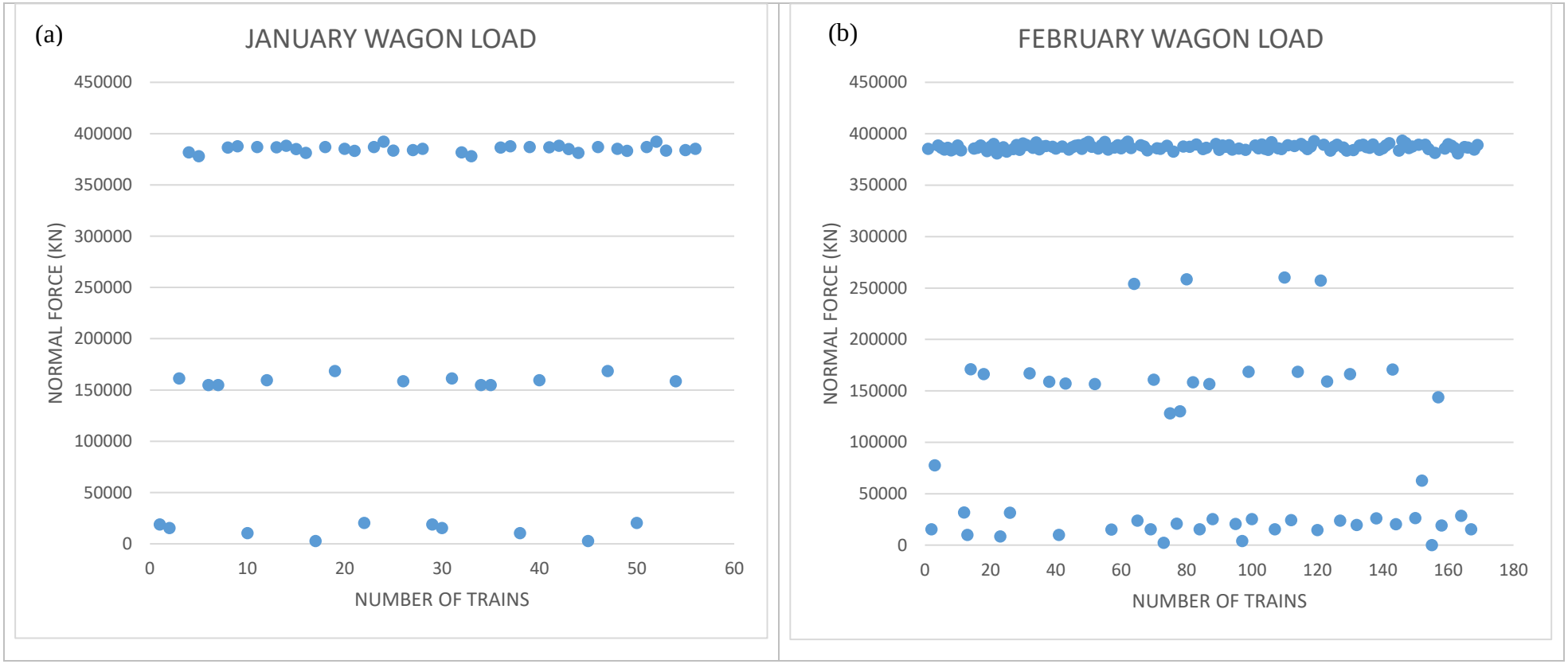

Figure 7.7: Wagon Loads - (a) January & (b) February

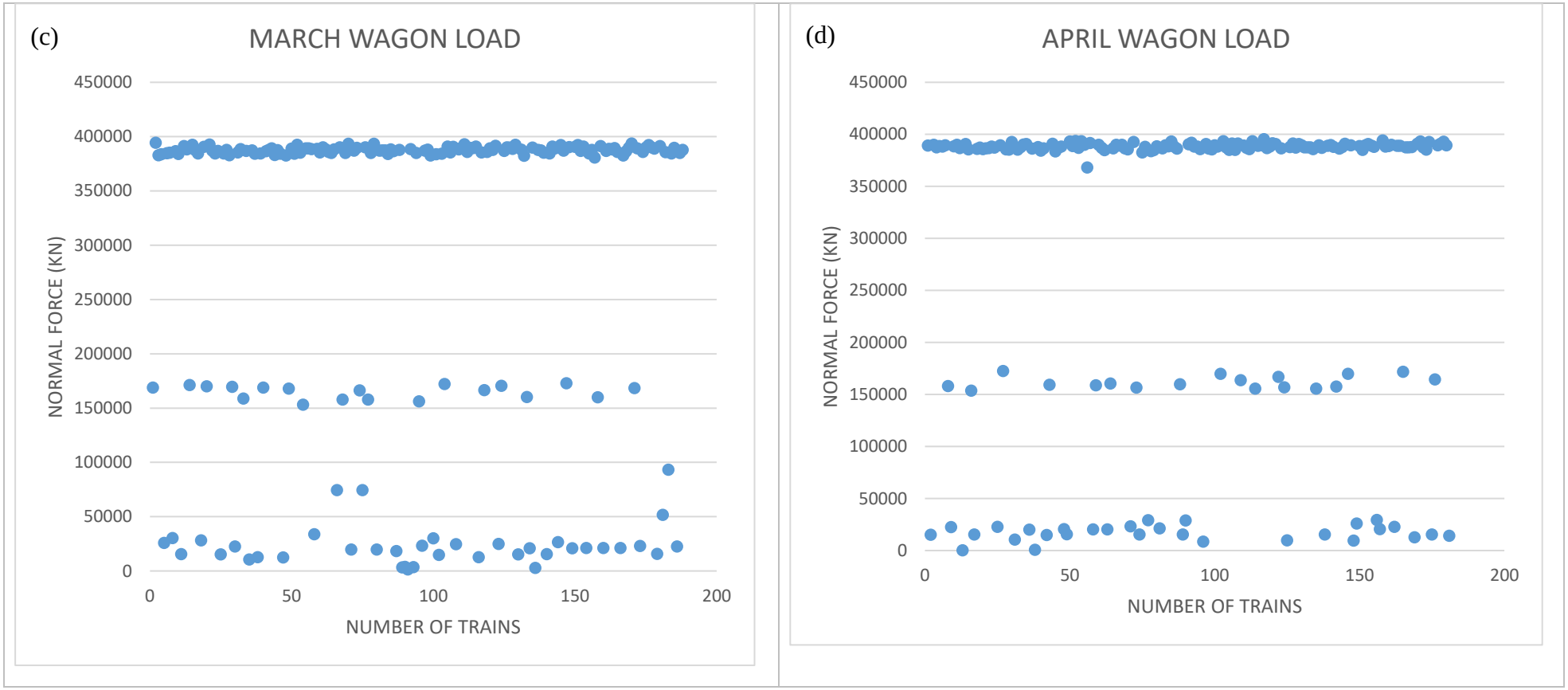

Figure 7.8: Wagon Loads - (c) March & (d) April

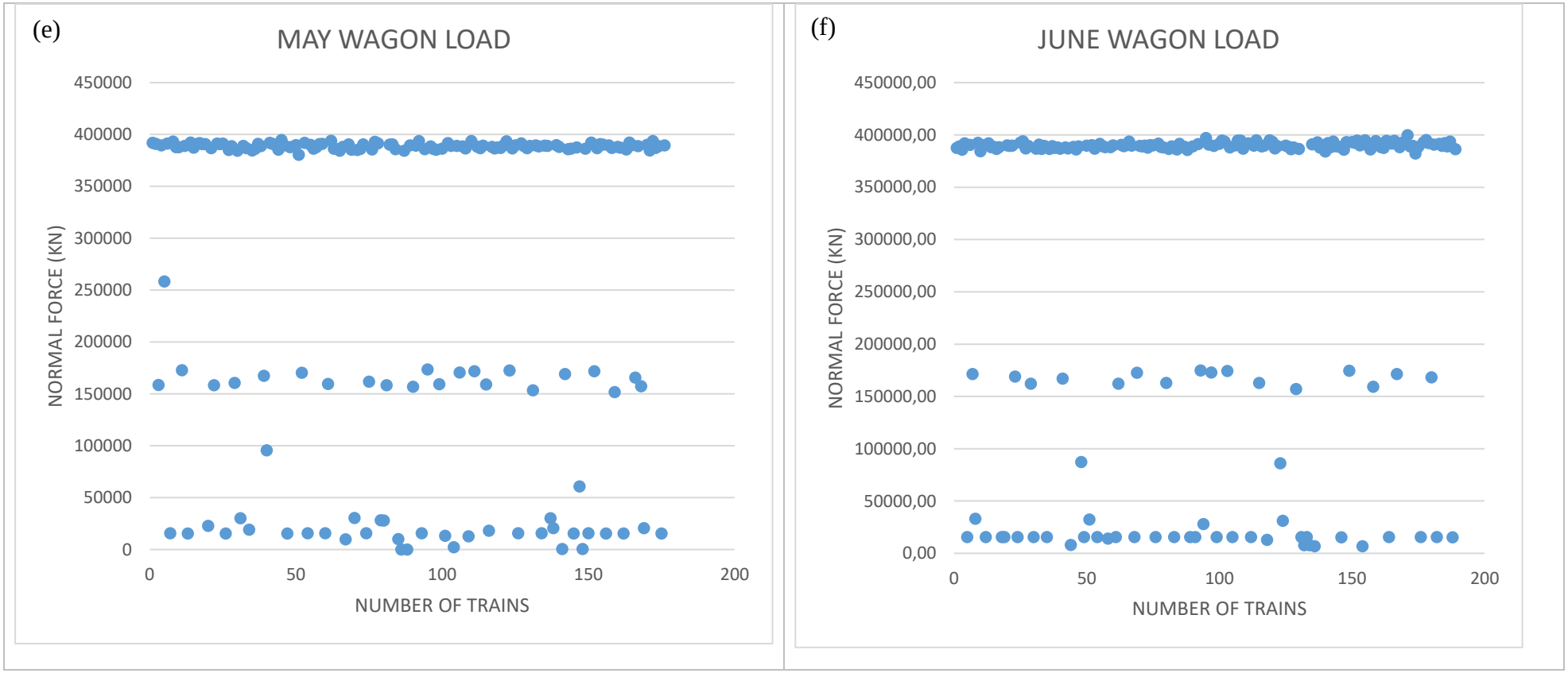

Figure 7.9: Wagon Loads - (e) May & (f) June

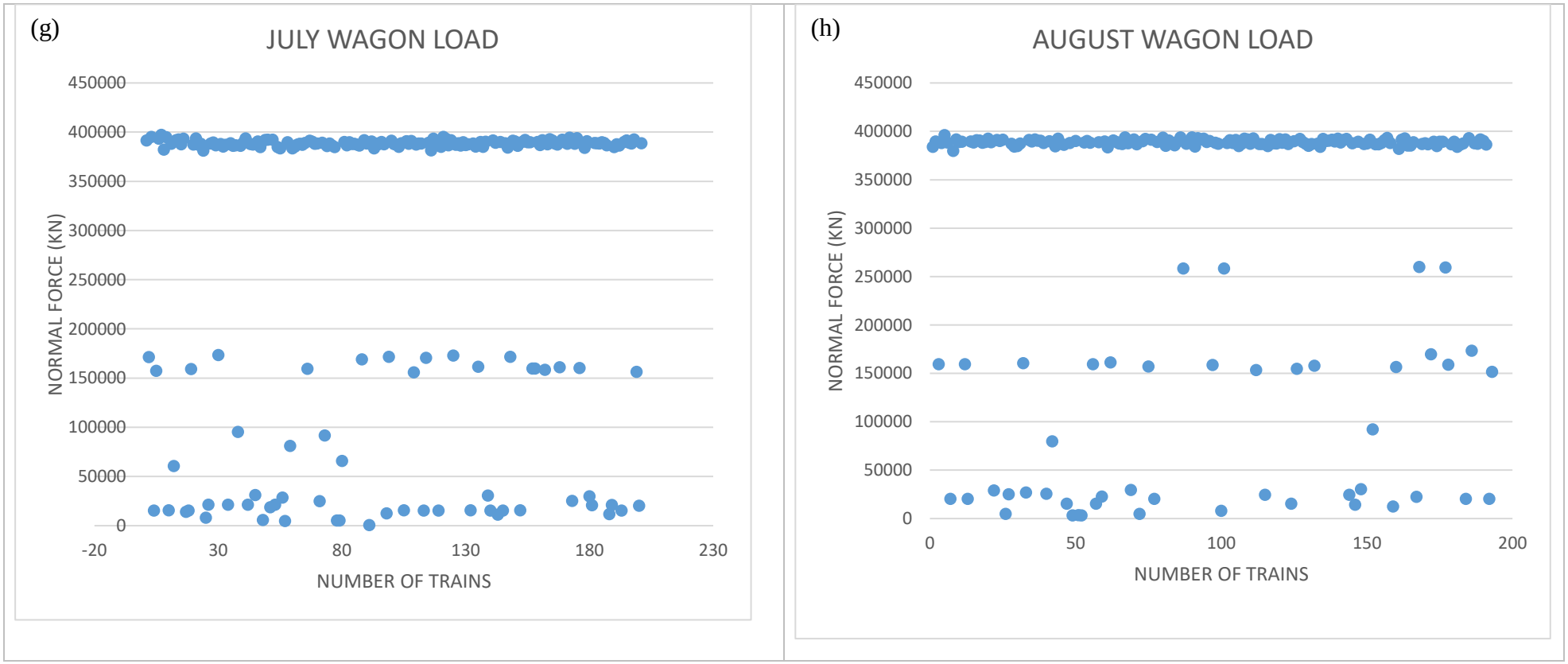

Figure 7.10: Wagon Loads - (g) July & (h) August

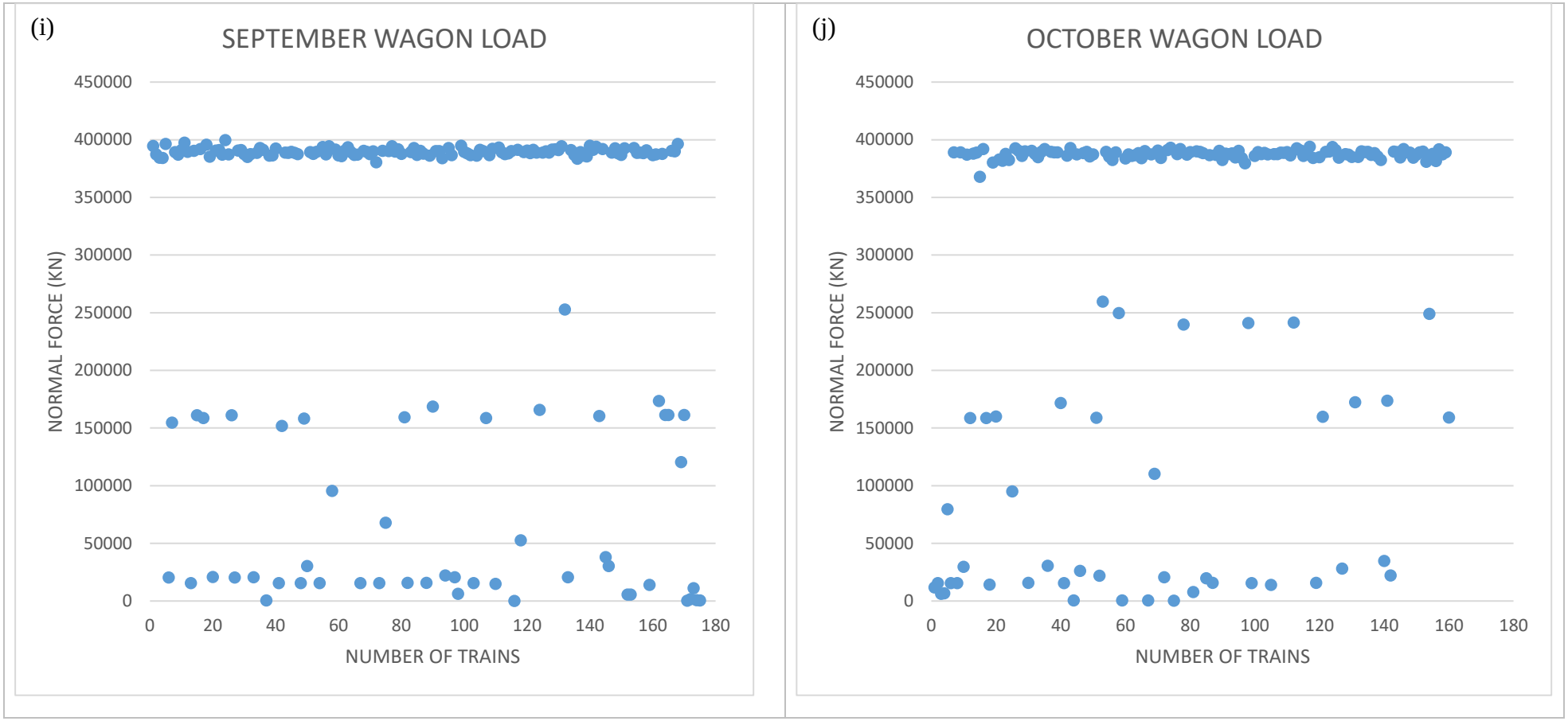

Figure 7.11: Wagon Loads - (I) September & (J) October

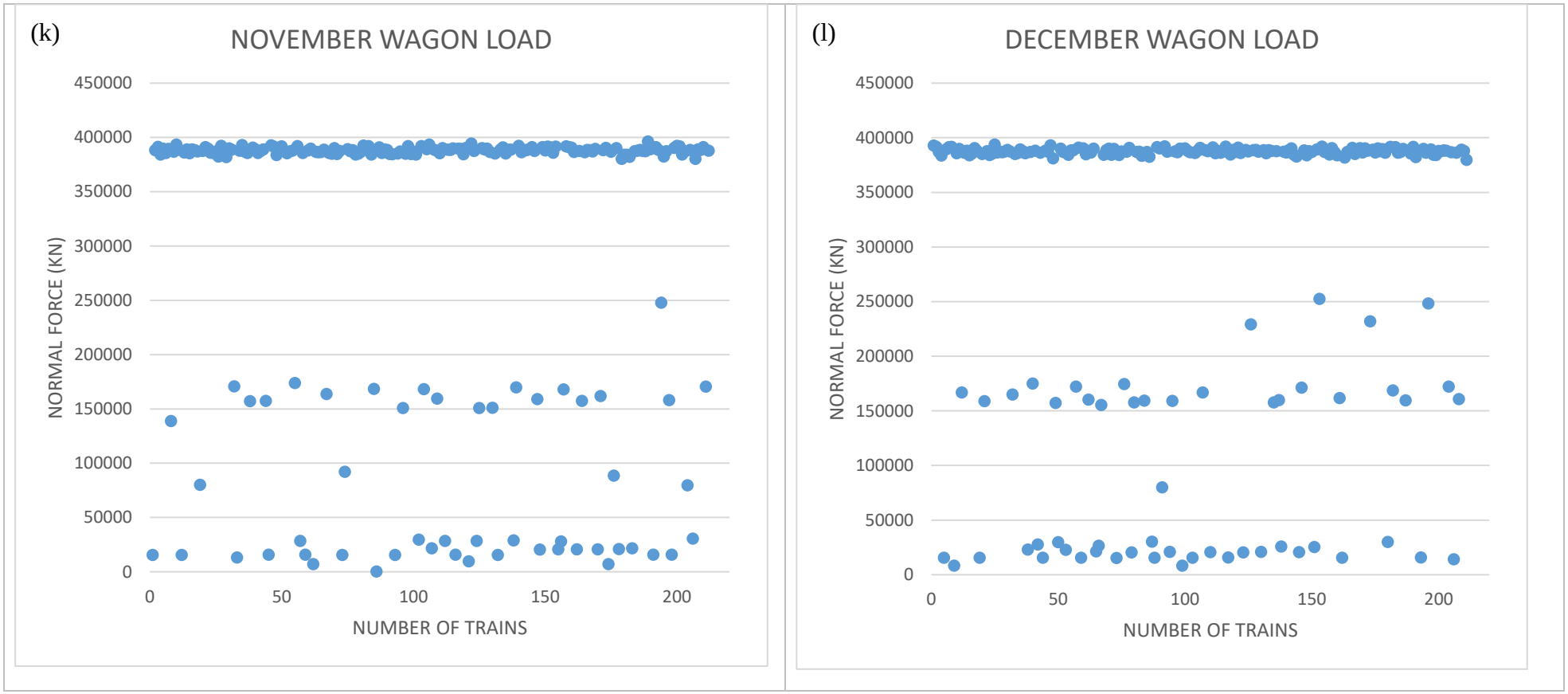

Figure 7.12: Wagon Loads. (k) November & (l) December

Appendix C: Speeds Statistical Summaries

Table 7.1: Monthly Statistical Summaries

		A		B		C		D		E		F	
		Loaded	**Unloaded**	**Loaded**	**Unloaded**	**Loaded**	**Unloaded**	**Loaded**	**Unloaded**	**Loaded**	**Unloaded**	**Loaded**	**Unloaded**
JANUARY	MEDIAN	42	47,8			40,8	46,5	46,1	48,2		50,2		51,1
	MAX	53,5	48,2			49,5	49,8	53,4	55,8		50,3		51,4
	MIN	21,2	26,6			25,1	25,4	12,3	24,8		50,1		50,6
	MEAN	36,83	40,77			39,93	42,91	44,25	46,79		50,2		51,1
	MODE	26,2	48,1			45,5	46,8	47,9	48,8		50,3		51,3
FEBRUARY	MEDIAN	43	47,7	46,55	47,8	44,7	47,8	46,3	47,8	46,9	45,2		
	MAX	49,7	54,1	48,9	49,4	53,9	60,7	56,2	61,5	47	45,5		
	MIN	27,3	0,1	25,8	40,1	33,5	40,6	25,8	22,5	46,8	44,44		
	MEAN	41,37	46,85	43,11	46,7	44,35	47,57	45,59	47,58	46,9	45,01		
	MODE	46,8	48,5	46,9	49,1	48,9	48,2	47,3	48,2	46,8	45,5		
MARCH	MEDIAN	42,1	47,1	42,4	48	45,6	47,1	46,3	47,9	47,3			
	MAX	52,2	52,5	43,3	50,1	54,5	51,7	59,6	64,1	47,3			
	MIN	9,2	37,6	39	44,7	38,7	38	15,1	17	47,3			
	MEAN	40,66	47,23	42,06	48,06	45,62	46,52	45,41	47,83	47,3			
	MODE	44,5	46,4	43	48	44	47,3	48,2	48,2	47,3			
APRIL	MEDIAN	42,8	47,6		47,2	46,5	47,4	46,1	47,7	42,8	45,75	43,2	
	MAX	59,9	61		48,8	54,7	51,4	60	55,1	45,8	45,8	47,2	
	MIN	4,8	30,4		40,8	10,4	39,3	5,5	9,8	42	45,7	35,5	
	MEAN	42,03	47,27		46,2	44,01	46,99	45,23	46,83	43,74	45,75	42,4	

Table 7.2: Monthly Statistical Summaries cont.

	MODE	44,9	44,5		47,3	47,2	48,9	48,2	48,2	42,8	45,7	45,2	
MAY	MEDIAN	41,6	46,8	39,7	48,2	45,6	47,3	46,1	47,5	44,6	48,75		
	MAX	50,8	53,2	43	49,9	54	53,5	58,7	59	49,8	55,4		
	MIN	31,2	38	35,8	42,7	24,4	39,6	6,8	26,1	43,3	42		
	MEAN	41,69	46,68	39,63	47,9	44,83	46,76	45,21	27,18	45,9	48,72		
	MODE	44,6	45,8	42,8	48,8	48,2	48,2	48,2	48,2	43,4	55,4		
JUNE	MEDIAN	40,2	46,4	45,4	46,9	43,8	47,9	45,1	47,3	44,5	50,84		
	MAX	48,7	54	47	50,3	51,4	53	54,8	59,7	45,9	52,19		
	MIN	8,2	12,2	34,8	8,8	11,8	9	3,2	9,7	38,5	16		
	MEAN	34,71	44,5	41,56	39,45	42,09	45,1	41,89	42,94	43,01	44		
	MODE	41,7	46,4	45,7	48,8	44	48,2	47,3	48,2	44,6	51,4		
JULY	MEDIAN	44,3	46,3	47,15	47,4	45,8	46,3	45,8	47,5	42,55	48,95		
	MAX	50,3	55,2	48,3	50,4	49,7	52,8	58,6	55,2	47,6	48,8		
	MIN	12	29,8	45,4	43,6	31,1	30,2	2,1	7	37,4	46,4		
	MEAN	42,49	45,61	47,01	47,59	44,92	45,61	44,34	45,92	42,53	48,09		
	MODE	45,5	44,5	47,3	47,3	45,3	48,2	48,2	48,2	37,6	47,7		
AUGUST	MEDIAN	45,1	46,8	45,1	48,9	45,4	47,3	46,1	47,8	45,65	49		
	MAX	56,8	54,2	48,2	49,5	53,8	51,6	58,3	61,4	45,7	49		
	MIN	28,2	39,5	43,4	40,8	34,1	32	14,2	20,8	45,6	49		
	MEAN	44,25	46,32	45,99	48,03	45,09	46,79	45,26	47,43	45,65	49		
	MODE	46,8	48,2	48,2	49,1	43,2	48,9	48,2	48,2	45,6	49		
	MEDIAN	45,1	46,8	45,9	47,1	43,8	46,7	45,7	47,6	63,2	44,7		

Table 7.4: Monthly Statistical Summaries cont.

SEPTEMBER	MAX	50,2	51,9	48	48,9	51	54,8	54,6	56,8	63,4	47,8		
	MIN	3,7	14,3	25,2	42,7	30,5	35	11,1	18,9	46,6	35,3		
	MEAN	43,55	45,76	37,25	42,7	43,1	45,95	44,67	46,9	59,96	43,99		
	MODE	45,3	48,2	46,2	47,7	43	48,5	48,2	48,2	63,4	47,6		
OCTOBER	MEDIAN	45,6	46,85	47,4	49	44,9	46,5	46,1	47,3				
	MAX	49,7	52,9	49,7	50	50,2	52,4	57,3	64,9				
	MIN	39,5	30,9	36,6	46,1	34,6	28,9	24,8	17,3				
	MEAN	45,41	45,12	44,44	48,8	43,87	45,81	45,36	46,75				
	MODE	47,6	47	47,8	49,1	45,9	46,4	48,2	48,2				
NOVEMBER	MEDIAN	43,9	47,1	45,8	48	46,1	47,5	46,1	48	48,85	48		
	MAX	51,5	54	49,4	52,4	55,1	53,6	64,5	55,9	48,9	48		
	MIN	28,9	39,8	35,8	44,4	35,2	37,5	17,8	26	48,8	48		
	MEAN	42,63	46,66	44,01	48,19	45,64	47,09	45,56	47,4	48,85	48		
	MODE	46,7	47	38	48,1	44,2	48,9	47,3	48,2	48,8	48		
DECEMBER	MEDIAN	45,5	47,1		45,7	43,3	47,4	46	47,9				
	MAX	56,3	163,2		49,6	53,2	55,6	57,9	62				
	MIN	32,8	7,3		33,2	28,5	23,7	26,1	23,5				
	MEAN	44,71	46,1		44,88	43,35	46,5	45,42	47,43				
	MODE	39,3	47,1		49,1	37,6	48,2	46,8	48,2				

Appendix D: Speed Profiles

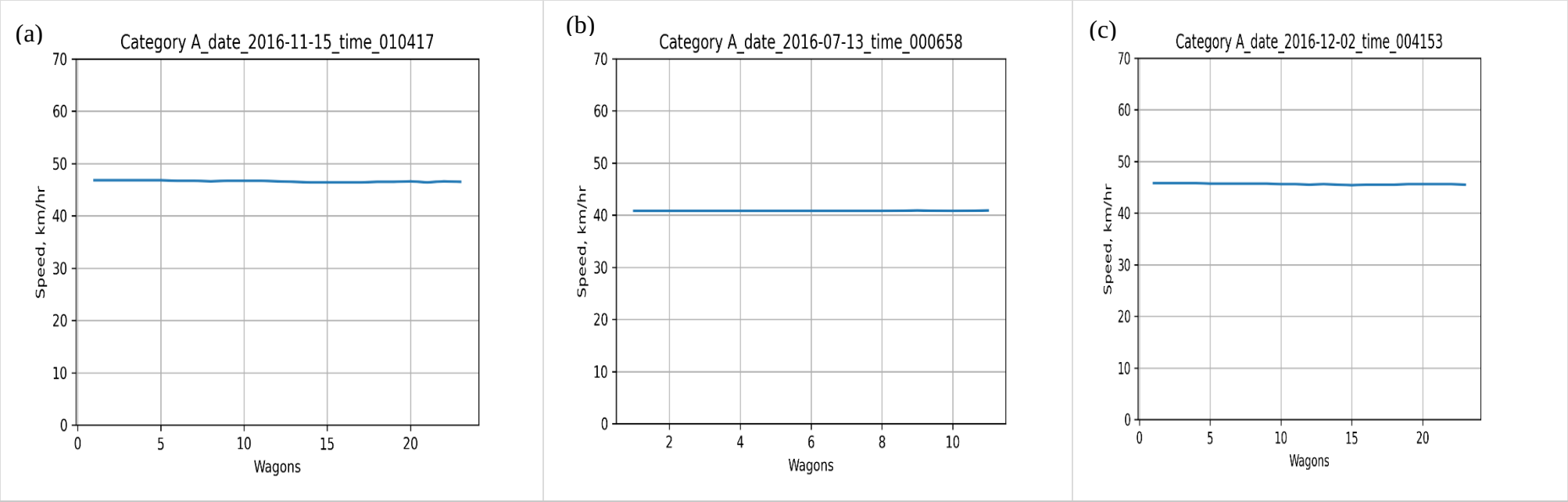

Figure 7.13: Loaded Category A Speed Profiles (a-c)

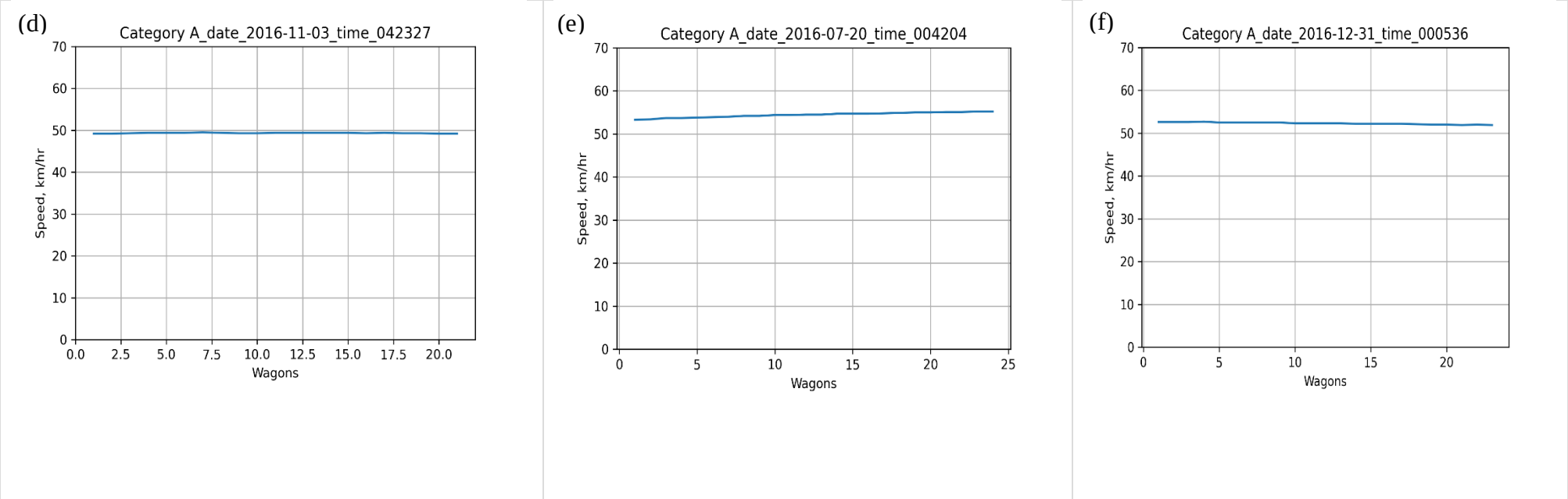

Figure 7.14: Unloaded Category A Speed Profile (d-f)

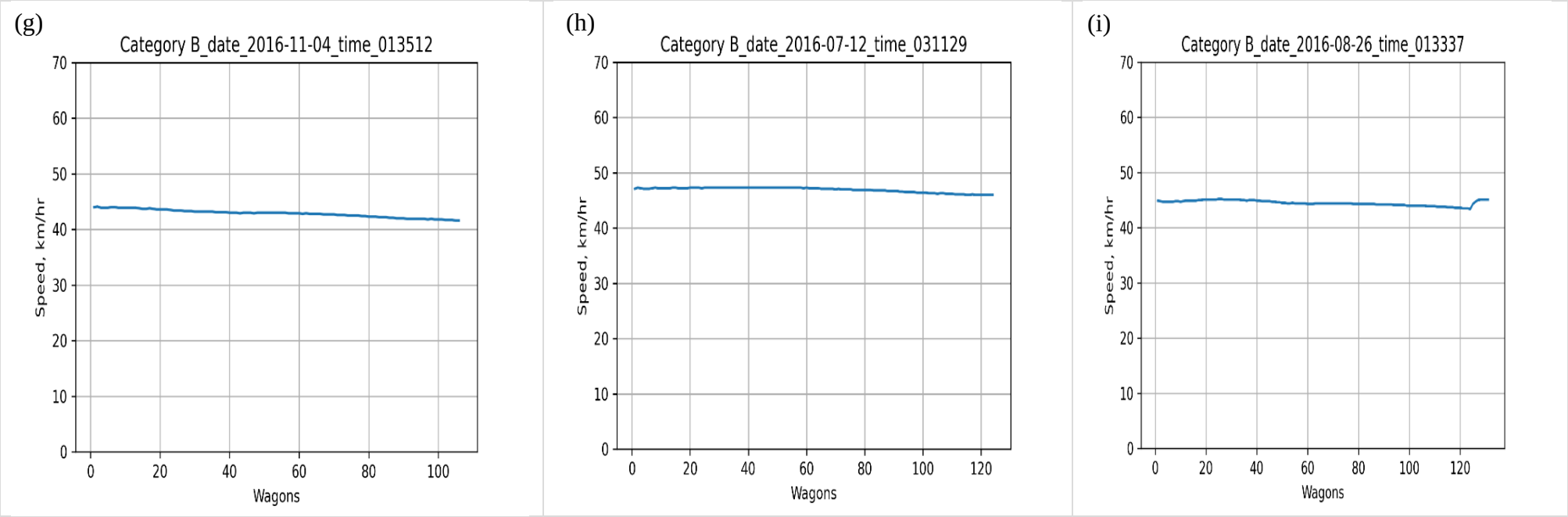

Figure 7.15: Loaded Category B Speed Profiles (g-i)

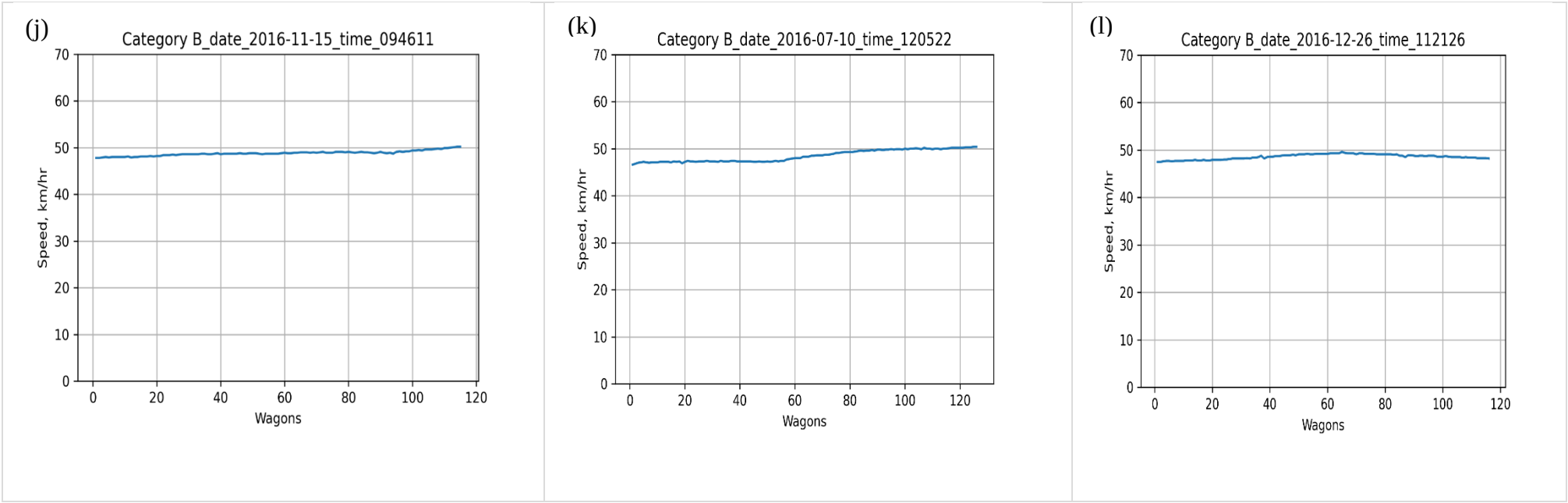

Figure 7.16: Unloaded Category B Speed Profiles (j-l)

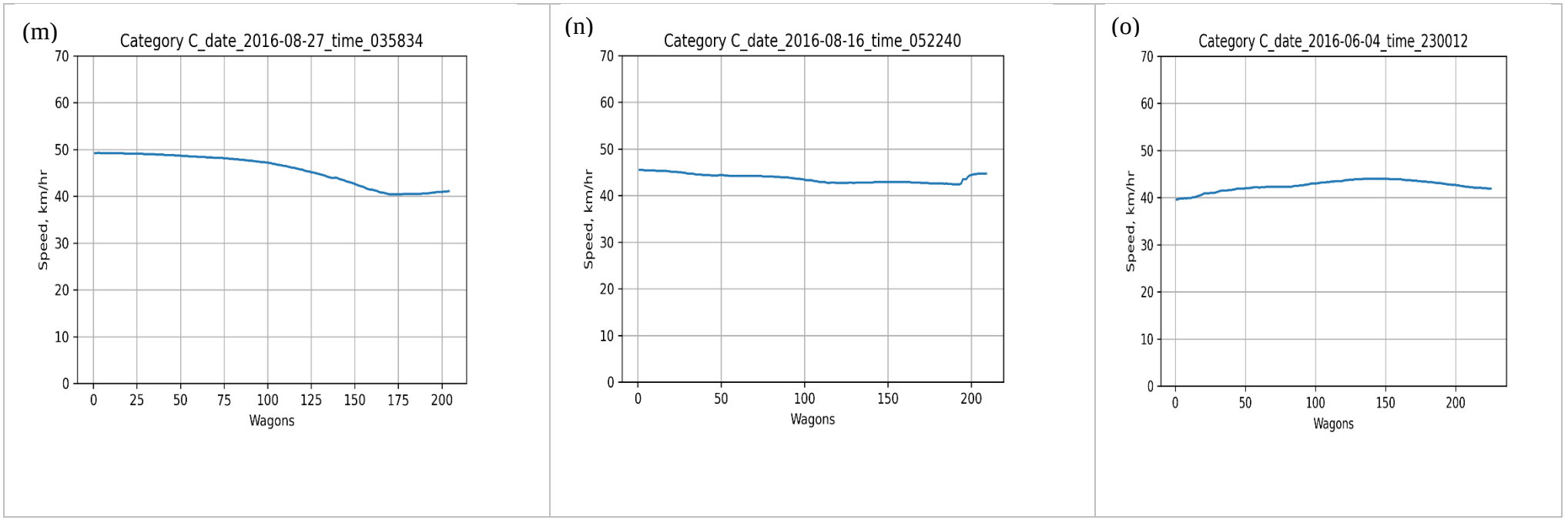

Figure 7.17: Unloaded Category C Speed Profiles (m-o)

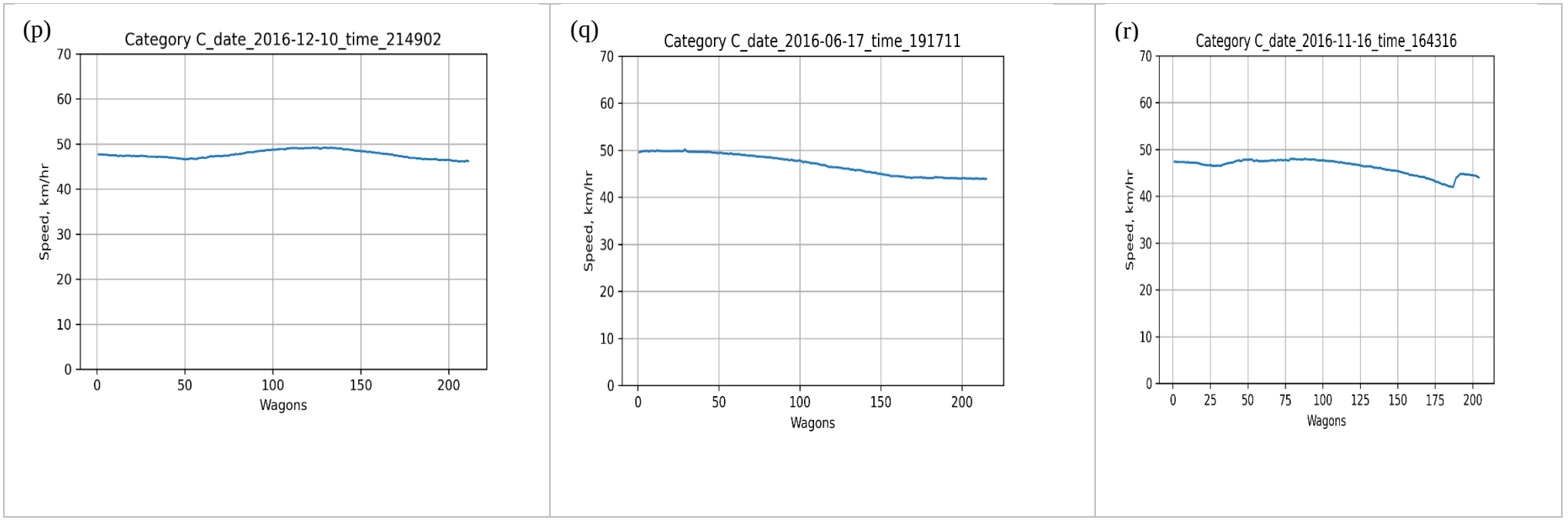

Figure 7.18: Unloaded Category C Speed Profiles (p-r)

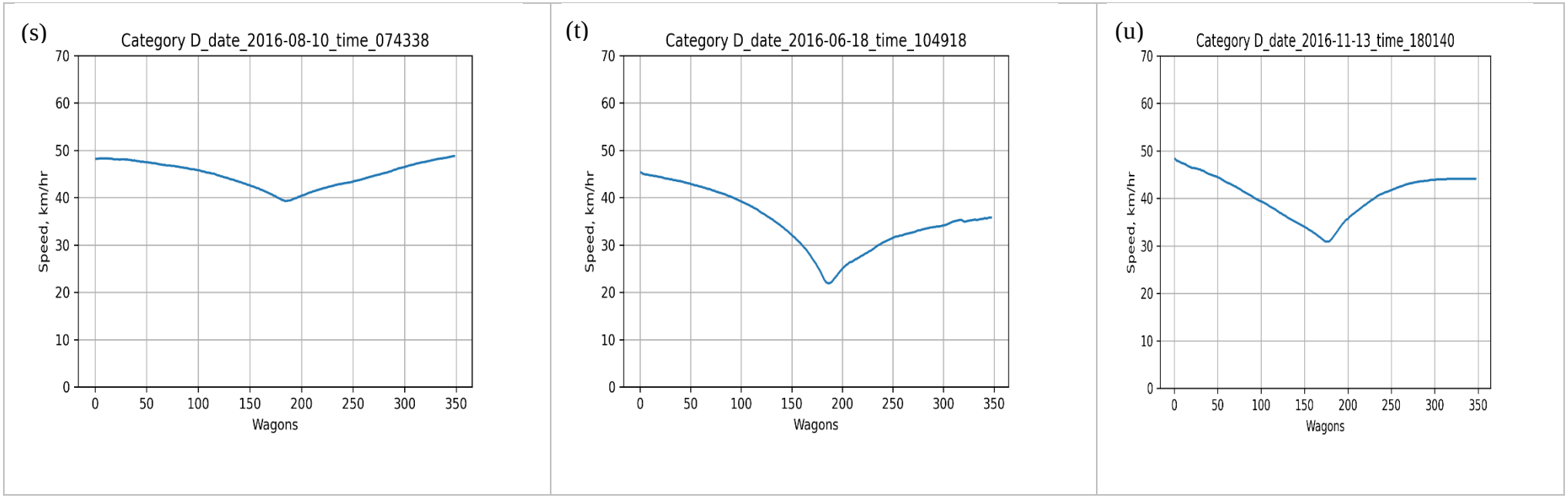

Figure 7.19: Loaded Category D Speed Profiles (s-u)

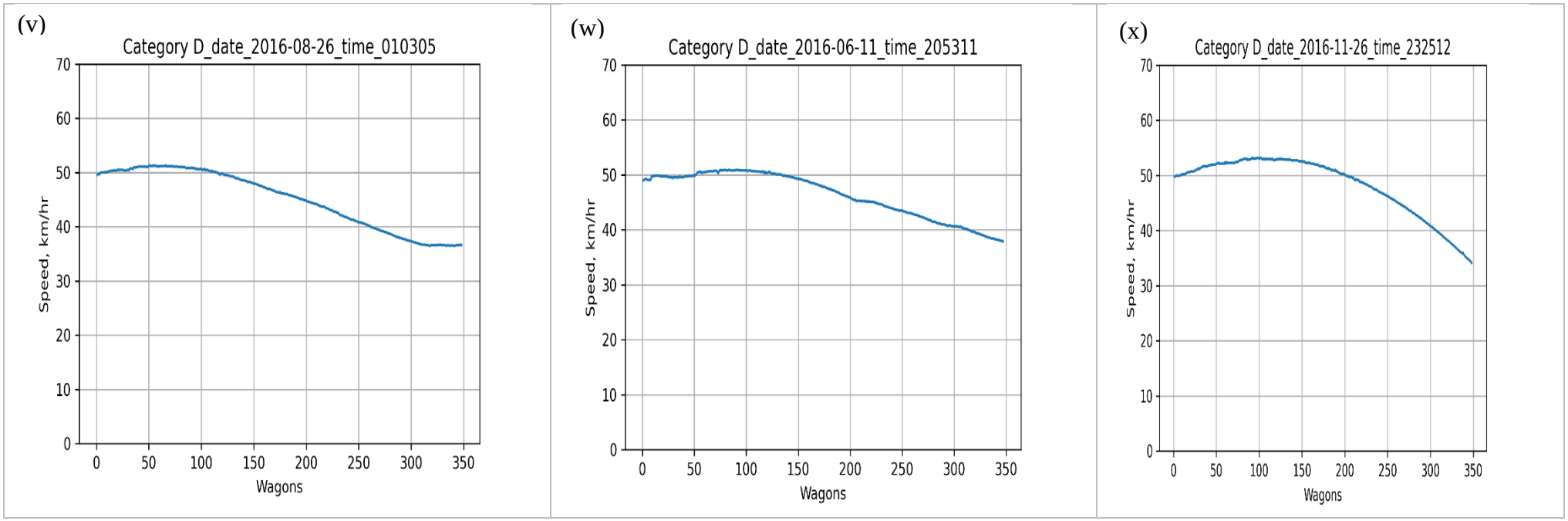

Figure 7.20: Unloaded Category D Speed Profiles (v-x)

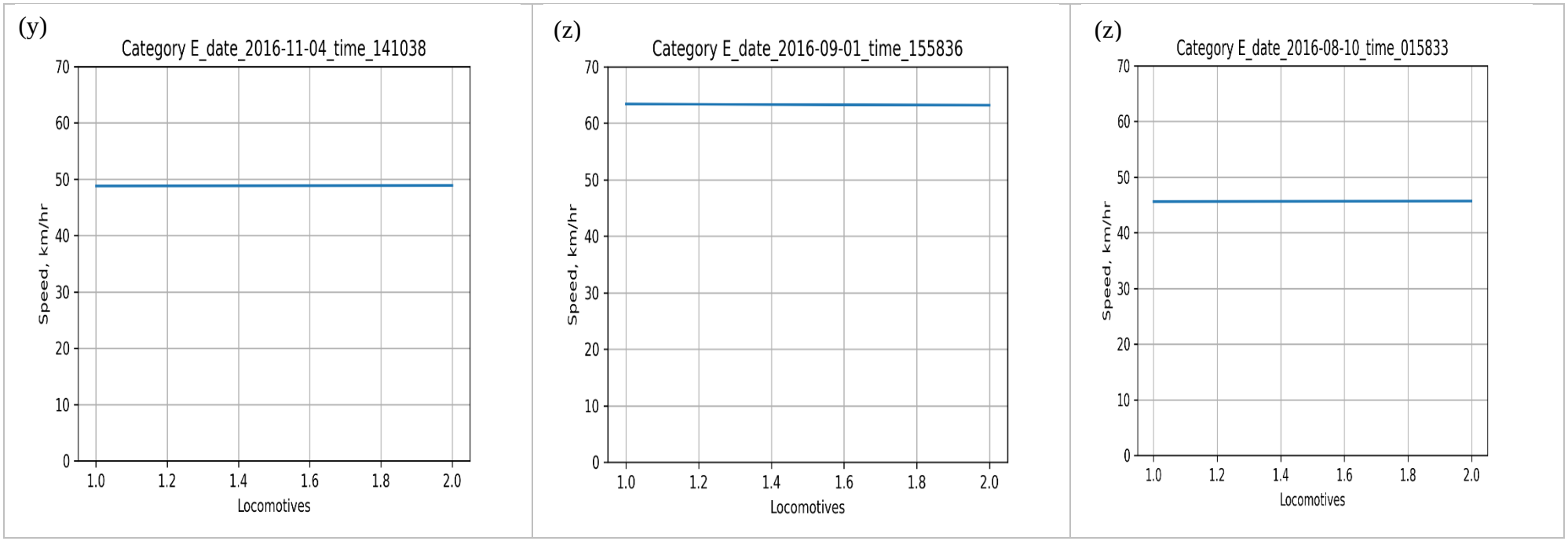

Figure 7.21: Category E Trains Speed Profiles

Appendix E: Rail Forces

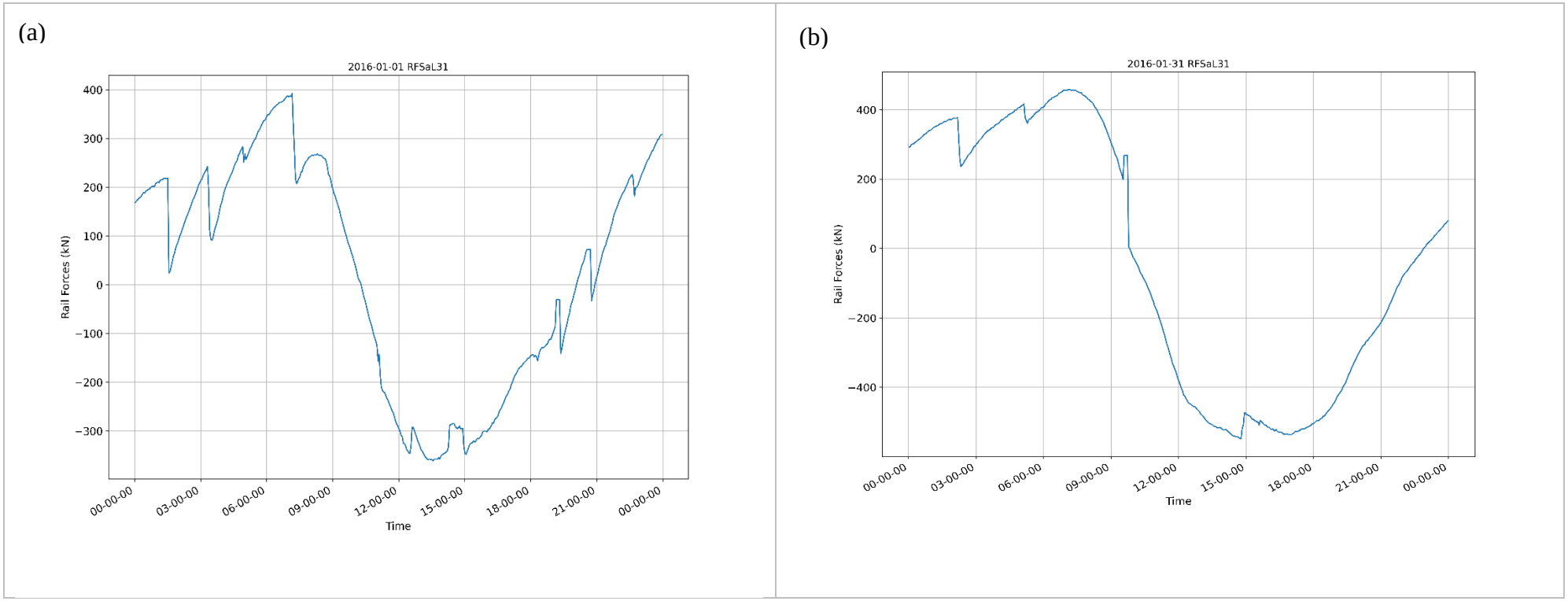

Figure 7.22: Rail Forces (a-b)

(c)

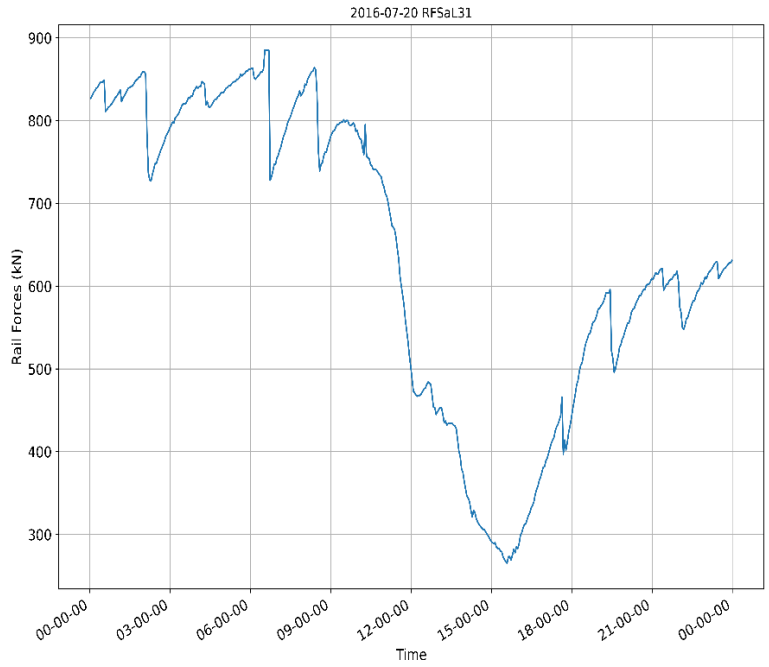

(d)

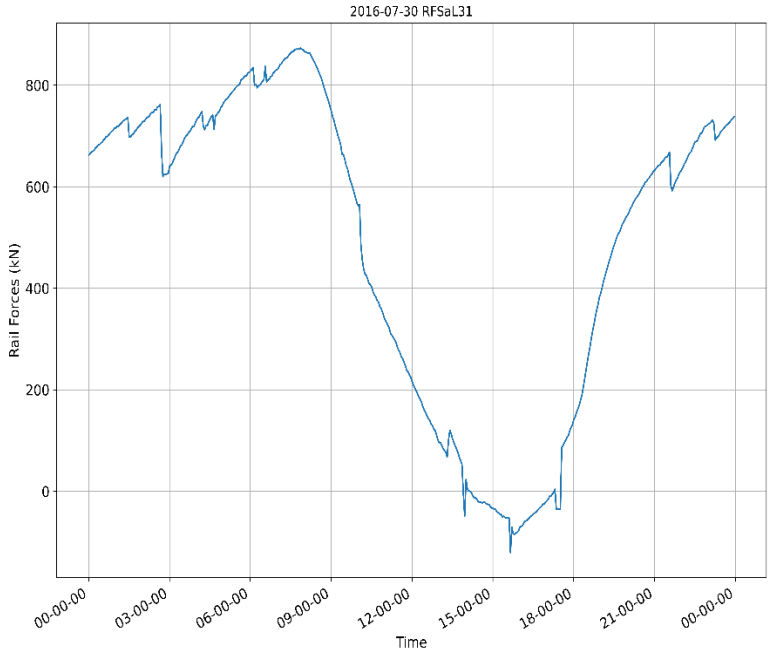

Figure 7.23: Rail Forces (c-d)

(e)

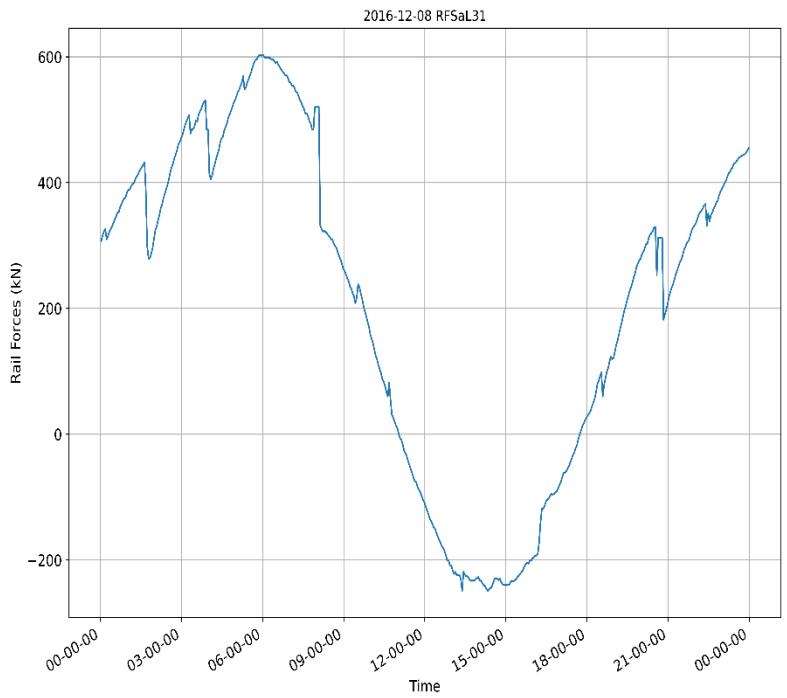

(f)

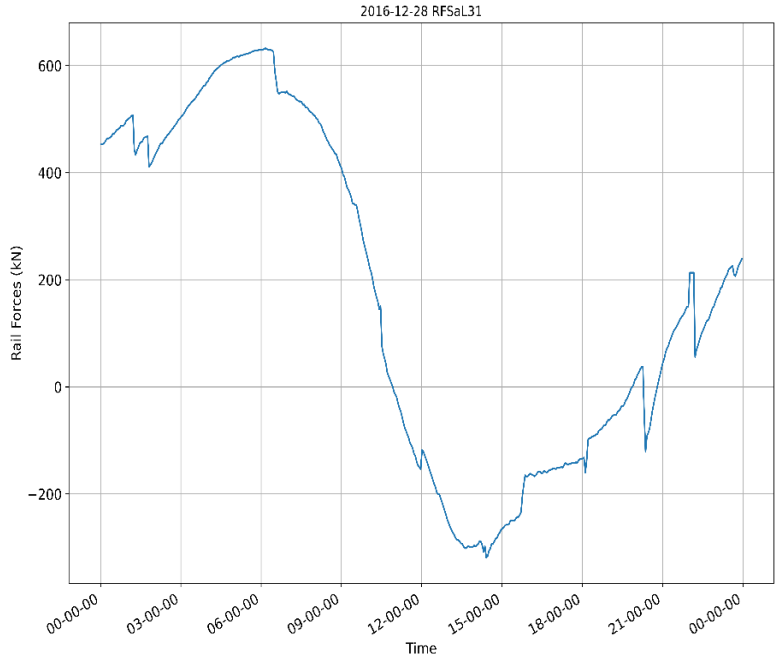

Figure 7.24: Rail Forces (e-f)

Appendix F: Rail Temperature

(a)

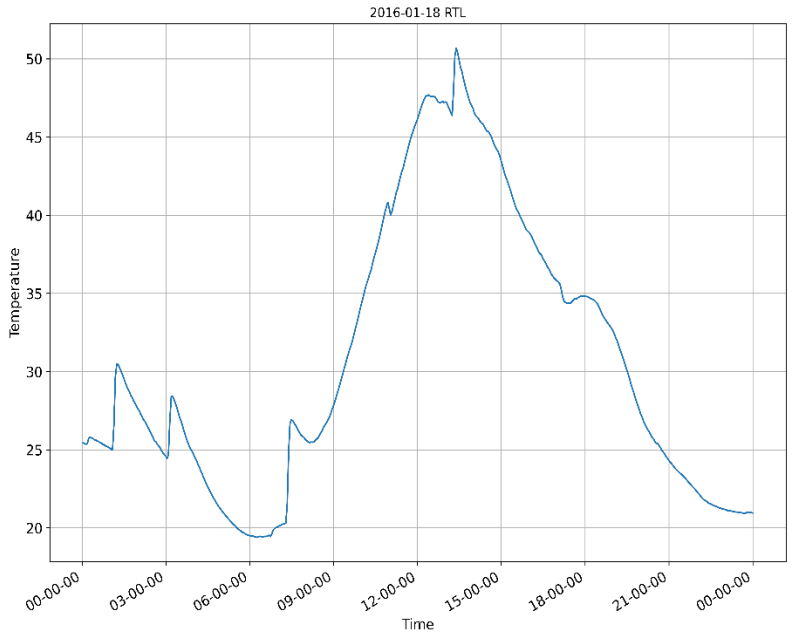

(b)

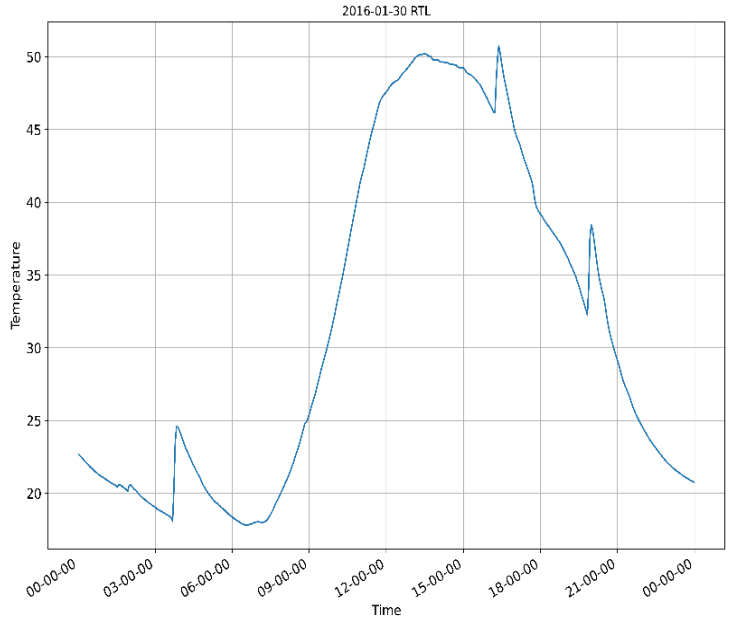

Figure 7.25: Rail Temperature (a-b)

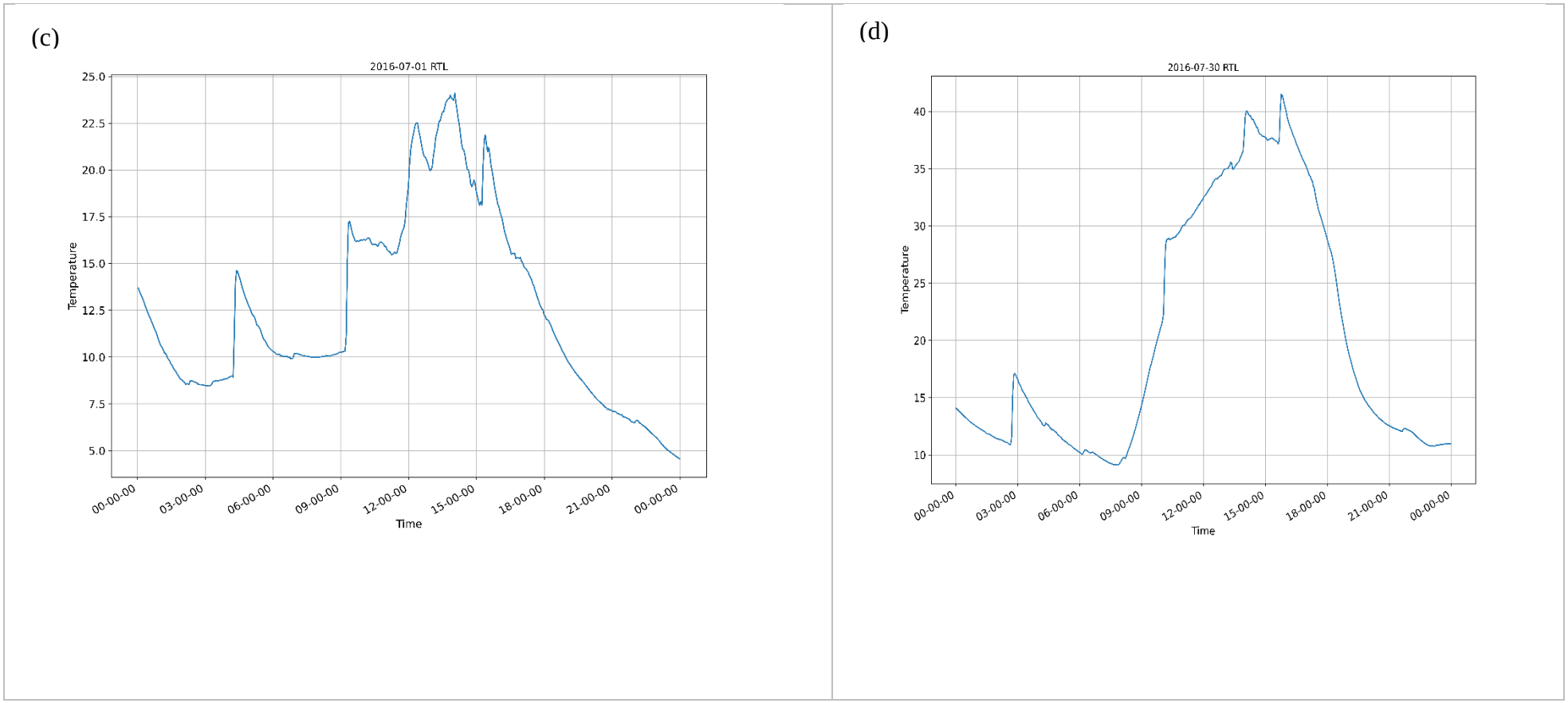

Figure 7.26: Rail Temperature (c-d)

(e)

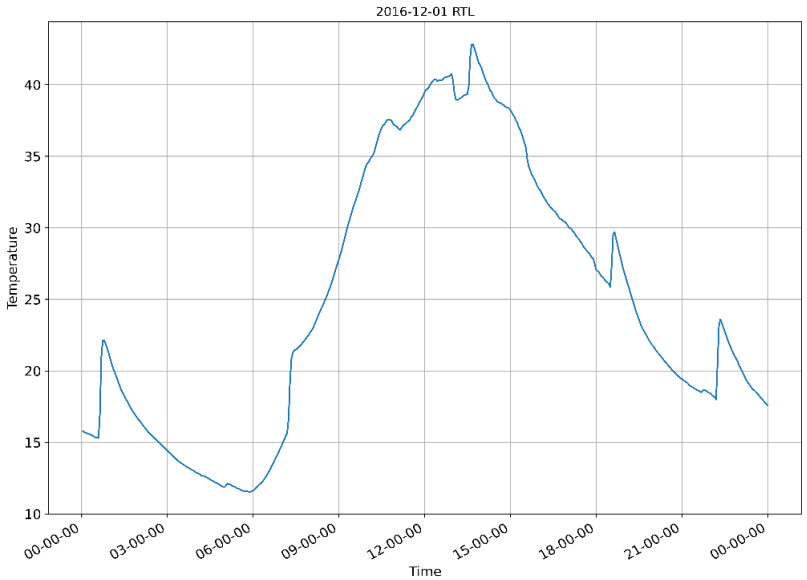

(f)

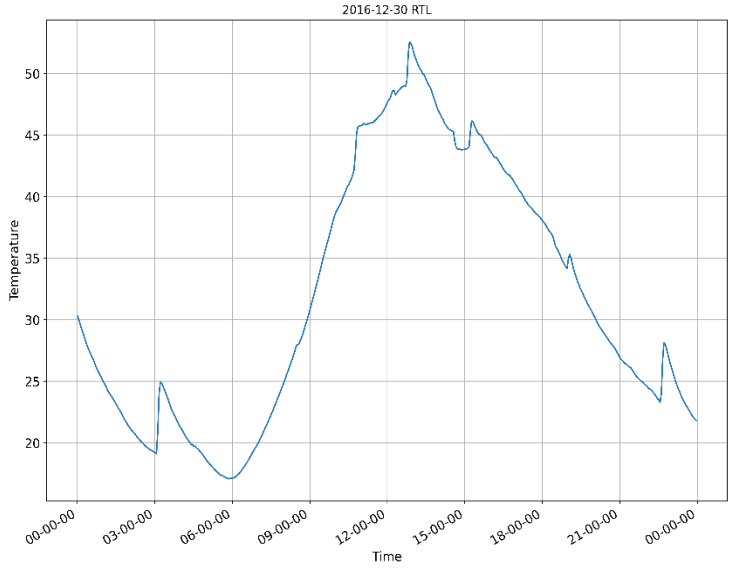

Figure 7.27: Rail Temperature (e-f)

Appendix G: Deck Expansion

(a)

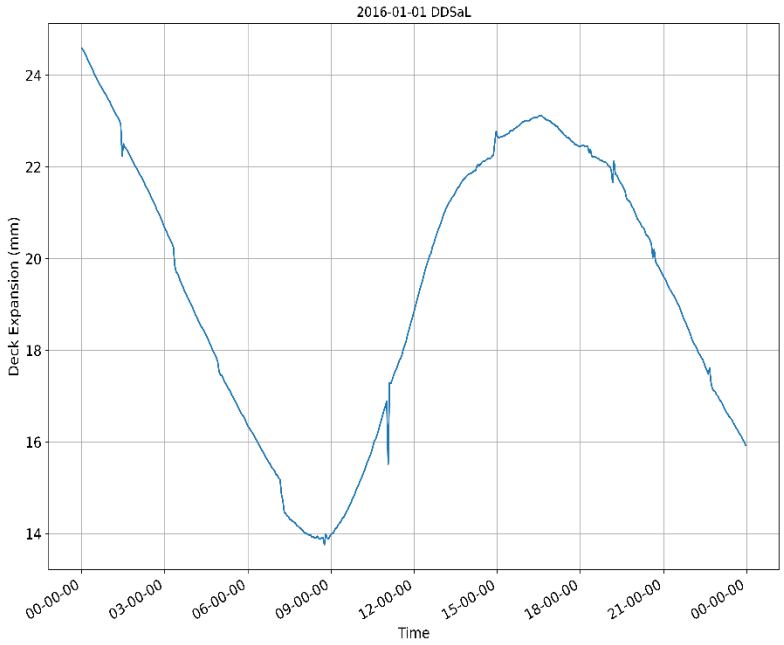

(b)

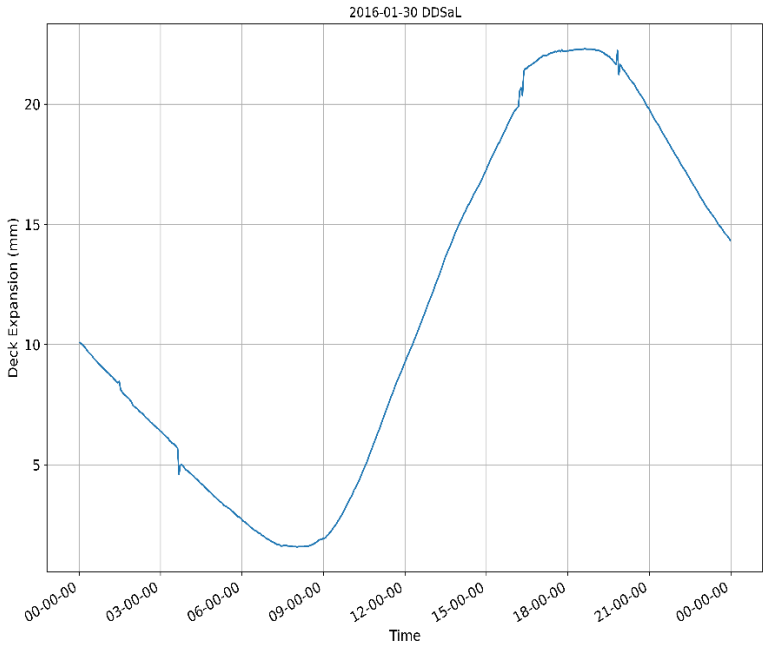

Figure 7.28: Deck Deflection (a-b)

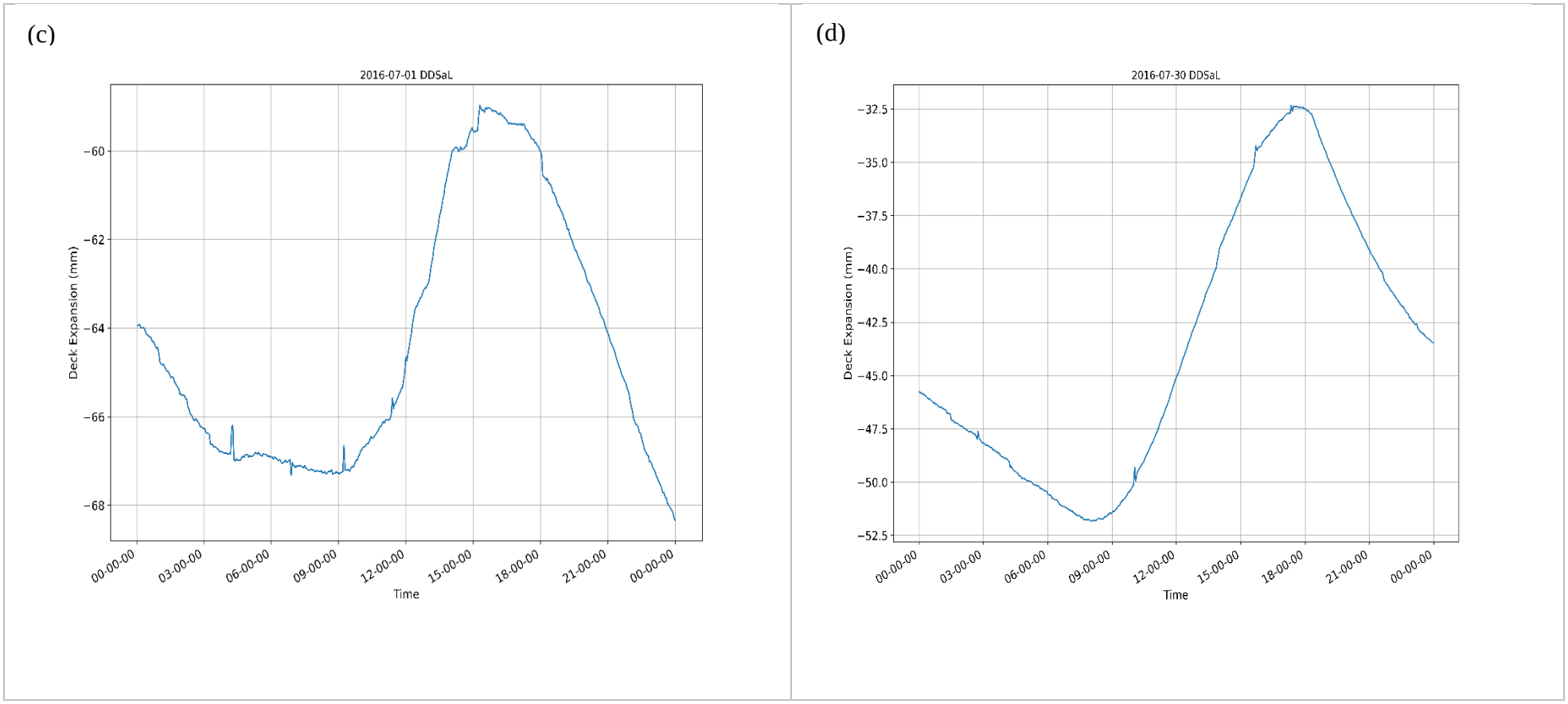

Figure 7.29: Deck Deflection (c-d)

(e)

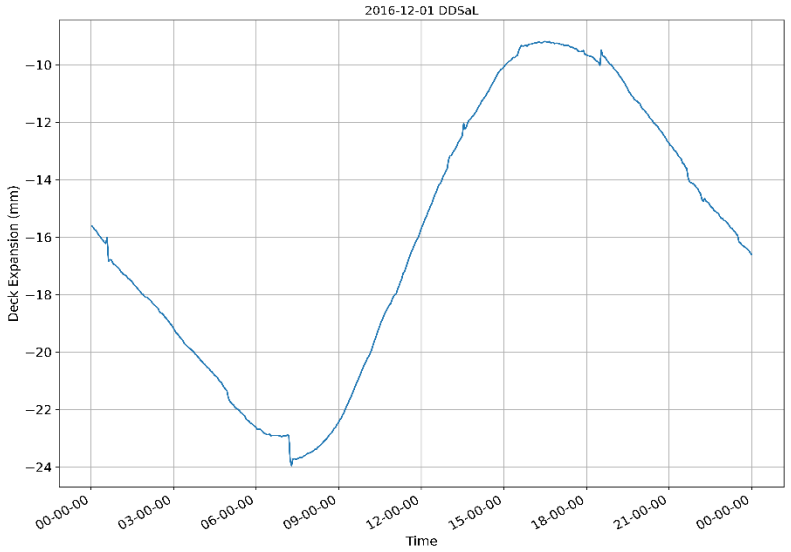

(f)

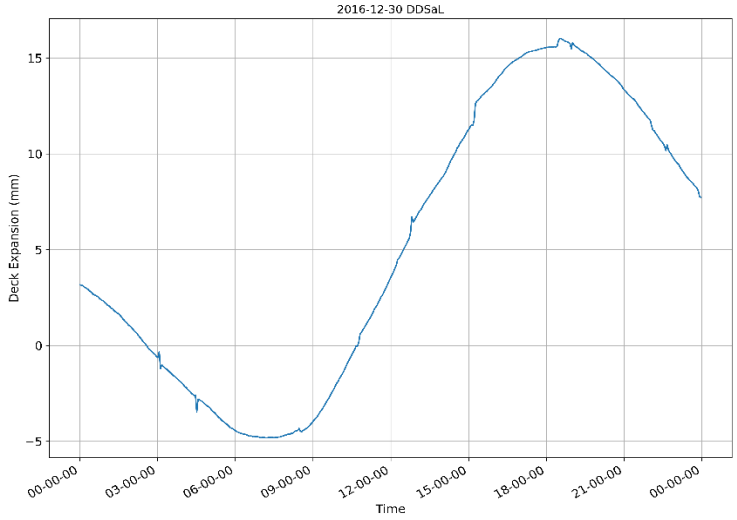

Figure 7.30: Deck Deflection (e-f)

Appendix H: Interaction Forces

Table 7.5: Braking, Traction and Temperature Forces

Date	Time	Upward	Downward	Temp change	Temp Force	Traction
27 Jan	11:18:23	-81	180	1	17,92	162,08
27 Jan	22:29:58	-10	-110	-5,5	-98,54	-11,46
06 Feb	05:56:45	-40	-151	-7	-125,42	-25,58
07 Feb	02:50:52	-40	-240	-8	-143,34	-96,66
07 Feb	15:37:28	11	91	-2	-35,83	55,17
04 Mar	13:02:04	-60	-40	2	35,83	-4,17
22 Apr	00:25:13	-40	-140	-6	-107,50	-32,50
22 Apr	22:59:36		-170	-7	-125,42	-44,58
09 May	09:32:58	-50	-180	-4	-71,67	-108,33
01 Jun	16:23:21	-30	-70	-4,5	-80,63	10,63
15 Jun	09:53:56	-30	-130	-5,6	-100,34	-29,66
25 Jun	15:53:38	-80	-100	-3	-53,75	-46,25
01 Jul	09:26:44	-51	-160	-7,2	-129,00	-31,00
20 Jul	06:47:00	-70	-210	-6	-107,50	-102,50
31 Jul	04:59:01		-180	-7,5	-134,38	-45,62
31 Jul	13:30:53	-19	-119	-7,4	-132,59	13,59

Appendix I: Descriptive Statistics

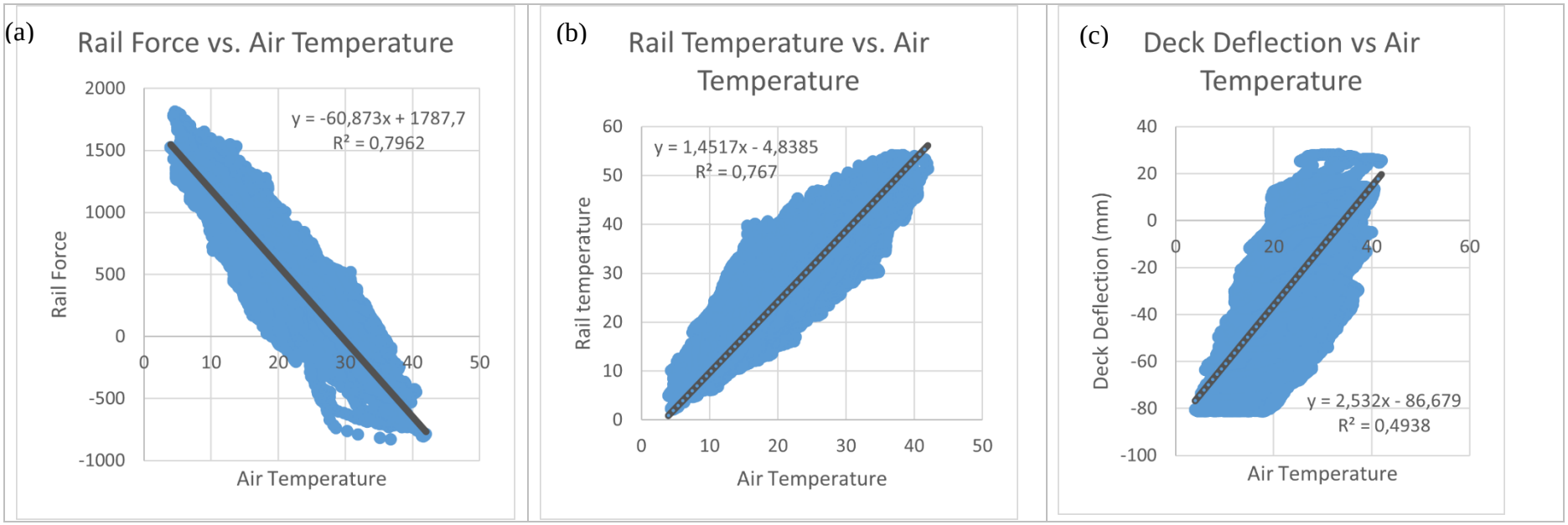

Figure 7.31: Regression models. (a). Rail force vs air temperature; (b). rail temperature vs. air temperature. (c). Deck Deflection vs. air temperature